

University of Montana

## ScholarWorks at University of Montana

---

Graduate Student Theses, Dissertations, &  
Professional Papers

Graduate School

---

2012

### Evolution and Architecture of an Incised Valley in the Upper Cretaceous Eagle Formation in South-Central Montana

Neal Auchter

*The University of Montana*

Follow this and additional works at: <https://scholarworks.umt.edu/etd>

**Let us know how access to this document benefits you.**

---

#### Recommended Citation

Auchter, Neal, "Evolution and Architecture of an Incised Valley in the Upper Cretaceous Eagle Formation in South-Central Montana" (2012). *Graduate Student Theses, Dissertations, & Professional Papers*. 1363.  
<https://scholarworks.umt.edu/etd/1363>

This Thesis is brought to you for free and open access by the Graduate School at ScholarWorks at University of Montana. It has been accepted for inclusion in Graduate Student Theses, Dissertations, & Professional Papers by an authorized administrator of ScholarWorks at University of Montana. For more information, please contact [scholarworks@mso.umt.edu](mailto:scholarworks@mso.umt.edu).

EVOLUTION AND ARCHITECTURE OF AN INCISED VALLEY IN THE UPPER  
CRETACEOUS EAGLE FORMATION IN SOUTH-CENTRAL MONTANA

By

NEAL CHRISTIAN AUCHTER

Bachelor of Arts, University of Wisconsin - Madison, Madison, Wisconsin, 2009

Thesis

presented in partial fulfillment of the requirements  
for the degree of

Master of Science  
in Geosciences

The University of Montana  
Missoula, MT

July 2012

Approved by:

Sandy Ross, Associate Dean of The Graduate School  
Graduate School

James R. Staub, Chair  
Department of Geosciences

Michael H. Hofmann  
Department of Geosciences

Christopher P. Palmer  
Department of Chemistry

## Evolution and Architecture of an Incised Valley in the Upper Cretaceous Eagle Formation in South-Central Montana

Chairperson: James R. Staub

The Santonian-Campanian Eagle Formation in south-central Montana is composed of a series of exceptionally well preserved regressive-transgressive cycles deposited on the western margin of the Cretaceous Interior Seaway. This study focuses on the genesis of a regionally correlative basal incision surface and the subsequent fill architecture of the informal middle member of the Eagle Formation. Three stratigraphic surfaces are traced continuously for up to 15 km and include the regressive surface of marine erosion (RSE), sequence boundary (SB), and transgressive surface of tidal-fluvial erosion (TSE). Within this sequence stratigraphic framework, 4 facies association, internal lower-order architectures (i.e. channel forms, lateral accretion sets, crevasse splays) and higher-order regional surfaces (i.e. sequence boundaries) are used to establish a three-phase depositional history of valley evolution: 1) fluvial incision during decreasing accommodation concomitant with fluvial deposition and sediment storage on abandoned terraces within the valley, 2) rapid increase in accommodation significantly outpaced sediment influx concurrent with seasonal fluctuations in fluvial discharge and landward migration of the turbidity maximum, producing a flood-dominated mud-rich central valley deposit, and 3) deceleration in the rate of relative sea level rise marked by a depositional shift to tidally influenced fluvial deposition, extensive valley widening, and coal development. The resulting valley architecture is a highly diachronous composite basal incision surface. The time-transgressive multi-phase nature of valley formation and infilling produced a fill profile with a mud-rich valley center flanked by stacked, sand-rich fluvial and tidal-fluvial deposits toward the valley margins. These findings contribute to the sequence stratigraphic interpretation of incised valleys along the Late Cretaceous Western Interior Seaway, serve as an outcrop analog for potential incised valley reservoirs, and have direct application in developing reservoir models for the Eagle Formation in south-central Montana and elsewhere.

## INTRODUCTION

Incised valleys can be generally defined as stratigraphic entities that form in response to a regional decrease in relative sea level. Within the context of coastal systems, incised valleys form under two fairly distinct phases, one dominated by fluvial processes during valley incision, and one influenced by fluvial, estuarine, and marine processes during subsequent infilling of the valley. As such incised valleys have been the focus of much research due to their potential for recording the complex sedimentary responses to changes in relative sea level through geologic time and their potential to host productive hydrocarbon reservoirs. Continuing research on incised valleys preserved in the stratigraphic record, modern analogs, and flume experiments have focused on understanding the generation and architecture of sequence stratigraphic surfaces, controls on sediment storage and the interplay between sediment supply and accommodation. This study focuses on outcrops in the informal middle member of the Eagle Formation in order to test the hypothesis that the erosional base of distinct channel deposits can be laterally correlated to define an incised valley. In testing this central hypothesis, key objectives include 1) documenting the lateral and vertical variability in stratigraphic architectures and sediment heterogeneity in strike-section and 2) developing a depositional context for the informal middle member of the Eagle Formation.

Much effort has been made in the last 30 years to unify the nomenclature and general interpretation of stratigraphic incised valleys. Key criteria of debate have included: 1) the nature of a sequence boundary as a component of an incised valley, 2) the relevance of lateral extent, 3) the scale relationship between incised valley and individual channel forms, 4) the stratigraphic architectures observed within the incised valley, and 5) the ability to identify valley walls and correlative interfluvial deposits within the system (e.g. Van Wagoner et al., 1990; Dalrymple et

al., 1992, 1994; Zaitlin et al., 1994; Holbrook, 2001; Posamentier, 2001; Ardies et al., 2002; Plink-Bjorklund, 2005; Boyd et al., 2006; Dalrymple and Choi, 2006; Gibling, 2006; Darmadi et al., 2007, Strong and Paola, 2008; Maynard et al., 2010; Holbrook and Bhattacharya, 2012). Various defining criteria have included assertions such that the basal incision surface be widely traceable though not explicitly defined as a sequence boundary (Gibling, 2006), that the basal incision surface is necessarily a sequence boundary (Maynard et al., 2010), that the basal incision surface (which is a sequence boundary), be correlated regionally on the interfluvium (Maynard et al., 2010), that incised valleys must include tributaries that drain the interfluvium (Posamentier, 2001), that the dimensions of the incised valley need be (Gibling, 2006) or need not be (Maynard, et al., 2010) an order of magnitude larger than those of the component channel forms in the system, and that the scale of erosional relief on the basal incision surface need be (Gibling, 2006) or need not be (Maynard et al., 2010) several times the scour depth of component channels. To address the differences between these and other previously formulated definitions for incised valleys, this study asserts a geometric based stratigraphic definition of an incised valley with three criteria as follows (Table 1):

1. The basal incision surface and correlative surfaces are regionally mappable and define a sequence boundary.
2. At least part of the incised valley fill is composed of multi-story channels.
3. The width (W) to thickness (T) ratio (W/T) of the valley is an order of magnitude greater than component channels.

Satisfying the 3-part definition offered in this study is intended to establish an incised valley as a regional-scale stratigraphic architectural entity formed in response to a lowering of base level. Criterion 1 (Lateral Extent) establishes the regional extent and sequence stratigraphic

significance of the basal incision surface which defines the incised valley. Criterion 2 (Vertical Profile) establishes that the depth of incision is greater than a single channel depth. This distinguishes an incised valley as a response to change in base level rather than an increase in sediment supply and/or fluvial discharge. The latter may incise to base level and produce significant widening under conditions of limited but not actually decreasing base level. Criterion 3 (System Dimensions) establishes the spatial and temporal framework of an incised valley as distinct from that of an individual channel such that scale and duration of valley formation as indicated by valley dimensions are significantly greater than individual channel processes of the component channels within the system. Width (W) is measured perpendicular to the elongate sediment body or perpendicular to measured paleoflow orientations, and maximum thickness (T) represents the site of maximum thickness for the fluvial body or valley fill. These terms are applied here in accordance with Gibling (2006) wherein the various W/T ratios of fluvial channel bodies and valley fills throughout the geologic record were reviewed. This dimensional relationship between incised valley and component channels is based solely on the dimensions of the component channels and reflects the process of generating the stratigraphic entity without placing specific size restrictions on either the valley or its component channels. Because there are no size restrictions on valleys or channels there is overlap in the potential dimensions of smaller incised valleys and larger individual fluvial bodies and highlights the point that channel geometry alone is insufficient to distinguish a fluvial channel body from an incised valley (Figure 1).

Within an incised valley system a variety of geomorphic bodies and sedimentary processes can occur resulting in the variable preservation of local and regional stratigraphic architectures. Coastal incised valleys commonly exhibit an upward depositional pattern of

alluvial to estuarine to open marine strata (Zaitlin et al, 1994; Boyd et al., 2006; Dalrymple and Choi, 2006). This succession reflects the fluviially dominated nature of incision, wherein it is expected that some part of the base of the incised valley be defined by fluvial deposits. The subsequent transition to increasing marine (tidal and/or wave) conditions reflects the landward shoreline trajectory during valley infilling. Component channel types within the valley may include some combination of braided channels, low sinuosity channels, and meandering channels (Dalrymple et al., 1992, 1994; Dalrymple and Choi, 2006; Gibling, 2006). Facies may include sandstone, mudstone, carbonate, and paleosol as well as possible coal development.

Characteristic sedimentary features include inclined heterolithic strata, tidal rhythmities, brackish water to marine fossils and/or trace fossil assemblages, large-scale cross beds, paleoflow orientations directed landward and/or seaward, and a tripartite estuarine facies distribution in plan form (Zaitlin et al., 1994; Posamentier, 2001; Ardies et al., 2002; Plink-Bjorklund, 2005; Blum and Aslan, 2006; Boyd et al., 2006; Dalrymple and Choi, 2006; ; Gibling, 2006; Darmadi et al., 2007; Yoshida et al., 2007; Li et al., 2010; Maynard et al., 2010 ). Sequence stratigraphic evaluation of incised valleys has produced a number of stratigraphic models for incised valleys occurring under varying amounts of tidal and wave influence, with specific attention focused on tidally dominated and wave dominated incised valley systems (Zaitlin et al., 1990, 1994; Dalrymple et al., 1992, 1994; Allen and Posamentier, 1993; Eberth, 1996; Boyd et al., 2006; Dalrymple and Choi, 2006). Such models focus on the relative influence of fluvial discharge, tidal influence, and/or wave influence in order to predict the nature and relative position of specific facies along the longitudinal profile of an incised valley. A cornerstone for these models is the concept that directionally opposed vectors of fluvial discharge and wave and/or tidal flow produce a tripartite energy distribution of dominantly fluvial energy, dominantly wave and/or

tidal energy, and a zone of energy minimum where the vectors of fluvial flow and wave and/or tidal flow approach equal magnitudes of opposite direction (Zaitlin et al., 1990, 1994; Dalrymple et al., 1992, 1994; Boyd et al., 2006; Dalrymple and Choi, 2006). These energy zones are generally assumed to represent a tripartite facies distribution of fluvially sourced sandstones and mudstones, finer central valley deposits such as siltstones and mudstones, and estuarine and marine sourced sandstones.

In the case of a tidally dominated incised valley systems, facies models predict a seaward to landward progression of tidal sand bars and upper flow regime sand flats deposited under conditions dominated by tidal currents, to meandering tidal channel deposits in the central valley occurring under mixed-energy conditions with periods of significant tidal and fluvial influence, to increasing tidal-fluvial channel deposits with decreasing tidal influence as river currents increase in the landward direction (Zaitlin et al., 1990, 1994; Dalrymple et al., 1992, 1994; Boyd et al., 2006; Dalrymple and Choi, 2006). As tidal influence wanes in the landward direction beyond the energy minimum zone, it may be preserved stratigraphically as a progression from flow reversals to simple modification of flow reducing fluvial flow velocity and producing tidal backwater effects. Landward tidal effects may move longitudinally along the system on daily and monthly scales in response to tidal cycles, seasonal scales in response to fluctuations in fluvial discharge, decadal to centennial scales in response to drainage- or basin-wide changes in fluvial discharge, and larger geologic time scales in response to tectonic, eustatic, and/or climatically driven changes in the basin and incised valley system.

In wave dominated incised valley systems, models predict shoreface deposits with sand barriers and tidal inlets (i.e. spit systems, barrier islands) with associated flood tidal deltas in the distal portion of the valley, fine-grained sediments and organic muds occurring in the central



basin where opposing fluvial and wave energy produce an energy minimum zone, and fluvial deposits at the landward and fluvially dominated end of the valley (Zaitlin et al., 1990, 1994; Dalrymple et al., 1992, 1994; Boyd et al., 2006; Dalrymple and Choi, 2006). The basic concept is that upon establishing the relative influence and landward extent of tidal or wave influence the transgressive stacking patterns produced during transgression along the entire longitudinal profile of the incised valley can be reasonably predicted. Mixed-energy scenarios occurring between tide- and wave-dominated end members likely encompass the majority of ancient and modern incised valley systems and produce stratigraphic architectures and valley fill profiles that differ from these idealized stratal stacking models (Figure 2). Key factors such as longitudinal and lateral changes in the depositional processes through the course of valley evolution (Yoshida et al., 2007; Strong and Paola, et al., 2008; Li et al., 2010; Corbett et al., 2011), the relationship between accommodation space and sediment supply (Martinsen et al., 1999; Muto and Steel, 1999; Blum and Aslan, 2006 ) and the rate of marine transgression (Willis, 1997; Martin et al., 2009, 2011) all have significant impact on the architectures and valley-fill facies distributions that occur.

This study presents detailed sedimentological and sequence stratigraphic analysis of the informal middle member of the Eagle Formation (referred to as the middle member of the Eagle Formation) in south-central Montana. The stratal stacking patterns, facies distributions, and stratigraphic architectures recorded in the middle member of the Eagle Formation suggest that significant high frequency changes on the order of hundreds to thousands of years occurred in rate of relative sea level rise and depositional processes during a full cycle of change in accommodation produced a multiphase incised valley evolution resulting in compound stratigraphic incised valley architecture.

## **REGIONAL FRAMEWORK**

The Cretaceous Western Interior Seaway (KWIS) was located within a wide (~1500 km) north-south trending basin, which formed during the development of the retroarc foreland basin associated with the Sevier Orogeny. The Sevier Orogeny formed from Late Jurassic to Late Cretaceous time due to the convergence of the North American and Farallon plates (DeCelles, 2004; Liu et al., 2008, 2011). The resulting foreland basin formed and evolved in response to orogenic loading and flexural subsidence, and dynamic subsidence associated with subduction of the Farallon Plate. The combined interaction of orogenic loading and forebulge migration on the more proximal (western) edge of the basin (Pang and Nummedal, 1995; Currie, 1997; Catuneanu et al., 2000; White et al., 2002; Yang and Miall, 2009) and the dynamic subduction of the eastward-moving Farallon Plate (Liu, 2008, 2011) produced spatially and temporally variable subsidence profiles along the basin axis. The basin was further influenced by compressional deformation during the Laramide Orogeny beginning as early as the Campanian stage of the Late Cretaceous (DeCelles, 2004).

Variations in eustatic sea level (Miller et al., 2003, 2005; Plint and Kreitner, 2007), tectonic subsidence (Pang and Nummedal, 1995; Catuneanu, 2000; White, 2002; DeCelles, 2004; Liu, 2008, 2011), and lateral variations in sediment supply (Krystinik and Dejarnett, 1995; DeCelles and Currie, 1996; Catuneanu et al., 2000) over the course of the Sevier Orogeny produced a series of third order regressive-transgressive depositional cycles. Cycles are characterized by clastic wedges including coastal plain and shallow marine strata extending eastward away from the orogenic front and deposited along the western margin of the KWIS (Payenberg et al., 2002, 2003; Corbett et al., 2011; Kieft et al., 2011). During the Late Cretaceous, the stratal stacking patterns of these regressive-transgressive cycles became

increasingly complex and amalgamated. The Eagle Formation (Santonian – Campanian) represents part of one such third order regressive-transgressive cycle (sensu Miall, 2000) (Figure 3).

The Eagle Formation extends from northwestern Wyoming through central Montana into southern Alberta (equivalent Milk River Formation). Previous work in the Eagle Formation and generally contemporaneous packages along the KWIS has been carried out in central Wyoming extending south into the Book Cliffs of Utah (Willis, 1997; Willis et al., 1999; Martisen et al., 1999; Davies et al., 2005; Lee et al., 2005, 2007; Li et al., 2010, 2011; Corbett et al., 2011; Kieft et al., 2011), in south-central Montana (Hanson and Little, 1989, Hauer et al., 2009, 2010) and in north-central Montana extending north into southern Alberta and Saskatchewan (Rogers, 1994; Eberth, 1996; Ardies et al., 2002; Payenberg et al., 2002, 2003). The regional succession extends vertically from the Niobrara Formation to the Telegraph Creek Formation to the Eagle Formation, which is overlain by the Clagget and Judith River formations (Payenberg, 2002, 2003) recording a third order regressive-transgressive sequence (Figure 4). The Eagle Formation outcrops in several bands across central Montana, including the well exposed ‘rim rocks’ near Billings, Montana, which are the focus of this study. The outcrop belt in south-central Montana wraps around the Pryor Mountains and its regional exposure is likely a function of Laramide uplift of the Pryor Mountains and subsequent downcutting and valley widening by the Yellowstone River. As such, the outcrops exhibit a general dip of usually less than 5 degrees away from the Pryor Mountains. Previous work has established three members of the Eagle Formation in south-central Montana (Hauer et al., 2009, 2010; Staub, personal communication 2012). This study focuses on the middle member of the Eagle Formation within that stratigraphic context.

The study area is an area of about 100 km<sup>2</sup> oriented on a northeast-southwest transect approximately 20 km west of Billings, Montana. The Eagle Formation outcrops extensively throughout the study area as cliffs and buttes with outcrop faces oriented dominantly east-west and north-south. Outcrops are generally laterally continuous throughout the area and range from about 500 meters to several kilometers of continuous exposure per outcrop. The main study area is estimated to include 135 linear km of outcrop. These outcrops may be further subdivided to approximately 54 km of 80% or greater exposure, 42 km of 30 to 80% exposure, and 39 km of less than 30% exposure. Outcrops range in height from 15 to 30 meters. Outcrop orientations and continuity provide an ideal opportunity to observe and document two- and three-dimensional architectures in an overall strike (and shoreline) parallel orientation. Within the study area three key areas are discussed in detail due to their significance as part of the overall valley interpretation. These locations include Calamity Jane Horse Cache (herein referred to as Horse Butte), 88<sup>th</sup> Street, and Phipps Park (Figure 5).

## **DATA AND METHODS**

Fifty four detailed measured stratigraphic sections were measured at centimeter to decimeter scale in order to capture depositional characteristics at the scale of individual sedimentary facies. Data collected were used to document the specific lithofacies within the study area. Lithofacies are the basic building blocks for any sedimentologic study and are defined here based on the physical, observable sedimentary characteristics such as grain size, sedimentary structures, composition, bedding characteristics, sedimentary architectures, and bioturbation (Miall, 2000). Grain size classification is according to Wentworth (1922), and

bioturbation is listed as a bioturbation index ranging from 0 to 6 based on the classification scheme of MacEachern et al. (2005) (Figure 6). Based on these characteristics the rocks of the middle member of the Eagle Formation are best defined by 7 distinct lithofacies (hereafter referred to as facies), each representing a distinct depositional environment and associated specific sedimentary processes. These facies were grouped into 4 facies associations. Facies associations are defined here to represent a distinct suite of depositional processes occurring within a particular depositional environment (Miall, 2000).

Stratigraphic architectures and surfaces are important components for interpreting depositional environments, dominant sedimentary processes, and help tie facies and facies associations into a more regional stratigraphic context. Architectures and key stratigraphic surfaces were mapped throughout the study area by physically walking them out in the field, as well as using photomosaics covering virtually all available outcrop exposure within the study area. Regionally mapped architectures and surfaces were ground-proofed using the measured stratigraphic sections. Synthesis of these data using Petrel software was conducted to make regional stratigraphic correlations from measured sections and map the thickness of individual depositional packages.

## RESULTS

### Facies

#### *Facies 1: Mudstone, siltstone, and interbedded mudstone and sandstone*

Facies 1 comprises mudstone, siltstone, and interbedded mudstone, siltstone, and sandstone. Sand beds are well sorted and very fine-grained to fine-grained. Sand beds occur subordinately as thin (<1 cm thick) beds in mudstone and siltstone, and dominantly as structureless, parallel planar laminated, wave-ripple laminated, or hummocky cross-stratified (HCS) beds. Individual sand beds interbedded with mudstone and siltstone are typically 2 to 30 cm thick and do not show significant internal grading. Bedsets range from 30 to 400 cm thick. Bioturbation is highly variable throughout (BI = 2 to 6), with the most intense bioturbation occurring in the mudstone and siltstone intervals interbedded with structureless, laminated, or HCS beds. Ichnofauna include *Ophiomorpha*, *Palaeophycus*, and *Planolites*.

#### *Facies 2: Cross-stratified very fine- to fine-grained sandstone*

Facies 2 is composed of very fine-grained to fine-grained sandstone. Bedding and sedimentary structures include parallel to low angle parallel-laminations and planar, trough, sigmoidal, and herringbone cross-stratification. Thicker sandstone beds (50 to 110 cm thick) are generally trough and planar crossbedded. Thinner beds (15 to 30 cm thick) have a higher number of sedimentary structures indicating bidirectional paleoflow including herringbone cross stratification and sigmoidal cross bedding. Beds are sharp or erosionally based, and are arranged in bedsets with thicknesses ranging from 50 to 300 cm. Planar, trough, or sigmoidal crossbeds

are commonly lined by mud clasts. Locally, chert pebbles and disarticulated bivalve shells occur above more laterally extensive (10's to 100's of meters) erosional surfaces. Bioturbation is highly variable (BI = 0 to 5) and includes *Ophiomorpha*, *Skolithos*, *Palaeophycus*, *Planolites*, *Thalassinoides*, *Conichnus*, and *Rosselia*.

*Facies 3: Low-angle stratified sandstone and mudstone and cross-stratified sandstone*

Facies 3 includes fine-grained to medium-grained, moderately well-sorted sandstones, interbedded mudstone and sandstone, and mudstones. Sedimentary structures include low-angle laminated, thinly planar-parallel bedded, or convolute bedded sandstone, low-angle interbedded sands and muds, and mudstone beds. Thickness of low angle inclined strata range from laminae to 5 cm, and bedsets range from 50 to 250 cm thick. Bedsets are usually erosionally based and can include mud clasts near the base. Interbedded sands and muds occur subordinately as distinct bedsets within mudstone beds. Bedsets range from 5 cm to 50 cm thick. Stratigraphic architectures are characterized by 200 cm to 500 cm thick sand-dominated lateral accretion sets. The tops of most measured lateral accretion sets were erosionally truncated. No bioturbation was observed in Facies 3 (BI = 0).

*Facies 4: Unidirectional and bidirectional cross-stratified sandstone*

Facies 4 includes fine-grained, well-sorted cross-stratified sandstone and inclined heterolithic strata. Sedimentary structures include planar, trough, sigmoidal, and bidirectional cross-stratification, asymmetric ripples, planar lamination, and inclined heterolithic strata (IHS)

with occasional convoluted bedding. Trough and/or planar crossbeds can occur as erosionally based bidirectional cross-strata. Cross-stratified sandstones can include mud and carbonaceous drapes, mud clasts, and organic debris. Cross-stratified beds are typically sharp or erosionally based and range in thickness from 15 to 45 cm. Bedsets range from 30 cm to 200 cm thick. Complete IHS bedsets have thicknesses greater than 700 cm. Bioturbation was only observed near the top of Facies 4 on the bedding planes of planar cross-stratified packages and included *Skolithos*, *Planolites*, and *Lockeia* (BI = 1).

*Facies 5: Low-angle to horizontal sandstone, heterolithic strata, and mudstone*

Facies 5 is characterized by fine-grained sandstone, heterolithic strata (interbedded to interlaminated sand, silt, muddy sand, and sandy-silty mud), and mudstone. Sedimentary structures include low-angle laminated to thinly-bedded (<5 cm) sand and interbedded sand and mud, low-angle structureless to laminated fine-grained sand, planar-parallel structureless or laminated sand, horizontally laminated to thinly-bedded (<5 cm) heterolithic strata, and mudstone beds (~5 to 75 cm thick). Heterolithic strata and mudstone beds locally include load casts and ball and pillow structures. Bedsets range from less than 100 cm for heterolithic strata to over 400 cm in the case of massive and laminated sand. Bioturbation was observed in heterolithic strata characterized almost exclusively by *Planolites* (BI = 2), and in planar-parallel structureless or laminated sand beds characterized by *Skolithos* (BI = 3 to 6).



*Facies 6: Carbonaceous mudstone, coal and tonstein*

Facies 6 is characterized by carbonaceous mudstones that are normally overlain by a coal. The mudstones range from 5 to 70 cm thick. When not altered by pedogenesis, mudstones are structureless to laminated and contain varying amounts of organic debris and organic content generally increases upward. Toward the top these mudstones typically are root penetrated (rizoliths) and at some locations they are also iron mottled. The coal ranges from not present to 45 cm thick. The coal, where thin (< 20 cm), is dull (durain) with an irregular cleat spacing on the order of 10 cm or greater. The coal transitions upward in areas where thick (> 20 cm) to bright banded (clarain to vitrain) with cleat spacing on the order of 2 cm or less. Locally, in areas where the coal is thick, a thin volcanic ash fall (> 5 cm) is preserved near the base as a tonstein. The contact between the underlying mudstone and overlying coal is usually gradational. The top of the coal contains sand filled *Ophiomorpha* burrows at some locations (BI = 1 to 3).

*Facies 7: Bioturbated, heterogeneous sandstone*

Facies 7 is characterized by bioturbated, very fine-grained to fine-grained sandstone with variable mud content and local mud and peat rip-up clasts. Sedimentary structures include thinly bedded or laminated sandstone and structureless sandstone. Beds range from 1 cm to 3 cm and bedsets ranges from 3 to 10 cm thick. Facies 7 is highly bioturbated (BI = 5 to 6), characterized almost exclusively by *Thalassinoides*, *Palaeophycus*, and *Ophiomorpha*. Package thickness ranges from 25 to 200 cm thick.

## **Facies Associations**

### *Facies Association 1: Regressive Marine Interval*

Facies Association 1 (FA1) is composed of Facies 1 and 2. Thickness ranges from less than 5 m to greater than 10 m. FA1 records a shoaling upward succession extending from inner shelf and lower shoreface to middle and upper shoreface, interrupted by a well-defined erosion surface separating deposits of Facies 1 from deposits of Facies 2. Facies 1 preserves a continuous upward coarsening trend consistent with transition from shelf and lower shoreface deposits to middle shoreface deposits. Sedimentary structures associated with laminated mudstones and siltstones (Facies 1) commonly found at the base of FA1 were deposited in distal lower shoreface or shelf environments via low-density turbidity currents and suspension settle-out. Subordinate sand beds occurring within these laminated muds and silts were interpreted to be deposited during strong storm events wherein storm wave base was sufficiently lowered, and/or via remobilization of sediment from storm events of lesser strength (Dott, 1982 a; Rodriguez et al., 2001, 2012; Hampson and Storms, 2003). Gradational transition into interbedded sandstones and mudstones is characterized by vertically increasing net sand content. Individual sand beds increase from less than 1 cm thick to 10 to 30 cm thick, and thicker (10-30 cm) sand beds interbedded with mudstone display HCS bedding indicating event deposition within storm wave base under conditions of high oscillatory flow velocities (Dott, 1982 a, b; Dumas et al., 2005; Hampson and Storms, 2003; Pattison, 1995; Rodriguez, 2012). The gradual thickening of beds and presence of HCS are interpreted to reflect continued shoaling from the inner shelf (below storm wave base) to lower shoreface environment (within storm wave base).

The transition from Facies 1 to Facies 2 marks an abrupt shift from shelf and lower shoreface deposits to sandstones deposited above fair weather wave base within a middle shoreface setting. Beds preserved at the base of the succession include 50 to 110 cm thick planar and trough crossbeds that were deposited as migrating two- and three-dimensional dunes respectively. The size of these individual dunes, their erosional bases, and the occasional presence of mud clasts concentrated at the erosional bases and/or foresets indicate deposition in a high-energy shoreface environment (Davis and Hayes, 1984; Pattison, 1995). Bedding vertically passes from trough and planar crossbeds near the base to include sigmoidal and herringbone crossbeds and subordinate parallel planar laminated beds recording upper shoreface deposition near the top of FA1. Trough and planar cross beds were formed under unidirectional flow. Sigmoidal beds were formed under conditions of accelerating and/or decelerating flow generating pronounced foreset lamination, a transition in foreset angle, and re-activation surfaces at the tops of foresets. Herringbone bedding occurs under conditions of sequentially opposed flow vectors (e.g. landward then seaward) of generally equal magnitude (Clifton et al., 1971; McCabe and Jones, 1977; Dabrio, 1982; Hampson, 2000; Dumass et al., 2005; Hampson and Storms, 2003). All bedforms are not necessarily present in any single location, but generally reflect a trend of increasing bidirectional flow orientations.

The shoaling upward character of Facies Association 1 is interpreted as a regressive shoreface deposited on a wave influenced, mesotidal coast-line. The abrupt shift from Facies 1 to Facies 2 and the development of an erosional surface between these facies is interpreted as a rapid basinward shift in shoreline forcing this swift shoaling in depositional environment (Figure 7).

## *Facies Association 2: Regressive to Early Transgressive Valley Fill Deposits*

Facies Association 2 (FA2) comprises fluvially dominated channel deposits with periods of tidal influence (Facies 3) and their associated floodplain deposits (Facies 5) deposited within an incised valley system. FA2 ranges in thickness from less than 3 meters near the margins of the valley to greater than 12 meters in the valley center. The basal contact between FA2 and the underlying FA1 is erosive and marks the abrupt transition from the marine environment of FA1 to the dominantly continental deposits of FA2.

Channel deposits (Facies 3) include low angle thinly bedded to laminated sandstones, which locally include mud clasts, convolute bedding, and asymmetrical ripple lamination. Channel sand deposits can be sharply overlain by thick mudstone beds (Facies 3) or heterolithic strata and laminated to structureless sand (Facies 5). In the case of a thick mud package (> 500 cm thick), mud beds are horizontal to gently inclined interbedded with subordinate lateral accretion sets containing planar-parallel and unidirectional ripple lamination (88<sup>th</sup> Street). This mud-dominated channel fill with intervals of sand is interpreted to be a function of deposition within the turbidity maximum along the longitudinal profile of the valley system, where opposing fluvial and tidal influences produce a discrete zone of high suspended sediment concentration (Wolanski et al., 1995; Burchard and Baumert, 1998; Dalrymple and Choi, 2006; Phillips and Slattery, 2006; Mitchell, 2012). The turbidity maximum can be highly mobile along the longitudinal profile of an estuarine system responding to changes in tidal influence and/or fluvial discharge, representing a zone of potentially significant change in sedimentary characteristics and sediment storage (Wolanski et al., 1995; Phillips and Slattery, 2006). Subordinate sand-dominated lateral accretion sets are interpreted to reflect longitudinal shifts in the location of the turbidity maximum seaward (e.g. seasonal elevation in discharge or episodic

flood) of the strike-section recorded in the study area due to seasonal elevation in discharge. Overbank deposits laterally thinning away from the mud-dominated channel fill, characterized by low-angle to horizontal tabular sand beds interbedded with thin mud beds and laminae, are interpreted as levee deposits associated with periods of elevated flow and deposition of coarser grained sediment (Facies 5).

In the case of channel deposits overlain by heterolithic strata and laminated or structureless sand (Phipps Park), deposition is interpreted to be the result of complete or partial abandonment of the channel (e.g. avulsion, oxbow) resulting in deposition of mud and silt. Occasional reactivation of the channel and or flood deposition from adjacent active channels resulted in deposition of isolated sand beds. Heterolithic strata overlying low-angle cross-stratified sands (Facies 5) include thinly interbedded sands and muds (0.5 to 2 cm thick), soft sediment deformation, and minor bioturbation (BI = 1). Bioturbation is exclusively limited to *Planolites*, which is interpreted to represent active backfilling of temporary burrows, resulting in unlined burrows of texturally distinct character from the host sediment (Pemberton and Frey, 1982). Rapid infilling of burrows is consistent with occasional, rapid deposition. Sharply overlying the abandoned channel fill is a ~4 m thick laminated to structureless sand package thinning out to the northeast over a distance of ~ 150 meters. This discrete sand package is interpreted to be an abandoned channel fill deposited by proximal active channel deposition.

Facies Association 2 represents fluvially dominated channel deposits and their associated overbank/floodplain deposits (Facies 3 and 5). Tidal influence produced a landward progression of the turbidity maximum resulting in significant deposition of mud and fine-grained sediment in the active channel. The lateral variability of significant architectural elements such as lateral

accretion sets, abandoned channel fill(s), and heterolithic floodplain deposits indicate lateral channel mobility (meandering) during deposition of Facies Association 2 (Figure 8).

### *Facies Association 3: Late Transgressive Valley Fill Deposits*

Facies Association 3 (FA3) comprises a succession of tidal-fluvial channel deposits (Facies 4) and their associated floodplain deposits (Facies 5) capped by carbonaceous mudstone and coal (Facies 6). FA3 ranges in thickness from less than 3 m to greater than 10 m thick.

Channel deposits comprise unidirectional and bidirectional strata including planar, trough, and sigmoidal crossbeds (Facies 4). Both unidirectional and bidirectional strata can include mud and carbonaceous drapes, mud and/or peat clasts, and organic debris. Mud and carbonaceous drapes occurring on crossbeds and/or accretion sets, sigmoidal crossbedding, and bidirectional cross bedding represent a continuum of tidally modulated fluvial discharge indicators (McCabe and Jones, 1977; Plink-Bjorklund, 2005; Boyd et al., 2006; Dalrymple and Choi, 2006). Mud drapes are deposited in response to decreases in flow velocity, which reduces the carrying capacity of a given flow thereby depositing finer sediment (i.e. mud and silt). This may occur in strictly fluvial settings due to rapid fluctuations in fluvial discharge. It may also occur in tidal settings wherein flood tides, which are in general opposition to the direction of fluvial discharge, produce a decrease in the velocity of fluvial discharge (Thomas, 1987). Tidally induced modulation of fluvial flow during the onset of flood tides and ebb tides produces the necessary turbidity and slackwater conditions for deposition of finer-grained sediment on top of coarser grained strata. Mud drapes were observed to occur on all of the varieties of cross-strata discussed in this section. Sigmoidal cross-stratified beds display an up and/or down current

transition in the steepness of foreset angle. Such bedding forms under accelerating and changing flow conditions with sufficient magnitude to alter ripple and dune bedforms. Sigmoidal bedding is generally inferred to form under conditions of tidally modulated flow within a single tide and is especially diagnostic of tidal influence when the tops of crossbeds are planed off in a landward direction reflecting full flow reversal (Shanley et al., 1992; Plink-Bjorklund, 2005). Stronger flow reversals are manifested as bidirectional cross-stratified sandstone, which typically include planar or trough crossbeds. Beds are often erosionally based and can include mud drapes, mud clasts, and/or organic debris. The general stacking pattern of bedding in Facies 4 progresses from thin mud drapes at the base of FA3 (above erosion surface 2) to increasingly thick and prevalent mud drapes, sigmoidal crossbeds, and bidirectionally oriented crossbeds near the top of Facies 4 (below the organic rich mudstone and coal of Facies 6). A similar increase in the presence and prevalence of mud and carbonaceous drapes, and indications of flow reversals is observed toward the margins of the study area.

Well preserved lateral accretion sets at the margins of the study area include wavy and convolute bedding, paired mudstone and siltstone drapes, mud and carbonaceous laminae, and locally preserved asymmetric ripples (Facies 4). These inclined heterolithic strata may form as a function of rapid changes in fluvial discharge and/or due to tidal influence, and are interpreted to represent at least occasional tidal influence of point bar deposits (Thomas, 1987; Shanley et al., 1992; Hovikoski et al., 2008; Li et al., 2011; Fustic, 2012). The heterogeneity of these deposits (i.e. decrease in sandstone content as a function of increased abundance of mud and carbonaceous laminae) can vary appreciably between lateral accretion sets as well as both laterally and vertically within a single accretion set. Deposition of finer grained sediment via tidal modulation of flow is a dynamic process that can change on multiple spatial and temporal

scales as a function of diurnal or neap-spring tidal cycles, episodic changes in fluvial discharge due to storms, seasonal changes in fluvial discharge, channel dimensions, valley geometry, and the interplay of these various processes and conditions (Shanley et al., 1992; Willis et al., 1999; Boyd et al., 2006; Dalrymple and Choi, 2006; Phillips and Slattery, 2006; Yoshida et al., 2007). The heterogeneous nature of IHS characteristic of Facies 4, in combination with the vertical increase in mud drapes and bidirectional flow indicators throughout the study area, are interpreted to represent increasing tidal modulation of fluvial flow, and potentially seasonal variations thereof.

Abandoned channel fills and floodplain deposits (Facies 5) associated with tidal-fluvial channel deposits (Facies 4) include mudstone packages that locally preserve soft sediment deformation, interbedded sandstone and mudstone, and horizontal laminated tabular sand beds. Mudstone packages were deposited primarily as distal suspension settle-out of fine particles, with soft sediment deformation preserving deposition of coarser sediment during higher discharge events and/or flood stage cut-off channel deposits. Parallel stratified heterolithics were interpreted to be deposited as more proximal floodplain deposits via alternating traction transport (sand beds with ripples) and suspension settle out of mud and silt after flood-stage flow (Plink-Bjorklund, 2005). Parallel stratified sand beds with subordinate mud laminae also occasionally preserve unidirectional ripples and were deposited adjacent to active channel processes via traction transport. Bioturbation at the top of FA3 is characterized by *Palaeophycus* interpreted to occur under brackish water conditions representing tidal influence and a landward increase in salinity (Pemberton and Frey, 1982; Frey and Howard, 1990; Gingras et al, 2011).

Tidal-fluvial channel deposits and their associated floodplain deposits (Facies 4, 5) are capped throughout the study area by a succession of carbonaceous mudstone and coal (Facies 6)



that are associated with the filling of the incised valley and are included in FA3 together with the tidal-fluvial deposits. The succession ranges from less than 5 cm to over 100 cm thick, with coal thickness varying from not present to 45 cm. The succession may occur as exclusively carbonaceous mudstone, exclusively coal, or a combination of the two with carbonaceous mudstone capped by coal. Carbonaceous mudstone is deposited via suspension settle-out in a topographic low (e.g. swamp) under conditions of 1) sufficient lateral and/or vertical distance from active channel processes to prevent deposition of coarser sediment during flood stage(s) (Plink-Bjorklund, 2005), or deposition adjacent to channels dominated by fine-grained sediment (Phillips and Slattery, 2006). Coal formation occurs under conditions such that the generation of accommodation generally matches the rate of accumulation of organic matter and production of peat (Davies et al., 2005; Diessel et al., 2006; Staub, 2002). Key factors involved in producing coal deposits typically include a static or rising water table associated with local or regional subsidence, regional precipitation and climate, and the autocompaction of peat (Davies et al., 2005). Conditions where generation of accommodation matches peat production typically produce planar mires which reflect surface topography. Under conditions of sufficient water supply where rainfall exceeds evapotranspiration, surface doming can occur producing a raised mire which does not reflect surface topography (Staub, 1991, 2002 Staub and Esterle, 1993, Staub and Gastaldo, 2003). Thick (30 to 50 cm) coal laterally adjacent to channel deposits is interpreted to record raised mires, which restrict channel mobility within the incised valley system. Based on a Campanian paleolatitude of  $48^{\circ}\text{N}$  peat generation is estimated to be approximately 1 mm per year (Falcon-Lang, 2003; Diessel et al., 2000; Martin, 2010). As such the rate of accommodation increase during peat production would have been equal to approximately 1 mm per year. Carbonaceous mudstones are interpreted to be deposited in

topographic lows and distal floodplains of tidal-fluvial channel(s) restricted by the developing mire. Locally, the top of the coal included *Ophiomorpha* burrows infilled with sand. The occurrence of *Ophiomorpha* burrows in the top of the coal and their sand-filled nature represent a rapid inundation of the mire system.

Facies Association 3 represents tidal-fluvial channel deposits and associated floodplains, carbonaceous mudstones, and coal preserved under conditions of slowly increasing accommodation. These genetically related facies received variable but generally increasing tidal influence through the temporal evolution of the succession. The lateral variability of significant architectural elements including point bar deposits and abandoned channel fills indicates continued channel mobility during deposition of Facies 4, with increasing channel preservation to the southwest margin of the study area. The development of a mire system (coal) across the top of most of FA3 indicates a relatively slow (~ 1 mm per year) increase in accommodation (Figure 9).

#### *Facies Association 4: Transgressive Marginal Marine to Marine Interval*

Facies Association 4 (FA4) comprises a distinct package of bioturbated, heterogeneous sandstone (Facies 7) and upper to middle shoreface deposits (Facies 2). FA4 is generally truncated by erosion at the tops of outcrops, but has been measured up to 800 cm thick. The high density and low diversity of ichnogenera assemblages present in Facies 7 are strong indicators of brackish water or otherwise stressed conditions occurring within marginal marine systems (Howard and Frey, 1984; Frey and Howard, 1990; Buatois et al., 2005; MacEachern et al., 2005; Spila et al., 2005; Gingras et al., 2011). Stressors such as a variable salinity gradient favor

organisms that exhibit short temporal ranges or behavioral and/or physical adaptability (Howard and Frey, 1984; Spila et al., 2005; Gingras et al., 2011). In addition to high density and low diversity, additional ichnological indicators of stressed conditions include dominantly simple morphological structures typically produced by trophic generalists, assemblages commonly dominated by a single or few ichnogenera, and ichnotaxa that represent marine assemblages rather than a mixture of marine and freshwater assemblages (Howard and Frey, 1984; Spila et al., 2005; Gingras et al., 2011). *Ophiomorpha* and *Thalassinoides* are both singular or branching burrow networks interpreted to be the feeding and dwelling burrows of arthropods (e.g., shrimp), and can occur in most marine environments where salinity and current energy are moderately high and the substrate is dominantly sand (Bromley and Frey, 1974; Frey et al., 1978; Howard and Frey, 1984; Frey and Howard, 1990). As such they fit the standard criteria for stressed marine conditions, and are interpreted to occur in a bay environment.

Facies 7 is sharply or gradationally overlain by shoreface sandstones of Facies 2. Facies 2 thickness measurements are variable due to exposure limitations, as this package occurs at the top of many of the outcrop exposures. Bioturbation intensity is spatially variable both vertically and laterally throughout the study area (BI = 1 to 5) with a significant increase in diversity.

Facies Association 4 represents a transgressive marginal marine to fully marine depositional system. The vertical transition of increasing size and diversity of ichnofauna, increasing bed and bedset thickness, and increased sediment sorting is consistent with increasing accommodation and continued marine inundation of the coastal system (Figure 10).

## **Regional Surfaces and Distribution of Facies Associations**

Regional mapping through walking out of surfaces, use of photomosaics, and correlation of measured sections has established 3 traceable, erosional surfaces observed throughout the study area. Measured depth of incision for the upper two erosional surfaces was measured from the top of the coal or base of the bay fill package (representing the top of the incision fill package) down to the erosional surface of interest. The amount of middle and upper shoreface sands (Facies 2) preserved below these surfaces, while not used in measuring incision depth, offer additional evidence for the depth of incision.

### *Erosion Surface 1*

Erosion Surface 1 is associated with the marine deposits of FA1 and marks an abrupt and sharp based basinward shift of facies from shelf and lower shoreface deposits of facies 1 to middle and upper shoreface deposits of facies 2. The erosional surface can be traced throughout the study area and ranges from ~12 to 16 meters below the datum (Figure 11).

### *Erosion Surface 2*

Erosion Surface 2 defines the mappable erosional contact between shoreface deposits (FA1) and fluvially dominated channel deposits and associated floodplain deposits (FA2). Erosion Surface 2 is defined not only as a laterally traceable physical surface, but also as a disconformable juxtaposition of fluvial channel deposits above marine shoreface deposits. Erosion Surface 2 is locally overlain by mud clasts.

The center of the study area represents the deepest point of incision at the 88<sup>th</sup> Street location). Maximum incision depth was 15 meters with less than 2 meters of middle-shoreface sandstone (Facies 2) preserved between Erosion Surface 2 and lower shoreface deposits (Facies 1) (Figure 11).

To the northeast of the 88<sup>th</sup> Street location Erosion Surface 2 has an incision depth of 5 to 8 m for a lateral distance of ~5 km. The incision depth increases again in the second area of deep incision, at the Phipps Park location. Incision depth was 13 meters with less than 3 meters of middle-shoreface sandstone (Facies 2) preserved between Erosion Surface 2 and lower-shoreface deposits (Facies 1). The incision depth of Erosion Surface 2 decreases to 5 to 8 meters continuing to the northeast margin of the study area (Figure 12).

To the southwest of the 88<sup>th</sup> Street location along the study transect, Erosion Surface 2 decreases in incision depth. At locations of minimum incision, incision depth was less than 3 meters with over 7 meters of middle and upper shoreface sands (Facies 2) separating Erosion Surface 2 from lower shoreface deposits (Facies 1).

### *Erosion Surface 3*

Erosion Surface 3 was mapped above Erosion Surface 2 from the 88<sup>th</sup> Street location to the northeast margin of the study area, forming a vertically stacked or nested stratigraphic profile. Along this part of the transect the vertical separation between Erosion Surface 2 and 3, defined by FA2, ranges from less than 3 to over 8 meters. Erosion Surface 3 also amalgamates with and/or truncates Erosion Surface 2 at the southwestern margins of the study area. Erosion Surface 3 extends beyond the lateral extent of Erosion Surface 2 approximately 3 km southwest

of the 88<sup>th</sup> Street location, where it incises directly into shoreface deposits (FA1) rather than fluvially dominated deposits occurring above Erosion Surface 2 (FA2) (Figure 13). Deposits occurring above Erosion Surface 3 throughout the study area are defined by tidal-fluvial channel deposits, associated floodplain deposits, and carbonaceous mudstone and coal (FA3).

### **Distribution of Facies Associations**

Shoreface deposits (FA1) are notably thinnest (2 to 4 m thick) at the two central locations of deepest incision (13 to 15 m of incision) and thicken flanking these locations to the northeast and southwest (Figure 14). The valley center, the 88<sup>th</sup> Street location, preserves the thickest package of fluvially dominated sediment (FA2 ~11 m thick). FA2 thins away from the valley thalweg, but increases in sand content. The thickest tidally influenced fluvial deposits (FA3 ~10 m thick) occur ~5 km northeast of the valley center and thin laterally to the northeast and southwest. The isopach map of FA2 and FA3, which includes the full valley fill sequence, is shown in figure 15A. General channel dimensions within the valley fill sequence were measured based on thickness of lateral accretion sets and/or the thickness and width of preserved channel forms. Channels measured in FA2 had a width of ~110 m and depth of ~9 m at 88<sup>th</sup> Street (W/T ratio of approximately 12 to 1), and a width of ~100 m and depth of ~8 m at Phipps Park (W/T ratio of approximately 12 to 1). Channels measured in FA3 had a width of ~90 m and depth of ~6 m at 88<sup>th</sup> Street (W/T ratio of approximately 15 to 1), and a width of ~60 m and depth of ~5 meters at Horse Butte (W/T ratio of approximately 12 to 1). Clear distinction of FA3 channel margins at Phipps Park is lacking but channel width is estimated to be at least 100 m and depth of ~8 m (W/T ratio of approximately 12 to 1).

Coal thickness is also variable across the transect demonstrating an inverted thickness profile from that of the valley fill thickness, with thickest deposits flanking the locations of deepest incision (Figure 15B). Thickest deposits are located ~3 km southwest of the deep incision at the 88<sup>th</sup> Street location and ~2.5 km northeast of the deep incision at the Phipps Park location. The thinnest coal, and locations with no coal, occur at locations with the thickest tidal-fluvial channel deposits (Phipps Park).

The isopach map of the bay fill deposits (Facies 7 of FA4) show an inverted thickness profile compared to that of the coal, with a distinctly thicker profile in the locations of deep incision and thickest tidally influenced deposits at the Phipps Park location (Figure 15C). The bay fill package thins laterally toward the northeast and southwest margins of the study area where depth of incision is less and coal is generally thicker (Figure 14).

## **DISCUSSION**

### **Sequence Stratigraphic Framework**

A central aspect of sequence stratigraphy is documenting and interpreting the interplay between sediment supply and accommodation (Van Wagoner et al., 1988, 1990; Muto and Steel, 1997; Martinsen, 1999; Blum and Tornqvist, 2000; Blum and Aslan, 2006; Martin et al., 2009 a, b; Strong and Paola, 2008). A sequence is interpreted to represent a full cycle of change in relative sea level with the sequence boundary defined by a subaerial erosion or hiatal surface indicating the lowest position of base level for that sequence (Van Wagoner et al., 1988; Hunt and Tucker, 1992; Catuneanu et al., 2009). This position of a sequence boundary within a full cycle of change in relative sea level aids differentiation between processes occurring in response

to decreasing accommodation, and those occurring in response to increasing accommodation. On the more fluviially influenced landward end of the system, however, changes in fluvial discharge and sediment supply can significantly alter stratal stacking patterns and modify time-transgressive surfaces such as the sequence boundary. As such it need not be the case that all phases of a cycle are actually preserved (Catuneanu et al., 2009). Key sequence stratigraphic surfaces that develop during periods of decreasing, static, and increasing relative sea level are used to distinguish relative temporal position within a given sequence. Sequence stratigraphic surfaces observed in the middle member of the Eagle Formation were identified based on the lateral extent and continuity of physical surfaces and/or distinct vertical shifts in facies.

#### *Regressive Surface of Marine Erosion (RSE)*

The erosive transition from inner shelf and lower shoreface (Facies 1) to middle and upper shoreface deposits (Facies 2) defined by Erosion Surface 1 reflects a basinward shift in facies in response to decreasing accommodation and is interpreted here to be a regressive surface of marine erosion (RSE) (*sensu* Hunt and Tucker, 1992). The regressive surface of marine erosion develops on the inner shelf as a function of basinward shoreline trajectory in wave-dominated shoreface systems (Hunt and Tucker, 1992; Helland-Hansen and Martinsen, 1996, Plint and Nummedal, 2000, Posamentier and Morris, 2000). It is generally defined as a sharp or erosional contact between proximal (i.e. landward) shoreface sands above distal shoreface and shelf deposits dominated by significantly finer sediments such as silt and mud. Similar sharp surfaces can also form due to limited accommodation space and/or high sediment supply associated with prograding deltas. As such, interpreting the RSE to mark the beginning of the



Falling Stage Systems Tract (sensu Hunt and Tucker, 1992) requires additional contextual evidence. Contextual evidence is drawn from the stratal relation to subsequent surfaces and development of an incised valley, which indicate a regional response to falling relative sea level rather than progradation driven by high sediment influx. Erosion of the underlying interbedded sandstone and mudstone, as well as contemporaneous fluvial incision and sediment bypass during decreasing accommodation is the likely source of the abundant mud clasts and drapes at the erosive surface and subsequent erosional surfaces observed in Facies 2.

#### *Sequence Boundary -(SB)*

Erosion Surface 2 separates the disconformable superposition of fluvial channel and associated floodplain deposits (FA2) above shoreface deposits (FA1), representing the most basinward shift of facies during deposition of the middle member of the Eagle Formation and therefore is interpreted as a sequence boundary (SB). The SB is laterally mappable for over 15 km across the entire study area. Incision along the SB is variable with the deepest point of incision at the 88<sup>th</sup> Street location (~15 m) and minimum incision along the margins of the study area (~3 m). The lateral extent and continuity of the SB is interpreted to represent a regional response to falling relative sea level. The deepest incision at the 88<sup>th</sup> Street location records the lowest position of base level for the sequence.

### *Transgressive Surface of Tidal-Fluvial Erosion (TSE)*

Erosion Surface 3 represents a deceleration in the rate of accommodation generation occurring subsequent to the development of SB1, and is interpreted here to define a laterally extensive transgressive surface of tidally influenced fluvial erosion (TSE). In the center of the study area extending from the 88<sup>th</sup> Street location to the Phipps Park location, the TSE occurs above the SB, defining the erosional boundary between the underlying FA2 and overlying FA3 thus forming a nested stratigraphic architecture. At more lateral positions to the southwest of the 88<sup>th</sup> Street location, TSE defines the disconformable superposition of tidal-fluvial channel deposits and associated floodplain deposits (FA3) above shoreface deposits (FA1). At these marginal southwestern positions (such as Horse Butte), the temporally distinct TSE defines a composite sequence boundary, amalgamating with the SB to form a continual erosive surface separating underlying shoreface deposits from overlying valley fill deposits.

### **Incised Valley Architecture and Three-Phase Fill History**

The formation and subsequent infilling of an incised valley generally entails a sequence of some order, recording various stages of valley incision and valley infilling. The regional-scale valley architecture resulting from an amalgamated diachronous composite sequence boundary produced by two temporally distinct erosional surfaces (SB and TSE) is interpreted to define the basal incision surface of a compound incised valley (*sensu* Holbrook, 2001).

### *Phase 1: Falling Stage - Lowstand*

Phase 1 of valley system evolution began with fluvial incision in response to falling relative sea level. During decreasing accommodation fluvial downcutting may have developed 1) as a knickpoint occurring at some significant slope break such as a previous regressive shoreline or the shelf break from which point incision propagated landward, or 2) via entrenchment in response to tectonic tilting or uplift of the alluvial plain at rates equal to or less than the rate at which the fluvial system could cut down in response (Posamentier, 2001). The former mode of incision establishes a buttress valley (*sensu* Holbrook and Bhattacharya, 2012) and produces a time-transgressive incision surface along the longitudinal valley profile, and the latter mode occurs simultaneously along the longitudinal valley profile. The strike-section available to this study does not allow for distinction between these two potential modes of incision. Regardless of the temporal development of the basal incision surface and sequence boundary along the longitudinal profile of the system, the strike-section profile records a time-transgressive basal incision surface. At any one cross-sectional position along the valley profile valley formation occurred by fluvial incision via one or more individual fluvial bodies. Based on the dimensional relationship between incised valley and the associated component channel(s) outlined above, valley downcutting can only occur over some part of the entire strike-section valley profile at any given point in time.

During decreasing relative sea level standard fluvial geomorphic processes such as channel meandering, flood plain deposition, channel cutoffs generating oxbows, and system-wide avulsions continue to occur. Recent studies have shown that during falling stage and lowstand, fluvial downcutting is expected to occur throughout the valley profile via diachronous channel migration, reworking of previous channel deposits, and channel avulsions (Strong and

Paola, 2008; Blum and Garvin, 2009; Martin et al., 2011; Holbrook and Bhattacharya, 2012). Fluvial incision may occur via one or multiple channels during falling stage before establishing a final valley thalweg during lowstand, potentially producing one or more ‘failed valleys’ during falling stage (Hofmann et al., 2009). Sediment deposited during falling stage and lowstand is expected to exist within the valley system on abandoned terraces, ‘failed valleys’, and floodplains of active fluvial channels concurrent with fluvial downcutting producing a ‘cut and cover’ valley evolution (sensu Holbrook and Bhattacharya, 2012). The Phipps Park location is interpreted to represent such falling stage fluvial deposits. Overlying the deep incision at Phipps Park defined by the SB are sand-dominated lateral accretion sets (~7 m thick) terminating at a mud- and sand-filled abandoned channel (Figure 16 A). These deposits may have been preserved by any of the potential processes previously discussed during fluvial downcutting (e.g., avulsion, abandoned terrace, ‘failed valley’).

The 88<sup>th</sup> Street location records the deepest incision for this incised valley system. As such it records the position of the active trunk channel and valley thalweg during lowstand (Figure 16B). The lowstand deposits recorded at the 88<sup>th</sup> Street location are characterized by sand-rich fluvial lateral accretion sets and low angle laminated and thinly bedded sands at the basal incision surface.

#### *Phase 2: Late lowstand – early transgression*

The transition to increasing accommodation during early transgression is marked by a significant change to mud-dominated valley deposits at the 88<sup>th</sup> Street location (Figure 16C). This sharp transition and thick fluvial mud-dominated package may record 1) backstepping of

the system, placing the longitudinal position of the study area within at least seasonal range of the turbidity maximum, 2) system-wide changes in sediment supply, or 3) some combination of both.

Mesotidal (2 to 4 m) to macrotidal (>4 m) conditions can occur even in wave-dominated coastal settings due to hypersynchronicity as a function of coastal morphology (Short, 1991; Dalrymple and Choi, 2006). Development of an embayment during valley evolution further basinward could produce hypersynchronous conditions causing an increase in tidal energy for some distance upstream (Dalrymple and Choi, 2006). The dominantly fine grain size found within the central study area (silt and mud) would be expected to be replaced by coarser sediment deposition both landward (fluvially dominated) and basinward (more significantly tidally influenced) of the study area. The thin sandstone accretionary surfaces within the mud-dominated fill would likely indicate changes in fluvial discharge such as seasonal or episodic floods, shifting deposition of coarser sediment longitudinally basinward into the study area. Recent studies integrating climate models, isotope records, sedimentology, and taphonomy assert monsoonal precipitation patterns within the Campanian Western interior (Fricke et al., 2010; Foreman et al., 2011). Seasonal monsoons would suggest significant longitudinal mobility of the turbidity maximum and the nature of sediment deposited in response to significant increases in fluvial discharge (Geyer, 1993; Wolanski et al., 1995; Staub et al., 2000; Phillips and Slattery, 2006; Wu, 2012). Such sedimentary patterns and fluvial architectures are observed at the 88<sup>th</sup> Street location.

In the case of changes in sediment supply, the 88<sup>th</sup> Street location would record deficient sediment influx from fluvial discharge, producing an underfilled valley. Deficiency in sediment influx can be the result of decreased sediment supply and/or decreased stream power (Blum and

Tornqvist, 2000). The result is aggradation and storage of coarser sediment further landward along the longitudinal profile than the strike-section preserved in the study area. Deposition would be restricted to the 88<sup>th</sup> Street location established during the final stage of fluvial downcutting and dominated by suspension settle-out of fine grained sediment. Deposition of sand-dominated lateral accretion sets would be interpreted to record seasonal increases in stream power and/or sediment supply (i.e. floods), which is consistent with annual or lower frequency monsoonal precipitation flood events (Fricke et al., 2010; Foreman et al., 2011). The underfilled nature of the valley would produce laterally variable sedimentary scenarios within the incised valley system, with active fine-grained deposition in the ‘sediment-starved’ 88<sup>th</sup> Street location concurrent with continued sediment storage and potential subaerial exposure of falling stage deposits such as ‘failed valleys’ and abandoned terraces. The Phipps Park FA2 sediments are an example of preserved falling stage sediment during underfilled deposition at 88<sup>th</sup> Street.

### *Phase 3: Late transgression*

Phase 3 of valley evolution marks a notable shift to increased tidal influence. The base of Phase 3 is defined by the trasgressive surface of tidal-fluvial erosion (TSE), which is laterally traceable throughout the study area and observed to truncate both fluvial deposits in the center of the study area and shoreface deposits near the margin of the study area. The erosional nature and lateral extent of the TSE indicates a distinct shift in the relationship between accommodation and sediment supply due to a significant deceleration in the rate of relative sea level rise. The result is a complex valley architecture defined by nested erosional surfaces in the valley center which

extend laterally and amalgamate into a diachronous composite sequence boundary and basal incision surface along the valley margins (Figure 16D).

Recent experimental work focusing on shoreline migration, fluvial incision and development of incised valleys, and sequence stratigraphic architectures (Strong and Paola, 2008; Hofmann et al., 2009; Martin et al. 2009 a, b, 2011) has documented complex stratigraphic architectures as a function of time-transgressive system evolution. These studies demonstrate diachrony in valley formation dominated by downcutting during rapidly decreasing relative sea level, represented here by the SB, and shifting to increased valley widening during decelerating relative sea level fall and during relative sea level rise, represented here by the TSE. Depositional widening during transgression modifies the original incision surface established during downcutting and does so at increasing lateral positions within the valley over the course of transgression (Strong and Paola, 2008). The well preserved single and vertically stacked channel deposits observed on the southwestern margin of the study area at the Horse Butte location are interpreted as increasingly well preserved tidal-fluvial channels occurring later in valley evolution along the valley margin. Channel migration during valley widening erodes and reworks previously deposited regressive as well as previous lowstand and early transgressive deposits. The preservation of fluvial deposits formed during downcutting at the Phipps Park location (FA2) is a function of the initially rapid increase in accommodation before valley widening and tidal-fluvial channel erosion extended outward from the central lowstand position at the 88<sup>th</sup> Street location. These processes may be further complicated by higher frequency fluctuations in the rate of relative sea level rise.

Recent outcrop (Corbett, et al., 2011; Kieft et al., 2011 Li et al., 2010) and subsurface (Nordfjord et al., 2006; Darmadi et al., 2007; Lee et al., 2005, 2007; Maynard et al., 2010)

studies have documented similar complex stratigraphic architectures and composite sequence boundaries. Architectures documented in outcrop have expanded from the simple cut and fill model to include : 1) complex valley with nested basal surfaces occurring within a single valley boundary, 2) compound valley with a composite basal incision surface with one or more boundaries of regional significance, 3) compound-complex valley with a composite sequence boundary having one or more boundaries of regional significance and internal nested surfaces confined within the valley, 4) multivalley complex with multilateral and amalgamated surfaces overlying a regional erosive surface, and 5) stacked multivalley complex with vertically amalgamated multivalleys showing no intervening marine deposition (Dalrymple et al., 1994; Holbrook, 2001; Zaitlin et al., 1994, Li et al., 2010). Interpretation of valley widening in response to decelerating increase in accommodation for the middle member of the Eagle Formation, producing a composite basal incision surface reflects the time-transgressive nature of valley evolution asserted in these experimental, outcrop, and subsurface findings.

Further support for deceleration in the rate of relative sea level rise may be drawn from the development of coal across the majority of the valley fill package and its lateral thickness variation. Coal formation occurs under a specific set of environmental circumstances wherein the generation of accommodation space generally matches the rate of accumulation of organic matter and production of peat (Staub, 2002; Davies et al., 2005; Diessel et al., 2006). Key factors involved in producing peat deposits typically include a static or rising water table associated with local or regional subsidence, regional precipitation and climate, and the autocompaction of peat (Davies et al., 2005). Conditions where generation of accommodation matches peat production typically produce planar mires which reflect surface topography. Under conditions of sufficient water supply, where rainfall exceeds evapotranspiration, surface doming can occur producing a



raised mire which does not reflect surface topography and regional subsidence (Staub, 2002). In conditions where the rate of increase of accommodation significantly outpaces production of peat, the system is inundated (Davies et al., 2005, Diessel, 2006).

The development of coal at the top of the valley fill package indicates a sufficiently slow rate of increasing accommodation such that peat production generally matched or modestly exceeded that rate of increasing accommodation long enough to produce at least 45 cm of coal. Given the upward change from dull to bright banded coal in thick coal areas, the inverted thickness relationship between the coal and the immediately overlying facies 7 (marginal marine bay fill), the assertion of annual monsoonal precipitation pattern (Fricke et al., 2010; Foreman et al., 2011) and general greenhouse conditions of the Late Cretaceous (Miller et al., 2003, 2005), it is proposed that coal accumulation occurred in slightly raised mires on the interfluvies between the last active tidal-fluvial channels.

The thickness of coal can be used as a relative proxy for channel activity or active floodplain deposition, with little or no coal located next to the most recently active channels and thickest coal representing the most time since last channel activity. The largest area of little or no coal is observed at the Phipps Park location, which is interpreted to represent one of the last active channel locations within the valley system (Figure 16D). This interpretation is further supported by the thickness profile of the overlying bay fill package, which onlaps the thickest coal deposits and has a generally inverted thickness profile.

The thickest bay fill deposits occurring at the Phipps Park area are interpreted to reflect the most available accommodation due to its unfilled nature as a function of recent channel activity. Inundation of the topographic low at Phipps Park is consistent with the onlap

relationship with adjacent coal. The sand-filled nature of burrows into the top of the coal also indicates rapid inundation of the valley system, filling subaerial burrows in the peat with sand. Continued drowning of the system is recorded by the transition from the bay fill deposits to the overlying fully marine shoreface deposits (Facies 2 of FA4) (Figure 16E).

The final inundation of the valley is marked by the marginal-marine bay fill deposit (Facies 7 of FA4) overlying the terrestrial carbonaceous mudstone and coal (Facies 6 of FA3). The sand filled burrows at the top of the coal are a significant feature of this transition in depositional setting. The sand-filling of burrows in the coal is interpreted to represent rapid flooding and drowning of the coastal swamp indicating an abrupt increase in the rate of relative sea level rise.

### **Implications for valley evolution**

The relative sea level curve derived from the 3-phase valley evolution outlined above and the stratal relationships on which the interpreted valley evolution is based imply significant regional changes in the interplay between some combination of accommodation, sediment supply, stream power, and tidal influence. Driver(s) for the depositional changes during valley evolution observed in the middle member of the Eagle Formation are expected to be a combination of autogenic factors such as changes in coastal morphology that necessarily occur during downcutting, lateral widening, and infilling of an incised valley, and allogenic factors such as changes in climate and/or tectonics throughout valley evolution. Since changes in coastal and valley morphology are inherently a part of valley evolution, fluctuations in the rate of relative sea level rise are interpreted to be dominated by allogenic processes.

Changes in climate during valley evolution can have important implications for fluvial discharge, erosion rates and sediment supply, and longitudinal shifts in erosion and deposition (Blum and Aslan, 2006). The existence of a monsoonal precipitation pattern suggested for the Campanian KWIS is consistent with subordinate low-angle sand beds in mud-dominated channel fill at 88<sup>th</sup> Street under both the turbidity maximum and sediment supply scenarios offered for Phase 2 of valley evolution. Similarly, seasonal variations in discharge and/or sediment supply could be sufficient to produce the heterogeneity observed in FA3 during Phase 3 which is characterized by mud and carbonaceous drapes and laminae. More likely, however, would be the case of seasonal modification of tidal influence, shifting tidal range from mesotidal to microtidal during seasonally high discharge associated with monsoonal precipitation patterns for example. Coal development during Phase 3 may also be consistent with monsoon precipitation patterns, however, coal development can also occur as a function of maritime climate and increased precipitation with sufficient proximity to the shoreline. The combination of tidal indicators such as mud drapes and flow reversals and coal development would indicate a paleogeographical position of only 10's of kilometers inland from the transgressing shoreline. As with the scenarios of turbidity maximum and underfilled valley deposition suggested for Phase 2, monsoonal precipitation patterns and higher precipitation as a function of coastal climate are not mutually exclusive.

Changes in climate during infilling of the incised valley (Phase 2 and 3), whether in the form of seasonal (monsoonal) floods, maritime climate, or some other factor could vary fluvial discharge and sediment supply to effectively match the rate of accommodation generation. The expected result would be aggradation and laterally migrating fluvial and/or tidal-fluvial channels. Lateral migration of channels would form the transgressive surface of tidal-fluvial erosion and

laterally the valley margins through continued channel processes. Coal development (i.e. peat mires) during later stages of slowed accommodation generation and proximity to shoreline would effectively limit continued channel migration. The coal distribution in the study area would support such an interpretation, with the Phipps Park location representing the last active channel flanked by thick and potentially raised peat mires.

Tectonic influence can also have important implications for changes in depositional regime throughout valley evolution. As previously noted, the strike-section available in the study area is insufficient to distinguish between knickpoint and eustatically driven change in relative sea level, and entrenchment and tectonically driven change in relative sea level. Tectonic tilting of the alluvial plain during valley infilling could produce increased erosion rates and stream power resulting in higher sediment supply. The result would be expected to be a shift from incision to aggradation as previously discussed under climatically driven increase in sediment supply. A potential driver for tilting or full uplift of the alluvial plain could be the occurrence and migration of the forebulge within the Campanian foreland basin. The forebulge within the Late Cretaceous foreland basin is projected to occur ~200 to over 300 km east of the Orogenic front, with a maximum crest age of 88.8 ma along the Montana/Wyoming border (Currie et al., 2002). While not temporally coincident with the maximum projected forebulge crest, the Eagle Formation was deposited approximately 300 km east of the orogenic front (Payenberg et al., 2002). The time-transgressive nature of forebulge migration to the north along the foreland basin axis and regionally coincident location with Eagle deposition may have sufficiently influenced the rate of increasing accommodation to facilitate development of the TSE during valley widening and coal development. As with most geologic end-member scenarios, valley evolution

during the middle member of the Eagle Formation in south-central Montana probably records a combination of both climatic and tectonic influence.

## **IMPLICATIONS FOR RESERVOIR DEVELOPMENT**

Channel and incised valley fill deposits are of significant interest due to their ability to host large quantities of water and hydrocarbons within their successions (Van Wagoner et al., 1990; Zaitlin and Shultz, 1990). The geometries established during incision essentially function as ‘containers’ for three-dimensional depositional packages of variable continuity and heterogeneity (Dalrymple et al., 1994; Ardies et al., 2002; Dalrymple and Choi, 2006). Prolific Cretaceous incised valley reservoirs with reserves in excess of 50 million barrels of oil equivalent (Mmboe) include the Athabasca Oil Sands of Western Canada (66500 Mmboe), Messla-Faregh field of the Sirte Basin, Libya (1500 Mmboe), Cut Bank field of the Western Canada Sedimentary Basin and Montana (199 Mmboe), Highlight field of the Powder River Basin, Wyoming (108 Mmboe), Churches Buttes field of the Green River Basin, Wyoming (77 Mmboe), South Glenrock field of the Powder River Basin, Wyoming (75 Mmboe), Adena field of the Denver Basin, Colorado (60 Mmboe), and Clareton field of the Powder River Basin, Wyoming (60 Mmboe) (Boyd et al., 2006). A number of gas and oil plays in northern Montana and southern Alberta currently in production are also thought to occur in fluvial and incised valley fill deposits (Ardies et al., 2002; McCrimmon and Arnott, 2002.)

Late Cretaceous strata within the Western Interior Seaway also host significant reserves of natural gas. Active fields producing gas from the Eagle Formation within Montana include the Tiger Ridge field in north-central Montana, Eagle-equivalent units on the Cedar Creek anticline,

the Pumpkin Creek field, and the Liscom Creek field in southeastern Montana (Shurr and Ridgley, 2002). These reservoirs have estimated porosities of up to 25% and effective permeability up to 150 md (Bayliff, 1975). Estimates of the biogenic gas reserves in Cretaceous strata within Montana range from 10 to 41 trillion cubic feet (tcf), with over 880 bcf recovered (McCrimmon and Arnott, 2002; Rice and Spencer, 1996; Shurr and Ridgley, 2002). The Eagle-equivalent Milk River Formation occurring along depositional strike in Alberta and Saskatchewan is estimated to host 15 tcf of biogenic gas (Rice and Claypool, 1981; Fishman et al., 2001). Despite proven production to the north, the reservoir potential of the Eagle Formation in south-central Montana occurring along depositional strike is still poorly understood. No incision fill deposits have been previously identified or regionally mapped in the Eagle Formation of south-central Montana prior to this study.

The stratigraphic architectures and fill profile of the incised valley system observed in the middle member of the Eagle Formation in south-central Montana have important implications for regional subsurface prediction and general sequence stratigraphic interpretation. This study demonstrates significant vertical and lateral variability in stratigraphic architectures and sediment heterogeneity as a function of fluctuating rates of relative sea level rise and the diachronous nature of valley evolution. These complex valley stacking patterns necessitate continued study of reservoir analogs in outcrop in order to improve the prediction of location, connectivity, and continuity of potentially viable reservoir packages within incised valleys.

Existing incised valley models (e.g. Dalrymple and Choi, 2006) predict a basic stratal stacking pattern of sand-dominated fluvial deposits at the base of the incised valley and decreasing net-to-gross sand content vertically and laterally due to increasing tidal influence and lateral transition to mud flat and salt marsh deposits on the valley interflaves. Traditional

exploration models have thus primarily targeted central valley deposits. Results from recent outcrop analog studies (Yoshida et al, 2007; Sixsmith et al., 2008; this study) have documented complex lateral variations in stratigraphic architectures and facies distributions that motivate continued and detailed study of these systems. This study demonstrates that preserved valley architectures and the valley morphology develop in response to variations in accommodation generation. Central valley deposits were far more heterogeneous and mud-dominated than would generally be predicted. Valley widening and fluctuations in accommodation and/or the rate of change in accommodation produced more sand-rich tidal-fluvial deposits than would be predicted. Sand-dominated tidal-fluvial channel deposits with a more 'traditional' stratal stacking pattern occurred at a predictable lateral offset from the valley center of ~5 km. Implications from this and related studies are that incised valley systems are sensitive to the rate of increasing accommodation, the interplay between accommodation and sediment supply, and changes in valley and coastal morphology through the course of valley evolution. High resolution control on the longitudinal and lateral relationship between temporally distinct surfaces may prove instrumental in correctly identifying stratal stacking patterns within the incised valley, as these surfaces may amalgamate to form complex architectures at reservoir scale (100's of m to 10's of km). This study offers one such example, wherein the optimal reservoir potential exists near the valley edges flanking a mud-dominated valley center.

## **CONCLUSION**

The informal middle member of the Eagle Formation in south-central Montana is interpreted as an incised valley system. The valley fill succession records a three-phase valley

evolution: 1) fluvial downcutting in response to decreasing accommodation, 2) rapid increase in accommodation and development of a mud-dominated valley center, and 3) deceleration in the rate of relative sea level rise allowing valley widening, sand-dominated tidal-fluvial channel deposition, and peat development. The transgressive surface of tidal-fluvial erosion generated during valley widening extends laterally beyond the limits of a fluvially incised sequence boundary to produce a composite basal incision surface and composite sequence boundary. Stratigraphic architectures of the incised valley and its component channel forms satisfy the stratigraphic definition of an incised valley in that 1) the basal incision surface is a (composite) sequence boundary, 2) the subsequent fill deposits indicate a disconformable basinward shift in facies, juxtaposing fluvial deposits on top of middle and upper shoreface deposits, 3) the incised valley is composed of vertically and laterally stacked multi-story channels, and 4) the width (W) to thickness (T) ratio (W/T) of the incised valley ( $W/T = \sim 1000$ ) is an order of magnitude greater than the component channel forms within the system ( $W/T = \sim 15$ ). Key findings are as follows:

- Incision during falling stage includes time-transgressive channel migration and storage of channel deposits concurrent with fluvial downcutting. Strata deposited during valley incision are locally preserved as lateral accretion sets and abandoned channel deposits.
- Lowstand to early transgressive deposits are characterized by mud-dominated fluvial deposits in the valley center.
- Deceleration in the rate of relative sea level rise changed the relationship between accommodation space and sediment influx. As a result valley fill shifted to tidally influenced fluvial deposits, which generated a regionally extensive erosional surface and widened the valley profile.



- The erosional surface generated during transgression and valley widening extends laterally beyond the limits of the lower sequence boundary and defines a diachronous, composite sequence boundary and basal incision surface.
- The multi-phase valley evolution produced a valley fill profile with a mud-rich valley center flanked by more traditionally stacked, sand-rich fluvial and tidally influenced fluvial deposits toward the outer valley.

## REFERENCES

- Allen, G.P., and Posamentier, H.W., 1993, Sequence stratigraphy and facies model of an incised valley fill: the Gironde Estuary, France. *Journal of Sedimentary Petrology*, v. 63, p. 378-391.
- Ardies, G.W., Dalrymple, R.W., and Zaitlin, B.A., 2002, Controls on the geometry of incised valleys in the Basal Quartz unit (Lower Cretaceous), western Canada sedimentary basin. *Journal of Sedimentary Research*, v. 72, p. 602-618.
- Bayliff, W.H., 1975, Performance review of Tiger Ridge and Bullock gas units. In: *Energy resources of Montana: Montana Geological Society 22<sup>nd</sup> Annual Publication*, p. 31-37.
- Blum, M.D., and Tornqvist, T.E., 2000, Fluvial responses to climate and sea-level change: a review and look forward. *Sedimentology* v. 47 (suppl. 1) p. 2-48.
- Blum, M.D., and Aslan, A., 2006, Signatures of climate vs. sea-level change within incised valley-fill successions: Quaternary examples from the Texas Gulf Coast. *Sedimentary Geology*, v. 190, p. 177-211.
- Blum, M.D., and Garvin, M., 2009, Role of incised valley systems in source-to-sink sediment routing and storage: examples from the late Quaternary northern Gulf of Mexico margin. *AAPG Search and Discovery Article #50248*.
- Boyd, R., Dalrymple, R.W., and Zaitlin, B.A., 2006, Estuarine and Incised-Valley Facies Models. *SEPM Special Publication No. 84*, p. 171-235
- Bromley, R.G., and Frey, R.W., 1974, Redescription of the trace fossil *Gyrolithes* and taxonomic evaluation of *Thalassinoides*, *Ophiomorpha* and *Spongeliomorpha*. *Bulletin of the Geological Society of Denmark*, v. 23, p. 311-335.

- Buatois, L.A., et al., 2005, Colonization of brackish-water systems through time: Evidence from the trace-fossil record. *Palaios* v. 20, p. 321-347.
- Burchard, H., and Baumert, H., 1998, The formation of estuarine turbidity maxima due to density effects in the salt wedge. A hydrodynamic process study. *Journal of Physical Oceanography*, v. 28, p. 309-321.
- Catuneanu, O., Sweet, A. R., and Miall, A. D., 2000, Reciprocal stratigraphy of the Campanian-Paleocene Western Interior of North America. *Sedimentary Geology*, v. 134, p. 235-255.
- Catuneanu, O., et al., 2009, Towards the standardization of sequence stratigraphy. *Earth Science Reviews* v. 92, p 1-33.
- Clifton, H.E., Hunter, R.E., and Phillips, R.L., 1971, Depositional structures and processes in the non-barred high-energy nearshore. *Journal of Sedimentary Petrology*, v. 41, no. 3, p. 651-670.
- Corbett, M.J., Fielding, C.R., and Birgenheier, L.P., 2011, Stratigraphy of a Cretaceous coastal-plain fluvial succession: the Campanian Masuk Formation, Henry Mountains Syncline, Utah, USA. *Journal of Sedimentary Research*, v. 81, p. 80-96.
- Currie, B.S., 1997, Sequence Stratigraphy of nonmarine Jurassic-Cretaceous rocks, central Cordilleran foreland-basin system. *GSA Bulletin*, v. 109, no. 9, p. 1206-1222.
- Currie, B.S., 2002, Structural configuration of the Early Cretaceous Cordilleran foreland-basin system and Sevier thrust belt, Utah and Colorado. *The Journal of Geology*, v. 110, p. 697-718.
- Dabrio, C.J., 1982, Sedimentary structures generated on the foreshore by migrating ridge and runnel systems on microtidal and mesotidal coasts of S. Spain. *Sedimentary Geology*, v. 32, p. 141-151.
- Dalrymple, R.W., Zaitlin, B.A., and Boyd, R., 1992, Estuarine facies models; conceptual basis and stratigraphic implications. *Journal of Sedimentary Research*, v. 62, pg. 1130-1146.
- Dalrymple, R.W., and Zaitlin, B.A., 1994, High-Resolution sequence stratigraphy of a complex, incised valley succession, Bobequid Bay-Salmon River estuary, Bay of Fundy, Canada. *Sedimentology*, v. 41, p. 1069-1091.
- Dalrymple, R.W., and Choi, K., 2006, Morphologic and facies trends through the fluvial-marine transition in tide-dominated depositional systems: A schematic framework for environmental and sequence-stratigraphic interpretation. *Earth-Science Reviews*, v. 81, p. 135-174.

- Darmadi, Y., Willis, B.J., and Dorobek, S.L., 2007, Three-Dimensional seismic architecture of fluvial sequences on the low-gradient Sunda shelf, offshore Indonesia. *Journal of Sedimentary Research*, v. 77, p. 225-238.
- Davies, R. Howell, J., Boyd, R., Flint, S., and Diessel, C., 2005, High resolution sequence-stratigraphic correlation between shallow-marine and terrestrial strata: Examples from the Sunnyside member of the Cretaceous Blackhawk Formation, Book Cliffs, eastern Utah. *AAPG Bulletin*, v. 90, no. 7, p. 1121-1140.
- Davis, R.A., and Hayes, M.O., 1984, What is a wave-dominated coast? *Marine Geology*, v. 60, p. 313-329.
- DeCelles, P.G., and Currie, B.S., 1996, Long-Term sediment accumulation in the Middle Jurassic-early Eocene Cordilleran retroarc foreland-basin system. *Geology*, v. 24, no. 7, p. 591-594.
- DeCelles, P.G., 2004, Late Jurassic to Eocene evolution of the Cordilleran thrust belt and foreland basin system, western USA. *American Journal of Science*, v. 304, p. 105-168.
- Diessel, C., Boyd, R., Wadsworth, J., Leckie, D., and Chalmers, G., 2000, On balanced and unbalanced accommodation/peat accumulation ratios in the Cretaceous coals from Gates Formation, Western Canada, and their sequence-stratigraphic significance. *International Journal of Coal Geology*, v. 43, p. 143-186.
- Diessel, C.F.K., 2006, Utility of coal petrology for sequence-stratigraphic analysis. *International Journal of Coal Petrology*, v. 70, p. 3-34.
- Dott, R.H.Jr., 1982 (a), 1982 SEPM presidential address: episodic sedimentation – how normal is average? How rare is rare? Does it matter? *Journal of Sedimentary Petrology*, v. 53, no. 1, p. 0005-0023.
- Dott, R.H. Jr., Bourgeois, J., 1982 (b), Hummocky stratification: significance of its variable bedding sequences. *GSA Bulletin*, v.93, p. 663-680.
- Dumas, S., Arnott, R.W.C., Southard, J.B., 2005, Experiments on oscillatory-flow and combined-flow bed forms: implications for interpreting parts of the shallow-marine sedimentary record. *Journal of Sedimentary Research*, v. 75, no. 3, p. 501-513.
- Eberth, D.A., 1996, Origin and significance of mud-filled incised valleys (Upper Cretaceous) in southern Alberta, Canada. *Sedimentology*, v. 43, p. 459-477.
- Falcon-Lang, H.J., 2003, Growth interruptions in silicified conifer woods from the Upper Cretaceous Two Medicine Formation, Montana, USA: implications for palaeoclimate and dinosaur palaeoecology. *Palaeogeography, Palaeoclimatology, Palaeoecology*, v. 199, p. 299-314.

- Fishman, N.S., Ridgley, J.L., and Hall, D.L., 2001, Timing of gas generation in the Cretaceous Milk River Formation, southeastern Alberta and southwestern Saskatchewan – Evidence from authigenic carbonates. In: Summary of Investigations 2001, Saskatchewan Geological Survey, v. 1, p. 125-136
- Foreman, B.Z., Fricke, H.C., Lohmann, K.C., and Rogers, R.R., 2011, Reconstructing paleocatchments by integrating stable isotope records, sedimentology, and taphonomy: A Late Cretaceous case study (Montana, United States). *PALAIOS*, v. 26, p. 545-554.
- Frey, R.W., Howard, J.D., and Pryor, W.A., 1978, Ophiomorpha: its morphologic, taxonomic, and environmental significance. *Palaeogeography, Palaeoclimatology, Palaeoecology*, v. 23, p. 199-229.
- Frey, R.W., and Howard, J.D., 1990, Trace fossils and depositional sequences in a clastic shelf setting, Upper Cretaceous of Utah. *Journal of Paleontology*, v. 64, p. 803-820.
- Fricke, H.C., Foreman, B.Z., and Sewall, J.O., 2010, Integrated climate model-oxygen isotope evidence for a North American monsoon during the Late Cretaceous. *Earth and Planetary Science Letters*, v. 289, p. 11-21.
- Fustic, M., et al., 2012, Recognition of down-valley translation in tidally influenced meandering fluvial deposits, Athabasca Oil Sands (Cretaceous), Alberta, Canada. *Marine and Petroleum Geology*, v. 29, p. 219-232.
- Gibling, M.R., 2006, Width and thickness of fluvial channel bodies and valley fills in the geological record: a literature compilation and classification. *Journal of Sedimentary Research*, v. 76, p. 731-770.
- Gingras, M.K., MacEachern, J.A., and Dashtgard, S.E., 2011, The potential of trace fossils as tidal indicators in bays and estuaries. *Sedimentary Geology*, doi: 10.1016/j.sedgeo.2011.05.007 (in press).
- Geyer, W.R., 1993, The importance of suppression of turbulence by stratification on the estuarine turbidity maximum. *Estuaries*, v. 16, no. 1, p. 113-125.
- Hampson, G.J., 2000, Discontinuity surfaces, clinoforms, and facies architecture in a wave-dominated shoreface-shelf parasequence. *Journal of Sedimentary Research*, c. 70, no. 2, p. 325-340.
- Hampson, G.J., and Storms, J.E.A., 2003, Geomorphological and sequence stratigraphic variability in wave-dominated, shoreface-shelf parasequences. *Sedimentology*, v. 50, p. 667-701.

- Hanson, M.S., and Little, L.D., 1989, Origins, stacking configurations, and facies distributions of genetic sequences, Eagle Sandstone, Billings, Montana. Montana Geological Society Field Conference, v. 1989, p. 141-150.
- Hauer, J., Oswald, O., Hendrix, M.S., Staub, J.R., 2009, An upper Cretaceous coal in the Eagle Formation of south-central Montana as an indicator for rapid transgression. Geological Society of America, Abstracts with Programs, v. 41, no. 7, p. A-551.
- Hauer, J., Oswald, O., Hendrix, M.S., Staub, J.R., and Jarvis, D.E., 2010, Evidence for forced regression in the Santonian-Campanian Eagle Formation in south-central Montana. AAPG International Conference and Exhibition Abstracts Volume CD-ROM, 815874.
- Helland-Hansen, W., and Martinsen, O.J., 1996, Shoreline trajectories and sequences: description of variable depositional-dip scenarios. Journal of Sedimentary Research, v. 66, no. 4, p. 670-688.
- Hofmann, M.H., Shultz, A., Suter, J.R., Hill, C., and Paola, C., 2009, Comparing allo- and autogenic depositional elements and key surfaces in the stratigraphic record – Results from two identical delta tank experiments. American Geophysical Union, abstract #EP52A-02.
- Holbrook, J., 2001, Origin, genetic interrelationships, and stratigraphy over the continuum of fluvial channel-form bounding surfaces: an illustration from middle Cretaceous strata, southeastern Colorado. Sedimentary Geology, v. 144, p. 179-222.
- Holbrook, J.M., and Bhattacharya, J.P., 2012, Reappraisal of the sequence boundary in time and space: case and considerations for an SU (subaerial unconformity) that is not sediment bypass surface, a time barrier, or an unconformity. Earth-Science Reviews, v. 113, p. 271-302.
- Hovikoski, J., Rasanen, M., Gingras, M., Ranzi, A., and Melo, J., 2008, Tidal and seasonal controls in the formation of Late Miocene inclined heterolithic stratification deposits, western Amazonian foreland basin. Sedimentology, v. 55, p. 499-530.
- Howard, J.D., and Frey, R.W., 1984, Characteristic trace fossils in nearshore to offshore sequences, upper Cretaceous of east-central Utah. Canadian Journal of Earth Science, v. 21, p. 200-219
- Hunt, D., and Tucker, M.E., 1992, Stranded parasequences and the forced regressive wedge systems tract: deposition during base-level fall. Sedimentary Geology, v. 81, p. 1-9.
- Kieft, R.L., Hampson, G.J., Jackson, C.A.L., and Larsen, E., 2011; Stratigraphic Architecture of a net-transgressive marginal- to shallow-marine succession: Upper Almond Formation, Rock Springs Uplift, Wyoming, USA., Journal of Sedimentary Research, v. 81, p. 513-533

- Krystinik, L.F., and Dejarnett, B.B., 1995, Lateral variability of sequence stratigraphic framework in the Campanian and early Maastrichtian of the Western Interior Seaway, in Van Wagoner, J.C., and Betram, G.T., eds., Sequence stratigraphy of foreland basin deposits: outcrop and subsurface examples from the Cretaceous of North America. AAPG, memoir 64, p. 11-26.
- Lee, K., et al., 2005, A ground-penetrating radar survey of a delta-front reservoir analog in the Wall Creek Member, Frontier Formation, Wyoming. AAPG Bulletin, v. 89, p. 1139—1155.
- Lee, K., et al., 2007, 3-D architecture and sequence stratigraphic evolution of a forced regressive top-truncated mixed-influenced delta, Cretaceous Wall Creek Sandstone, Wyoming, U.S.A. Journal of Sedimentary Research, v. 77, p. 303-323.
- Li, W., Bhattacharya, J.P., and Campbell, C., 2010, Temporal evolution of fluvial style in a compound incised-valley fill, Ferron “Notom Delta”, Henry Mountains region, Utah (U.S.A.). Journal of Sedimentary Research, v. 80, p. 529-549.
- Li, W., Bhattacharya, J., and Zhu, Y., 2011, Architecture of a forced regressive systems tract in the Turonian Ferron “Notom Delta”, southern Utah, USA. Marine and Petroleum Geology, v. 28, p. 1517-1529.
- Liu, L., Spasojevic, S., Gurnis, M., 2008, Reconstructing Farallon Plate subduction beneath North America back to the Late Cretaceous. Science, v. 232, no. 5903, p. 934-938.
- Liu, S., Nummedal, D., and Liu, L., 2011, Migration of dynamic subsidence across the Late Cretaceous United States Western Interior Basin in response to Farallon plate subduction. Geology, v. 39, no. 6, p. 555-558.
- MacEachern, J.A., Bann, K.L., Bhattacharya, J.P., and Howell, C.D.JR., 2005, Ichnology of deltas: organism responses to the dynamic interplay of rivers, waves, storms and tides *in* River deltas – concepts, models, and examples. SEPM Special Publication, no. 83.
- Martin, J., Paola, C., Abreu, C., Neal, J., and Sheets, B., 2009 (a), Sequence stratigraphy of experimental strata under known conditions of differential subsidence and variable base level. AAPG Bulletin, v. 93, no. 4, p. 503-533.
- Martin, J., Sheets, B., Paola, C., and Hoyal, D., 2009 (b), Influence of steady base-level rise on channel mobility, shoreline migration, and scaling properties of a cohesive experimental delta. Journal of Geophysical Research, v. 114, F03017.
- Martin, A.J., and Varricchio, D.J., 2010, Paleocological utility of insect trace fossils in dinosaur nesting sites of the Two Medicine Formation (Campanian), Choteau, Montana. Historical Biology, v. 23, no. 1, p. 15-25.

- Martin, J., Cantelli, A., Paola, C., Blum, M., and Wolinsky, M., 2011, Quantitative modeling of the evolution and geometry of incised valleys. *Journal of Sedimentary Research*, v. 81, p. 64-79.
- Martinsen, O.J. et al., 1999, Stratigraphic base level and fluvial architecture: Ericson Sandstone (Campanian), Rock Springs Uplift, SW Wyoming, USA. *Sedimentology*, v. 46, p. 235-259.
- Maynard, J. R., Feldman, H. R., and Alway, R., 2010, From bars to valleys: the sedimentology and seismic geomorphology of fluvial to estuarine incised-valley fills of the Grand Rapids Formation (Lower Cretaceous), Iron River Field, Alberta, Canada. *Journal of Sedimentary Research*, v. 80, p. 611-638.
- McCabe, P.J., and Jones, C.M., 1977, Formation of reactivation surfaces within superimposed deltas and bedforms. *Journal of Sedimentary Petrology*, v. 47, no. 2, p. 707-715.
- McCrimmon, G.G., and Arnott, R.W.C., 2002, The Clearwater Formation, Cold Lake, Alberta: a world class hydrocarbon reservoir hosted in a complex succession of tide-dominated deltaic deposits. *Bulletin of Canadian Petroleum Geology*, v. 50, p. 370-392.
- Miall, A.D., 2000, *Principles of Sedimentary Basin Analysis*. 3<sup>rd</sup>. Springer.
- Miller, K.G., et al., 2003, Late Cretaceous chronology of large, rapid sea-level changes: glacioeustasy during the greenhouse world. *Geology*, v. 31, p. 585-588.
- Miller, K.G., Wright, J.D, and Browning, J.V., 2005, Visions of ice sheets in a greenhouse world. *Marine Geology*, v. 217, p. 215-231. *Journal of Sedimentary Research*, v. 67, no. 6, p. 994-1000.
- Mitchell, S.B., 2012, Turbidity maxima in four macrotidal estuaries. *Ocean and Coastal management*, <http://dx.doi.org/10.1016/j.ocecoaman2012.05.030>.
- Muto, T., and Steel, R.J., 1997, Principles of regression and transgression: the nature of the interplay between accommodation and sediment supply.
- Nordfjord, S., Goff, J.A., Austin, J.A., and Gulick, S.P.S., 2006, Seismic facies of incised-valley fills, New Jersey continental shelf: implications for erosion and preservation processes acting during latest Pleistocene-Holocene transgression. *Journal of Sedimentary Research*, v. 76, p. 1284-1303.
- Pang, M., and Nummedal, D., 1995, Flexural subsidence and basement tectonics of the Cretaceous Western Interior basin, United States. *Geology*, v. 23, no. 2, p. 173-176.
- Pattison, S.A.J., 1995, Sequence stratigraphic significance of sharp-based lowstand shoreface deposits, Kenilworth member, Book Cliffs, Utah. *AAPG Bulletin*, v. 79, no. 3, p. 444-462.

- Payenberg, T.H.D., Braman, D.R., Davis, D.W., and Miall, A.D., 2002, Litho-and chronostratigraphic relationships of the Santonian-Campanian Milk River Formation in southern Alberta and Eagle Formation in Montana utilizing stratigraphy, U-Pb geochronology, and palynology. *Canadian Journal of Earth Science*, v. 39, p. 1553-1577.
- Payenberg, T.H.D., Braman, D.R., and Miall, A.D., 2003, Depositional environments and stratigraphic architecture of the Late Cretaceous Milk River and Eagle Formations, southern Alberta and north-central Montana: relationships to shallow biogenic gas. *Bulletin of Canadian Petroleum Geology*, v. 51, p. 155-176.
- Pemberton, S.G., and Frey, R.W., 1982, Trace fossil nomenclature and the *Planolites-Palaeophycus* dilemma. *Journal of Paleontology*, v. 56, no. 4, p. 843-881.
- Phillips, J.D., and Slattery, M.C., 2006, Sediment storage, sea level, and sediment delivery to the ocean by coastal plain rivers. *Progress in Physical Geography*, v. 30, p. 513-530.
- Plink-Bjorklund, P., 2005, Stacked fluvial and tide-dominated estuarine deposits in high-frequency (fourth-order) sequences of the Eocene Central Basin, Spitsbergen. *Sedimentology*, v. 52, p. 391-428.
- Plint, G.A., and Nummedal, D., 2000, The falling stage systems tract: recognition and importance in sequence stratigraphic analysis *in* Hunt, D., and Gawthorpe, R.L. (eds) *Sedimentary responses to forced regressions*. Geological Society of London, Special Publications v. 172, p. 1-17.
- Plint, G.A., and Kreitner, M.A., 2007, Extensive thin sequences spanning Cretaceous foredeep suggest high-frequency eustatic control: Late Cenomanian, Western Canada foreland basin. *Geology*, p. 735-738.
- Posamentier, H.W., and Morris, W.R., 2000, Aspects of the stratal architecture of forced regressive deposits *in* Hunt, D., and Gawthorpe, R.L. (eds) *Sedimentary responses to forced regressions*. Geological Society of London, Special Publications v., 172, p. 19-46.
- Posamentier, H.W., 2001, Lowstand alluvial bypass systems: incised vs. unincised. *AAPG Bulletin*, v. 85, p. 1771-1793.
- Rice, D.D., and Claypool, G.E., 1981, Generation, accumulation, and resource potential of biogenic gas. *American Association of Petroleum Geologists Bulletin*, b. 93, p. 1379-1401.
- Rice, D.D., and Spencer, C.W., 1996, Northern Great Plains shallow biogenic gas. In: 1995 National Assessment of United States Oil and Gas Resources – Results, Methodology, and Supporting Data. D.L. Gautier, G.L. Dolton, K.I. Takahashi and K.L. Varnes (eds.). U.S. Geological Survey Digital Data Series DDS-30. Release 2.



- Rodriguez, A.B., Fassell, M.L., and Anderson, J.B., 2001, Variations in shoreface progradation and ravinement along the Texas coast, Gulf of Mexico. *Sedimentology*, v. 48, p. 837-853.
- Rodriguez, A.B., Rodriguez, P.L., and Fegley, S.R., 2012, One-year along-beach variation in the maximum depth of erosion resulting from irregular shoreline morphology. *Marine Geology*, 291-294, p. 12-23.
- Rogers, R.R., 1994, Nature and origin of through-going discontinuities in nonmarine foreland basin strata, Upper Cretaceous, Montana: Implications for sequence analysis. *Geology*, v. 22, p. 1119-1122.
- Shanley, K.W., McCabe, P.J., and Hettinger, R.D., 1992, Tidal influence of Cretaceous fluvial strata from Utah, USA: a key to sequence stratigraphic interpretation. *Sedimentology*, v. 39, p. 905-930.
- Short, A.D., 1991, Macro-meso tidal beach morphodynamics: an overview. *Journal of Coastal Research*, v. 7, p. 417-436.
- Shurr, G.W., and Ridgley, J.L., 2002, Unconventional shallow biogenic gas systems. *AAPG Bulletin*, v. 86, p. 1939-1969.
- Sixsmith, P.J., et al., 2008, Facies architecture of a net transgressive sandstone reservoir analog: the Cretaceous Hosta Tongue, New Mexico. *AAPG Bulletin*, v. 92, no. 4, p. 513-547.
- Spila, M.V., Pemberton, S.G., and Sinclair, I.K., 2005, Comparison of marine and brackish/stressed ichnological signatures in the Ben Nevis and Avalon Formations, Jeanne d'Arc Basin. *Geological Association of Canada, Special Paper 43*, p. 73-94.
- Staub, J.R., 1991, Comparisons of central Appalachian Carboniferous coal beds by benches and a raised Holocene peat deposit. *International Journal of Coal Geology*, v. 18, p. 45-69.
- Staub, J.R., and Esterle, J.S., 1993, Peat-accumulating depositional systems of Sarawak, East Malaysia. *Sedimentary Geology*, v. 89, p. 91-106.
- Staub, J.R., Among, H.L., and Gastaldo, R.A., 2000, Seasonal sediment transport and deposition in the Rajang River delta, Sarawak, East Malaysia. *Sedimentary Geology*, v. 133, p. 249-264.
- Staub, J.R., 2002, Marine flooding events and coal bed sequence architecture in southern West Virginia. *International Journal of Coal Geology*, v. 49, p. 123-145.
- Staub, J.R., and Gastaldo, R.A., 2003, Late Quaternary sedimentation and peat development in the Rajang River Delta, Sarawak, East Malaysia *in* Sidi, F.H. et al., *Tropical deltas of southeast Asia – sedimentology, stratigraphy, and petroleum geology*. *SEPM Special Publication*, no. 76, p. 71-87.

- Strong, N., and Paola, C., 2008, Valleys that never were: time surfaces versus stratigraphic surfaces. *Journal of Sedimentary Research*, v. 78, p. 579-593.
- Thomas, R.G., et al., 1987, Inclined heterolithic stratification – terminology, description, interpretation and significance. *Sedimentary Geology*, v. 53, p. 123-179.
- Van Wagoner, J.C., Posamentier, H.W., Mitchum, R.W., Vail, P.R., Sarg, J.F., Loutit, T.S., and Hardenbol, J., 1988, An overview of the fundamentals of sequence stratigraphy and key definitions in Wilgus, C.K., Hastings, B.S., Kendall, C.G.St. C., Posamentier, H.W., Ross, C.A., and Van Wagoner, J.C. (eds), *Sea-level changes – An integrated approach*. SEPM Special Publication no. 42, p. 39-45.
- Van Wagoner, J.C., Mitchum, R.M., Campion, K.M., and Ramanian, V.D., 1990, Siliciclastic sequence stratigraphy in well logs, cores, and outcrops: concepts for high-resolution correlation of time and facies: American Association of Petroleum Geologists, *Methods in Exploration Series*, no. 7, 55 p.
- Wentworth, C.K., 1922, A scale of grade and class terms for clastic sediments. *The Journal of Geology*, v. 30, no. 5, p. 377-392.
- White, T., Furlong, K., and Arthur, M., 2002, Forebulge migration in the Cretaceous Western Interior basin of the central United States. *Basin Research*, v. 14, p. 43-54.
- Willis, B.J., 1997, Architecture of fluvial-dominated valley-fill deposits in the Cretaceous Fall River Formation. *Sedimentology*, v. 44, p. 737-757.
- Willis, B.J., Bhattacharya, J.P., Gabel, S.L., and White, C.D., 1999, Architecture of a tide-influenced river delta in the Frontier Formation of central Wyoming, USA. *Sedimentology*, v. 46, p. 667-688.
- Wolanski, E., King, B., and Galloway, D., 1995, Dynamics of the turbidity maximum in the Fly River Estuary, Papua New Guinea. *Estuarine, Coastal and Shelf Science*, v. 40, p. 321-337.
- Wu, J., Liu, J.T., and Wang, X., 2012, Sediment trapping of turbidity maxima in the Changjiang Estuary. *Marine Geology*, v. 303-306, p. 14-25.
- Yang, Y. T., and Miall, A. D., 2009, Evolution of the northern Cordilleran foreland basin during the middle Cretaceous: *Geological Society of America Bulletin*, v. 121, no. 3-4, p. 483-501.
- Yoshida, S., Steel, R.S., and Dalrymple, R.W., 2007, Changes in depositional processes – an ingredient in a new generation of sequence-stratigraphic models. *Journal of Sedimentary Research*, v. 77, p. 447-460.

Zaitlin, B.A. and Shultz, B.C., 1990, Wave-influenced estuarine sand body, Senlac heavy oil pool, Saskatchewan, Canada, in Barwis, J.H. McPherson, J.G., and Studlick, J.R.J., eds., *Sandstone Petroleum Reservoirs*: New York, Springer-Verlag, p. 363-387.

Zaitlin, B.A., Dalrymple, R.W., and Boyd, R., 1994, The stratigraphic organization of incised valley systems associated with relative sea level changes, *in* Dalrymple, R.W., Boyd, R., and Zaitlin, B.A., eds., *Incised-Valley Systems: Origin and Sedimentary Sequences*: SEPM, Special Publication, v. 51, p. 45-60.

## FIGURES AND TABLES

Examples of Criteria for Defining Stratigraphic Incised Valleys			
Lateral Extent	Vertical Profile	System Dimensions	Source
The basal erosion surface and correlative surfaces in extra-channel deposits can be traced widely, in some cases throughout the basin and between basins.	The scale of erosional relief on the basal surface is several times the depth of scour evident from component channel forms	The dimensions of the overall fluvial body are an order of magnitude larger than those of other channel forms in the system.	Gibling (2006)
An elongate, channel-shaped incision that can be correlated over a long distance	The base of the incision is a sequence boundary.	The sequence boundary can be correlated regionally on the interfluvial flooding surface/sequence boundary.	Maynard et al. (2010)
The basal incision surface and correlative surfaces are regionally mappable and define a sequence boundary.	Part of the incised valley fill is composed of multi-story channels.	The width (W) to thickness (T) ratio (W/T) of the valley is an order of magnitude greater than component channels.	This study

**Table 1.** Examples of criteria used to define stratigraphic incised valleys.

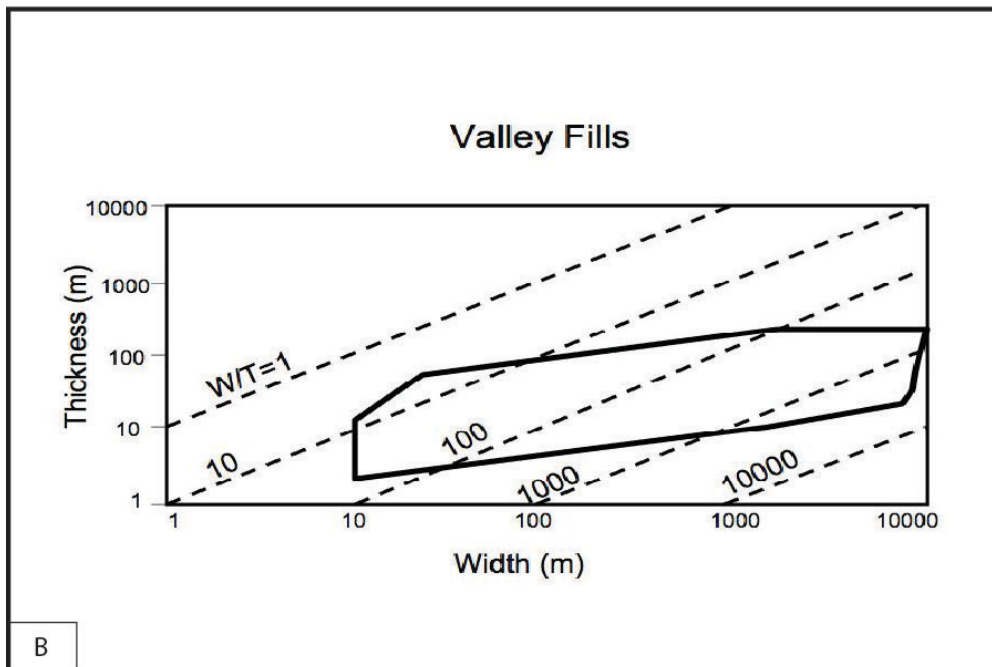
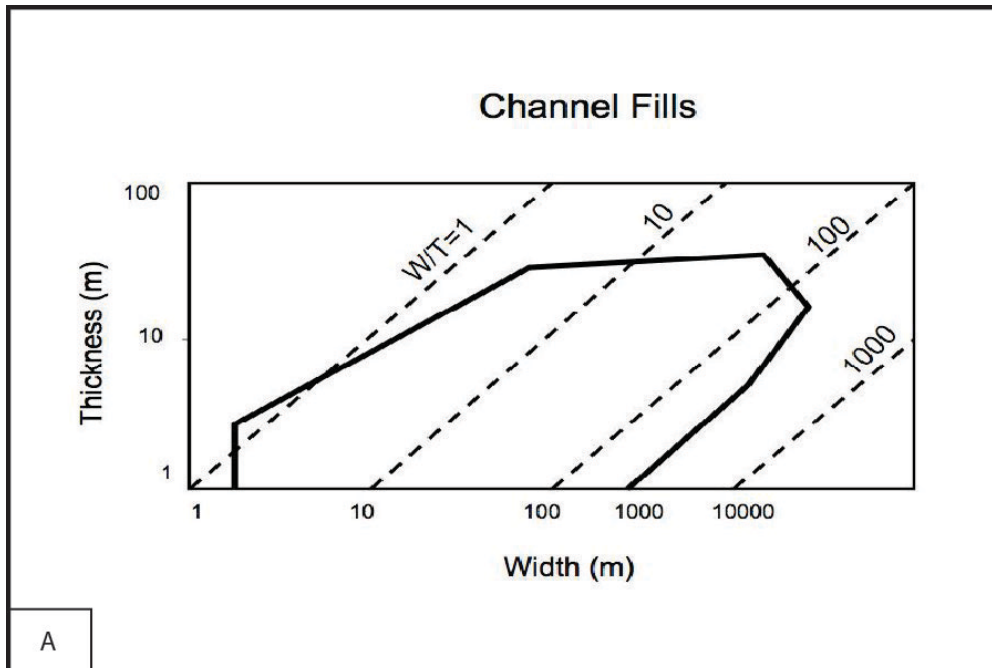


**Figure 1.** Width/Thickness ranges for: A) individual channel forms in meandering and fixed river systems, and B) stratigraphic incised valleys occurring in alluvial and marine strata (modified from Gibling, 2006).

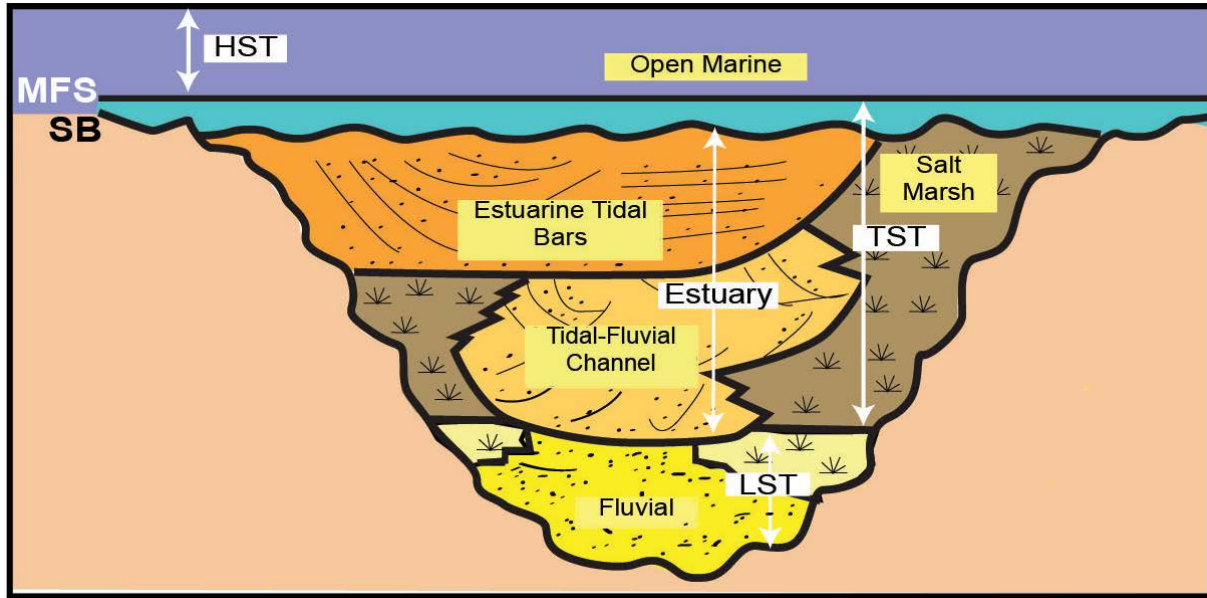


**Figure 2.** Predicted stratal stacking pattern for a tide-dominated incised valley with systems tracts noted. Sand-rich fluvial deposits occur at the base of the valley fill and expand laterally as a function of valley morphology. Sand packages become increasingly tidally influences, and are flanked by tidal flats and marshes (modified from Dalrymple and Choi, 2006).

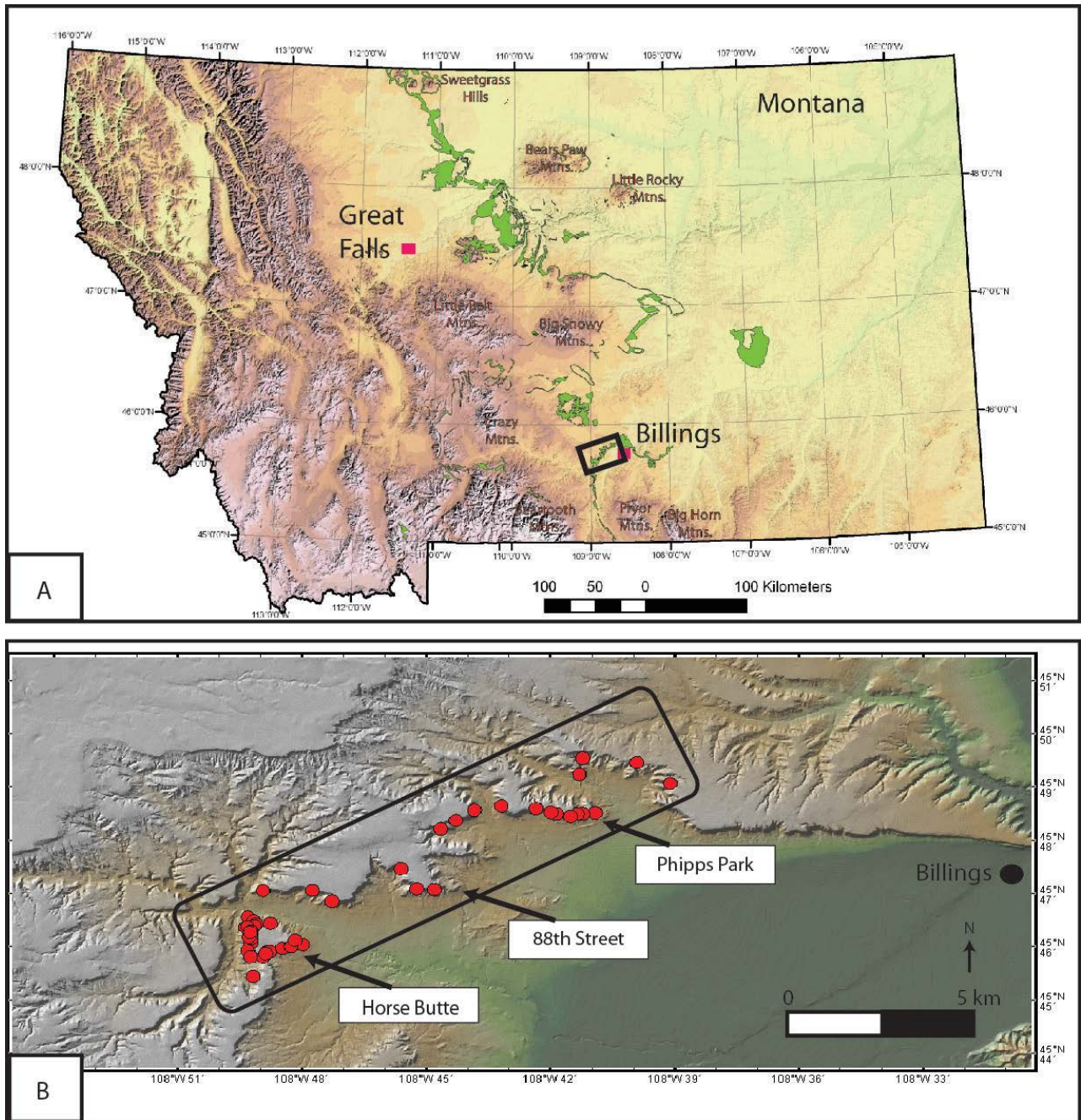


**Figure 3.** A) Outline of the Late Cretaceous Western Interior Seaway, and B) the location of the Santonian-Campanian Eagle Formation in south-central Montana relative to the Sevier orogenic front (modified from Payenberg et al., 2002).








PERIOD	STAGE	SOUTH-CENTRAL MONTANA	
UPPER CRETACEOUS	CAMPANIAN	BEARPAW	
		JUDITH RIVER	
		CLAGGETT	
		EAGLE	Upper member
			Middle member
	Lower member		
	SANTONIAN	TELEGRAPH CREEK	
		NIOBRARA	

**Figure 4.** Regional stratigraphy for the Upper Cretaceous in south-central Montana (modified from Payenberg, 2002).





**Figure 5.** A) Outcrop map of the Eagle Formation in Montana, with the study area noted (modified from Hauer et al., 2009). B) Study area located west of Billings Montana. Red dots indicate the location of measured sections. Locations discussed in text are highlighted.

Bioturbation Index (BI)	Classification	Visual Representation
0	No Bioturbation	
1	Sparse Bioturbation: distinct bedding with few observable traces	
2	Uncommon Bioturbation: distinct bedding with a low trace density	
3	Moderate Bioturbation: distinct bedding boundaries, traces are discrete but overlap is rare	
4	Common Bioturbation: bedding boundaries are indistinct, trace density is high and overlap is common	
5	Abundant Bioturbation: bedding is completely disturbed and may be just barely discernable	
6	Complete Bioturbation: total biogenic homogenization of sediment	

**Figure 6.** Classification scheme for bioturbation index (BI) values (from MacEachern et al., 2005).

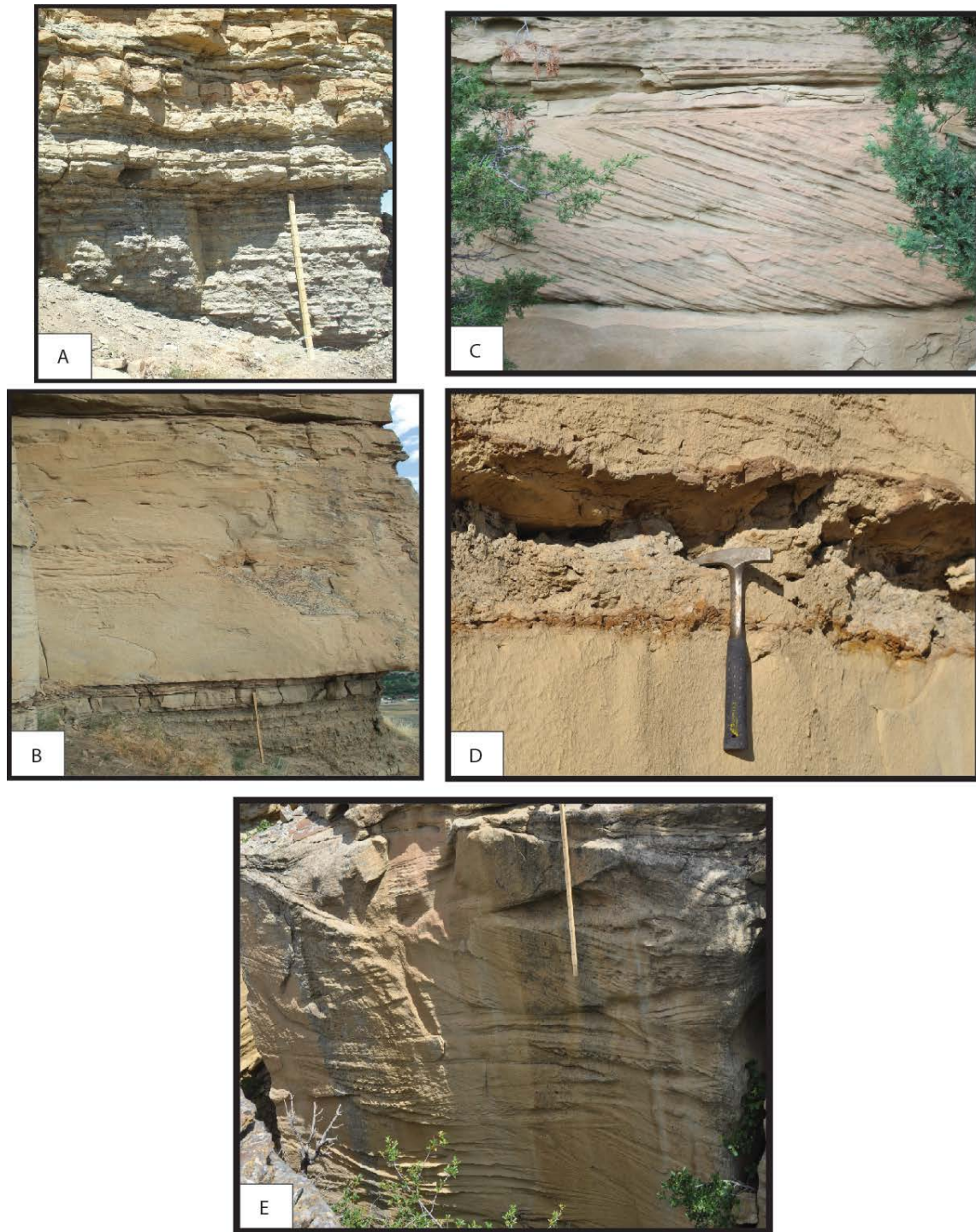


**Figure 7.** Sedimentary surfaces and features indicative of regressive shoreface deposition (FA1). A) Interbedded mud and silt (lower shoreface), B) Transition from lower shoreface to middle- and upper-shoreface (regressive surface of marine erosion), C) Planar cross-stratified bed occurring in Facies 2 (70 cm thick), D) sand-supported mud-clast conglomerate near the base of Facies 2, E) trough cross-stratification below the basal incision surface.

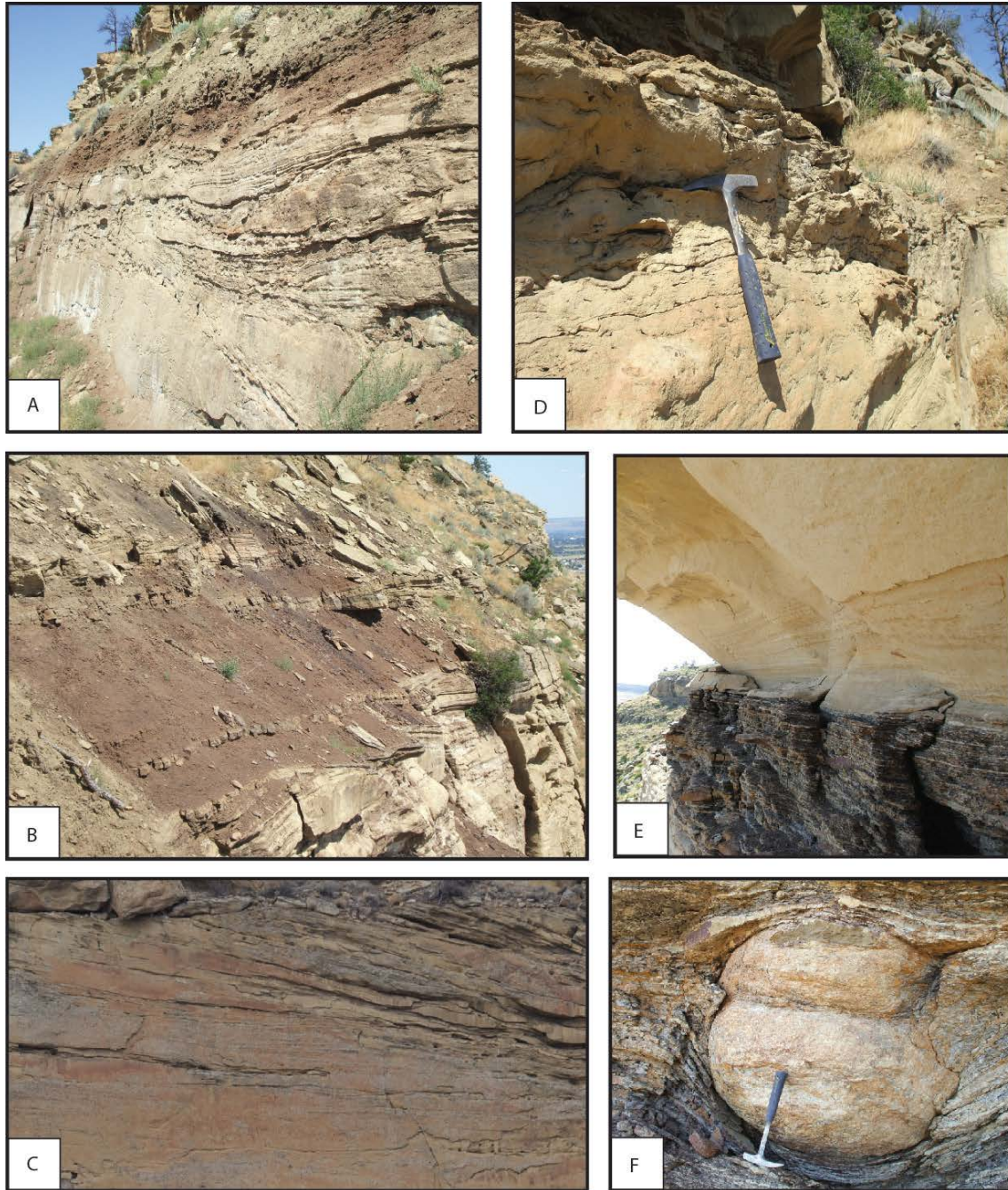


**Figure 8.** Fluvially dominated deposits and floodplain deposits characteristic of FA2. A) low angle lateral accretion set and laminated sand beds at the base of the 88<sup>th</sup> Street location, B) Mud-dominated valley center with subordinate sand-dominated lateral accretion sets at the 88<sup>th</sup> Street location, C) Sand dominated lateral accretion sets at the basal incision surface at the Phipps Park location, D) low angle and convolute sand beds with mud clasts above the basal incision surface at the Phipps Park location, E) heterolithic abandoned channel fill overlain by laminated-to-massive crevasse splay at the Phipps Park location, F) pseudo-nodule in the abandoned channel fill at the Phipps Park location.

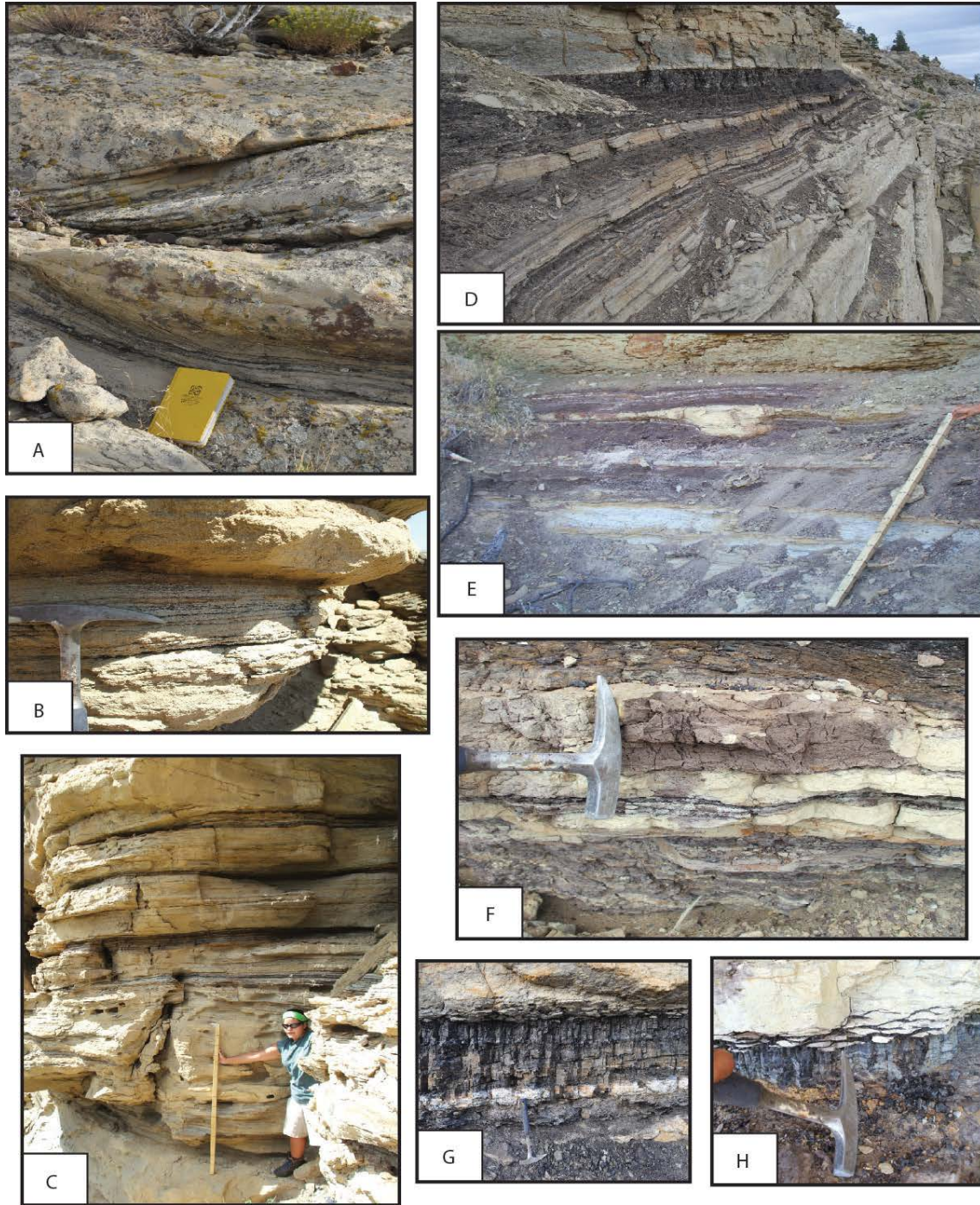


**Figure 9.** Tidal-fluvial deposits and associated floodplain deposits characteristic of FA3. A) bidirectional cross-stratification with paired carbonaceous drapes, B) paired silt and carbonaceous drapes, C) interbeds of laminated sand and interlaminated sand, silt, and mud, D) floodplain deposits overlain by carbonaceous mudstone and coal at the 88<sup>th</sup> Street location, E) mud-dominated flood-plain deposits with load cast and subordinate interlaminated sand and silt at the Horse Butte location, F) rizoliths below the coal at the Horse Butte location, G) 45 cm thick coal with tonstein near the base, H) coal with sand-filled *Ophiomorpha* burrows.



**Figure 10.** Bedding and surfaces characteristic of transgressive marginal marine to marine deposits (FA4). A) succession of carbonaceous mud (Facies 6), bay fill deposits (Facies 7), and middle- to upper-shoreface deposits (Facies 2), B) Bay fill package at the Phipps Park location, C) *Thalassinoides* burrow in the bay fill package, D) planar cross-stratified shoreface sands (Facies 2), E) sigmoidal cross-stratified sands (Facies 2)

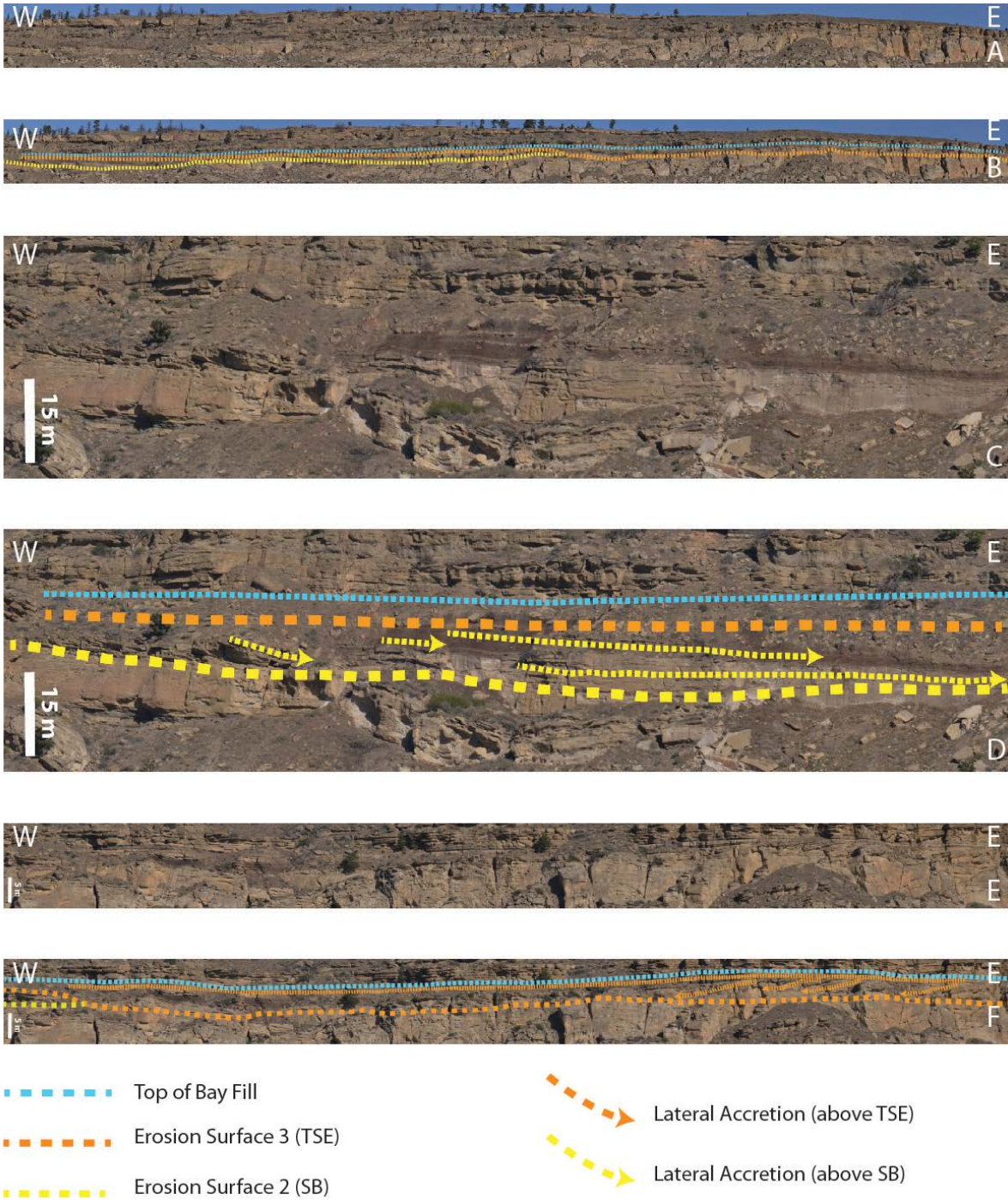


**Figure 11.** Stratigraphic architectures at the 88<sup>th</sup> Street location. All outcrop views are looking north. A, B) Uninterpreted and interpreted outcrop encompassing most of key architectures at this location. Surfaces include sequence boundary 1 (SB1), sequence boundary 2 (SB2), and the top of the bay fill package. C, D) Central mud-dominated valley fill representing the deepest point of incision within the study area. E, F) Channel form defined by incision surface SB2. SB2 truncates underlying shoreface deposits at the East end of the outcrop, and truncates the mud-dominated fluvial deposits and associated overbank deposits in the center of the outcrop.

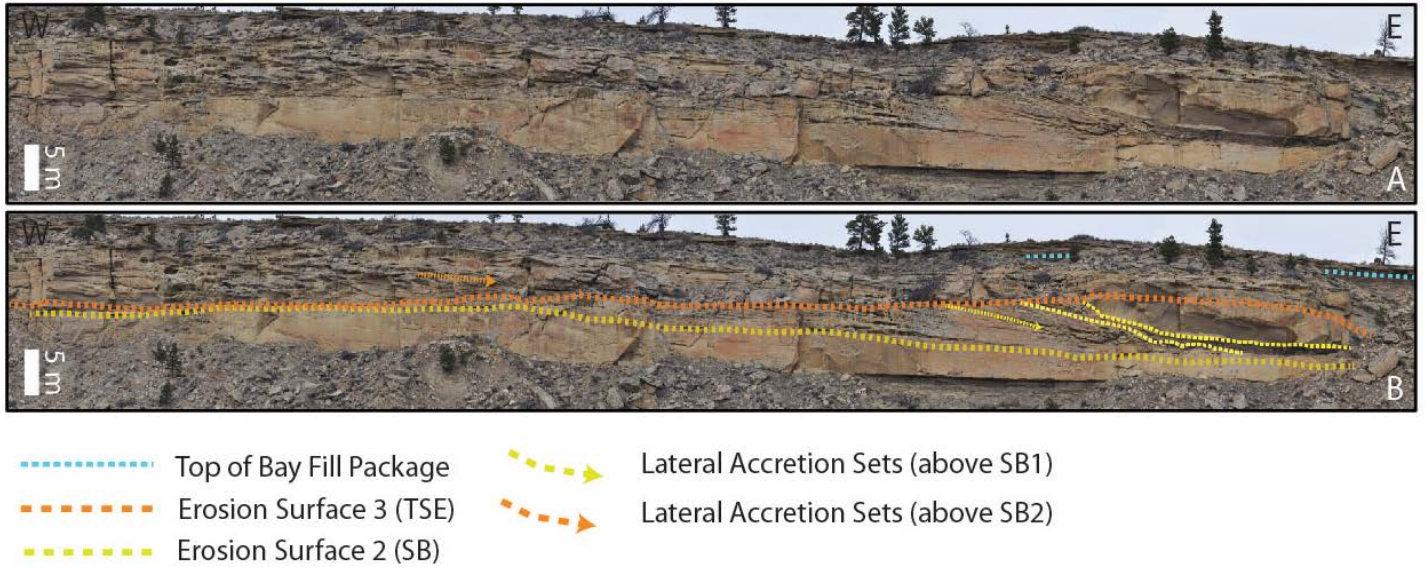
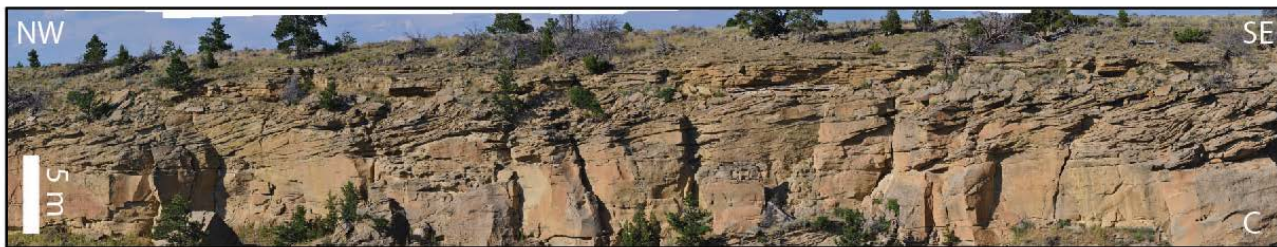


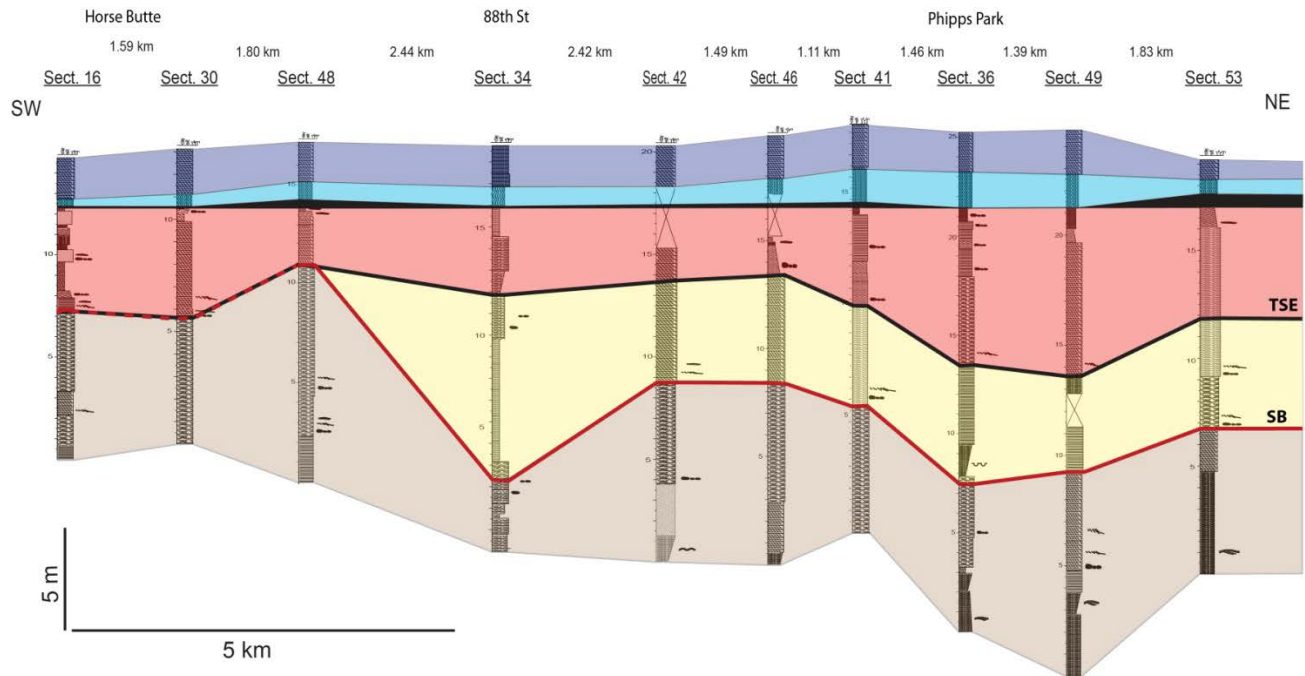
**Figure 12.** Stratigraphic architectures at the second location of deepest incision, ~5 km northeast of the 88<sup>th</sup> Street location at the Phipps Park location. A, B) Uninterpreted and interpreted outcrop mosaics. Fluvial deposits (FA2) overlying SB1 are truncated by tidal-fluvial deposits (FA3) overlying SB2.





- Top of Bay Fill Package
- Erosional base of tidal-fluvial channel
- Erosion Surface 3 (TSE)
- Lateral Accretion Sets (above TSE)

**Figure 13.** Stratigraphic architectures at the Horse Butte location, ~5 km southwest of 88<sup>th</sup> Street. A,B) Uninterpreted and interpreted southeast face of Horse Butte preserving 3 vertically stacked fluvial channels with increasing mud drapes and internal heterogeneity. The basal incision surface is defined by SB2. C,D) Uninterpreted and interpreted northwest face of Horse Butte, preserving a single channel deposit. The basal incision surface is defined by SB2, with well-preserved lateral accretion sets overlain directly by floodplain deposits, coal, and bay fill deposits.



**Facies**

- |   |  |  |
|---|--|--|
| FA1: Regressive Marine Interval                   | FA3: Coal  | Transgressive Surface of Erosion (TSE) |
| FA2: Regressive - Early Transgressive Valley Fill | FA4: Bay Fill Deposits                               | Sequence Boundary (SB)                 |
| FA3: Late Transgressive Valley Fill               | FA4: Transgressive Marginal Marine - Marine Interval |  |

**Base boundaries**

- Sharp
- Erosional
- Gradational

**Lithology**

- Sand
- Muddy sand
- Mudstone
- Carbonaceous shale
- Coal

**Sedimentary Features**

- wave ripple lamination
- Interbedded sand and mudstone
- Load casts
- Tabular planar bedding
- Planar cross-bedding
- Hummocky cross-stratification
- Mud clasts
- Mud drapes
- Trough cross-beds
- Coal clasts
- Accretionary surfaces

**Figure 14.** Stratigraphic correlation across the study transect based on measured stratigraphic sections.

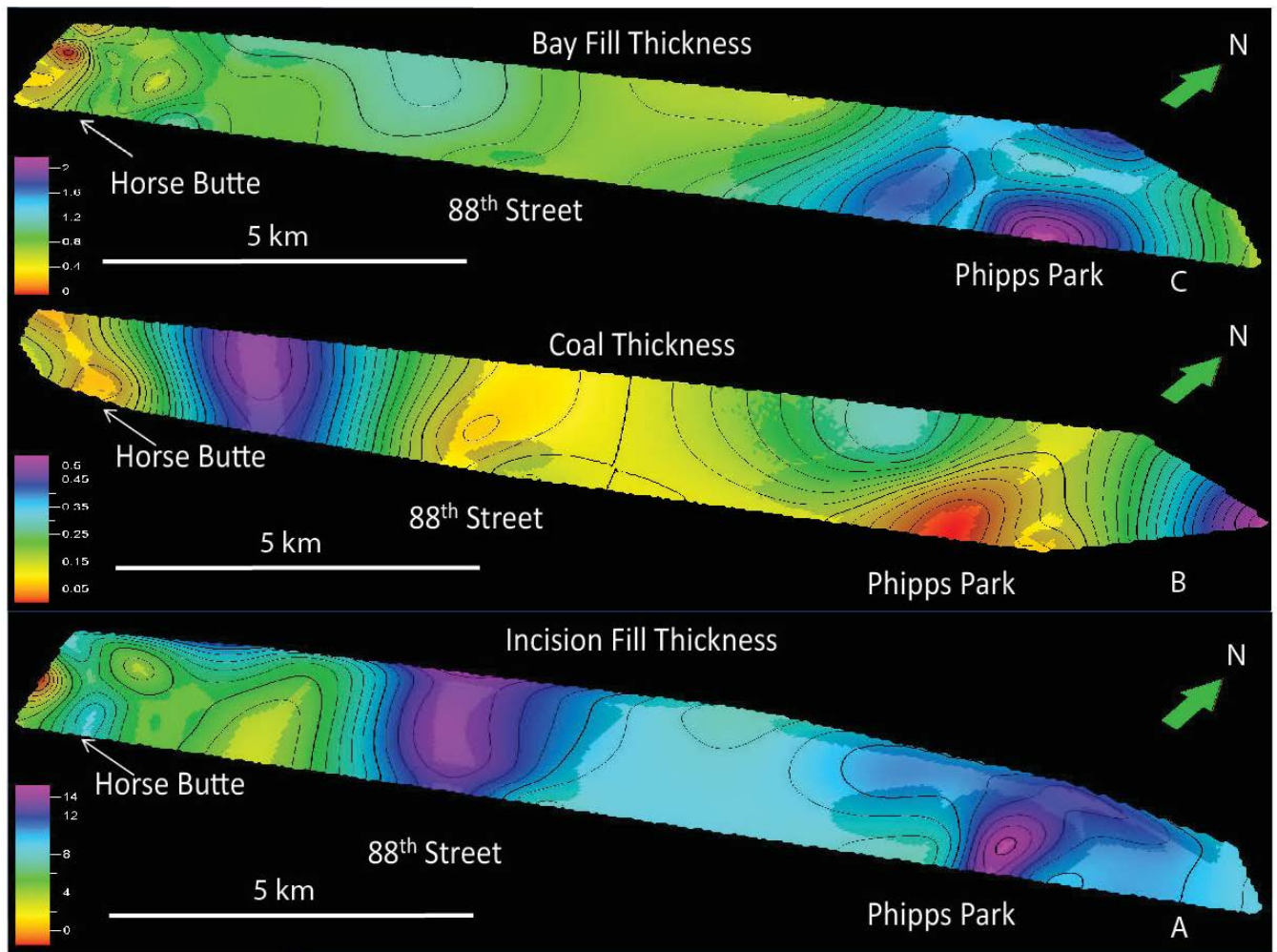


**Figure 15.** Isopach maps for key valley fill packages. A) Incision fill package including both fluvial and tidal-fluvial deposits and their associated floodplains (FA2 and FA3). Two distinct locations of deepest incision occur in the central study area (88<sup>th</sup> Street location) and ~5 km northeast of 88<sup>th</sup> Street (Phipps Park location). Incision between these two areas as well as continuing to the southwest of 88<sup>th</sup> Street is generally 5 to 8 m with one location of significantly less incision (~3 m). B) Coal thickness displays two locations of distinctly thicker coal flanking location of deepest incision occurring to the southwest of 88<sup>th</sup> Street and the northeast of Phipps Park. C). Bay fill package shows one location of distinctly thicker deposits occurring in the Phipps Park location.

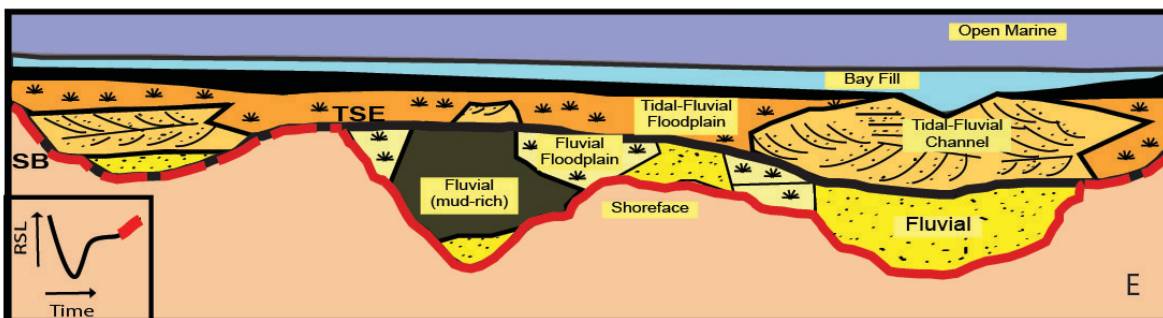
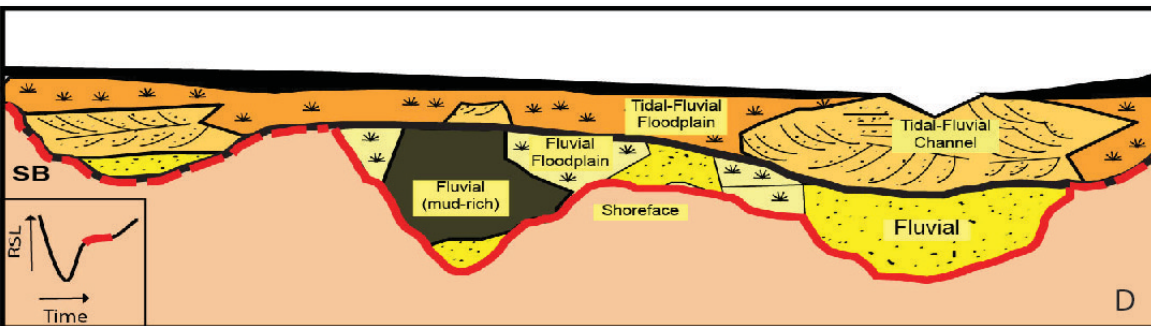
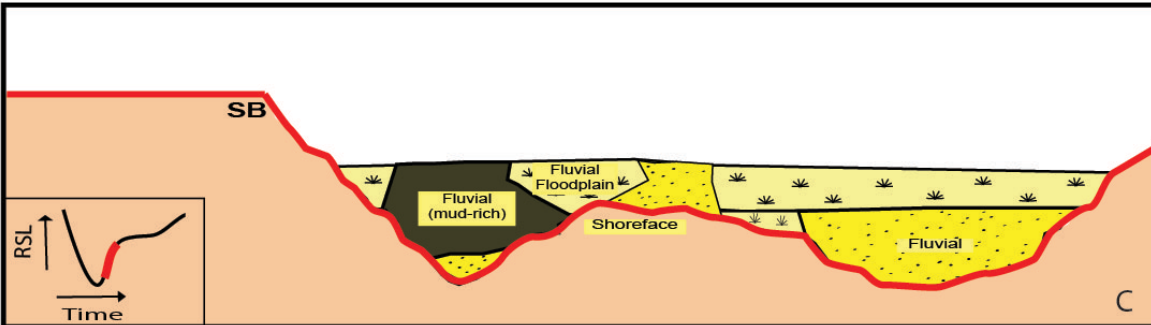
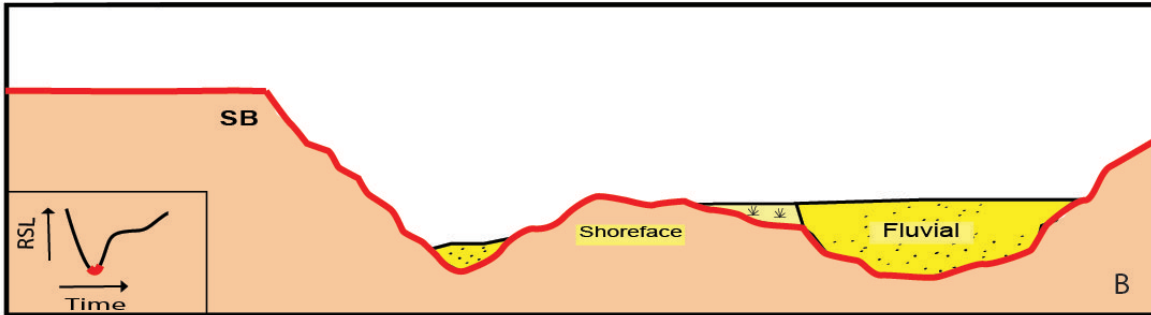
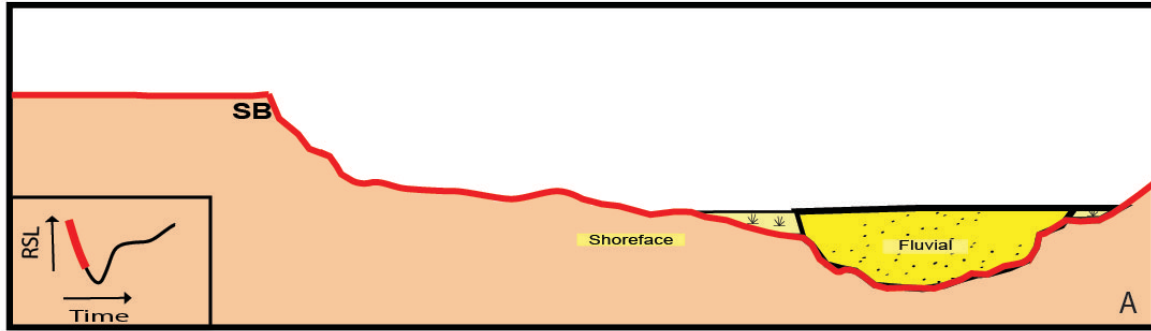


**Figure 16.** Conceptual model of valley evolution in the middle member of the Eagle Formation. A) First deep incision occurs in the northeast part of the study area during FSST (Phipps Park location), B) The trunk channel and deepest incision switch to the center of the study area (88th street location) and define the early LST through the onset of transgression, C) initial infilling of the valley during rapidly rising relative sea level is limited to the valley center and is mud-dominated. D) Deceleration in the rate of relative sea level rise results in valley widening and establishment of a lower rank sequence boundary via continued tidally influenced channel processes. E) With continued transgression and valley widening the system is capped by floodplain deposits and coals, followed by bay fill deposits marking complete inundation of the system, and finally a return to normal marine processes marked by shoreface deposits at the top of the package.

## APPENDIX A

### Thin Sections

50 Thin Sections were processed from hand samples collected at measured sections within the field area. Samples were pre-processed into billets before sending them to Spectrum Petrographics Inc. for processing. Some samples have small notches indicating stratigraphic up. Some samples also received microprobe polish. The sample list is shown as follows:

<u>Microprobe Polish</u>	<u>Stratigraphic Up</u>	<u>Unpolished</u>	<u>Stratigraphic Up</u>
16-02	X	16-06	
16-05	X	21-04	
21-07		32-08	
33-08	X	33-03	
33-09	X	33-04	
36-02		33-05	X
36-06		33-07	
36-08		36-01	X
36-14		36-03	X
36-16		36-04	
45-01		36-05	X
46-05	X	36-07	
47-01		36-10	
47-03		36-11	
47-07		36-12	
47-10		36-15	
49-05		46-03	X
50-01		46-06	
51-03		47-02	
51-08		47-04	
		47-08	
		47-09	
		49-02	
		49-04	X
		49-06	X
		49-07	
		50-02	
		51-02	
		51-04	

These samples are cataloged by the location of their measured sections and briefly described as follows:

Example:

**Measured Section Number** – brief description of the measured section.

*GPS Coordinates of the Measured Section (Latitude (Lat), Longitude (Lon))*

*Thin Section ID (correlative Spectrum ID) – brief description of the stratigraphic location of the sample*

**Measured Section 16** – channel form on the northwest face of Horse Butte

Lat: 45<sup>0</sup> 46.379 N      Lon: 108<sup>0</sup> 49.371 W

**16-02 (2GX-001)** – trough and planar cross-stratified, fine-grained sandstone just below the basal incision surface. [Facies 2: FA1]

**16-05 (2GX-002)** – fine-grained tabular sandstone bed (bed E) in the abandoned channel fill. This bed includes some very subtle bioturbation (BI = 1, bioturbation = *Skolithos* (?)). [Facies 5: FA3]

**16-06 (2GX-003)** – unique sandstone weathering (paleosol ?) below the carbonaceous mudstone. [Facies 6: FA3]

**Measured Section 21** – Thick carbonaceous shale and thin bay fill deposit between ‘the northwest channel’ and the ‘splay’ on the south face of Horse Butte.

Lat: 45<sup>0</sup> 45.935 N      Lon: 108<sup>0</sup> 49.320 W

**21-04 (2GX-004)** – fine-grained, cross-stratified sandstone with a bioturbation index of 3. Approximately 300 cm above the bay fill depositional package. [Facies 2: FA4]

**21-07 (2GX-005)** – 45 cm thick bay fill package. [Facies 7: FA4]

**Measured Section 32** – East side of the 88<sup>th</sup> Street outcrop.

Lat: 45<sup>0</sup> 47.066 N      Lon: 108<sup>0</sup> 44.089 W

**32-08 (2GX-048)** – 65 cm thick bay fill package. [Facies 7: FA4]

**Measured Section 33** – Center of the 88<sup>th</sup> Street outcrop.

Lat: 45<sup>0</sup> 47.114 N      Lon: 108<sup>0</sup> 44.925 W

**33-03 (2GX-006)** – horizontal, tabular-bedded fine-grained sandstone above the basal incision surface. [Facies 3: FA2]

**33-04 (2GX-007)** – sandstone bed from interbedded sandstones with silty mudstone layers. [Facies 3: FA2]

**33-05 (2GX-008)** – horizontal, tabular bedded fine-grained sandstone with abundant mud clasts and laminae. [Facies 5: FA3]

**33-07 (2GX-009)** – 85 cm thick bay fill package. [Facies 7: FA4]

**33-08 (2GX-010)** – asymptotically cross-stratified, fine-grained sandstone approximately 300 cm above the bay fill package. [Facies 2: FA4]

**33-09 (2GX-011)** – trough cross-stratified, fine-grained sandstone approximately 900 cm above facies association 7. [informal upper member of the Eagle].

**Measured Section 36** – Center of the Phipps Park outcrop.

Lat: 45<sup>0</sup> 48.513 N      Lon: 108<sup>0</sup> 41.227 W

**36-01 (2GX-012)** – silty sandstone near the base of the outcrop. [Facies 1: FA1].

**36-02 (2GX-013)** – discrete sandstone bed within the more heterogeneous and interbedded sandstone and mudstone near the base of the outcrop (HCS?). [Facies 1: FA1]

**36-03 (2GX-014)** – discrete sandstone bed from an interval of interbedded sandstone and shale beds near the base of the outcrop. [Facies 1: FA1]

**36-04 (2GX-015)** – shale bed from an interval of interbedded sandstone and shale beds near the base of the outcrop. [Facies 1: FA1]

**36-05 (2GX-016)** – trough cross-stratified, fine-grained sandstone below the basal incision surface. [Facies 2: FA1]

**36-06 (2GX-017)** - thinly bedded sandstone with abundant mud clasts directly above the basal incision surface. [Facies 3: FA2]

**36-07 (2GX-018)** – heterolithic strata interpreted to be abandoned channel fill. [Facies 5: FA2]

**36-08 (2GX-019)** – thick load cast within the heterolithic strata. [Facies 5: FA2]

**36-10 (2GX-020)** – sandstone from the interpreted crevasse splay (formerly the ‘sand plug’). [Facies 3: FA2]



**36-11 (2GX-021)** – horizontal planar, muddy sandstone with abundant mud clasts. [Facies 5: FA3]

**36-12 (2GX-022)** – very muddy sand with mud clasts. [Facies 5: FA3]

**36-14 (2GX-023)** – 180 cm thick bay fill package. [Facies 7: FA4]

**36-15 (2GX-024)** – low angle planar cross-stratified beds above the bay fill package. [Facies 2: FA4]

**36-16 (2GX-025)** – asymptotically cross-stratified, more heavily bioturbated (BI = 3) sandstone. [Facies 2: FA4]

### **Measured Section 45**

Lat: 45<sup>0</sup> 48.575 N      Lon: 108<sup>0</sup> 43.839 W

**45-01 (2GX-026)** – asymptotically cross-stratified sandstone approximately 75 cm above the bay fill package. [Facies 2: FA4]

### **Measured Section 46**

Lat: 45<sup>0</sup> 48.658 N      Lon: 108<sup>0</sup> 43.186 W

**46-03 (2GX-027)** – planar cross-stratified, fine-grained sandstone. [Facies 2: FA1]

**46-05 (2GX-028)** – cross stratified sandstone above the basal incision surface. [Facies 3: FA2]

**46-06 (2GX-029)** – muddy sandstone above the cross-stratified sandstone. [Facies 5: FA3]

**Measured Section 47** – Behind the memorial at the intersection of Lipp Rd. and Buffalo Trail Rd.

Lat: 45<sup>0</sup> 47.073 N      Lon: 108<sup>0</sup> 47.759 W

**47-01 (2GX-030)** – horizontal tabular sandstone bed in alternating sand and shale beds at the base of the outcrop. [Facies 1: FA1]

**47-02 (2GX-031)** – horizontal laminated sandstone below the interpreted regressive surface of marine erosion. [Facies 1: FA1]

**47-03 (2GX-032)** – cross-stratified sandstone with abundant mud clasts above the interpreted regressive surface of marine erosion. Sample from directly at the erosional surface. [Facies 2: FA1]

**47-04 (2GX-033)** – trough cross-stratified sandstone with mud clasts above the interpreted regressive surface of marine erosion. [Facies 2: FA1]

**47-07 (2GX-034)** – 110 cm thick bay fill package. [Facies 7: FA4]

**47-08 (2GX-035)** – second sample from slightly different lateral position in the bay fill package. [Facies 7: FA4].

**47-09 (2GX-036)** – horizontal planar lamination and asymptotic cross bedding approximately 150 cm above bay fill package. [Facies 2: FA4]

**47-10 (2GX-037)** – more steeply dipping planar and asymptotic cross beds, approximately 300 cm above bay fill package. [Facies 2: FA4]

#### **Measured Section 49**

Lat: 45<sup>0</sup> 49.249 N      Lon: 108<sup>0</sup> 41.307 W

**49-02 (2GX-038)** – sigmoidal and planar cross beds with mud drapes and clasts above the interpreted regressive surface of marine erosion. [Facies 2: FA1]

**49-04 (2GX-039)** – horizontal sandstone beds with abundant mud laminae and clasts just below significant talus interval. Beds coarsen up via loss of mud laminae and clasts. 49-04 is from the bottom of a bed with more mud content. [Facies 5: FA2]

**49-05 (2GX-040)** - horizontal sandstone beds with abundant mud laminae and clasts just below significant talus interval. Beds coarsen up via loss of mud laminae and clasts. 49-05 is from the top of a bed with less mud content. [Facies 5: FA2]

**49-06 (2GX-041)** – sandstone from the heterolithic strata in the middle of the outcrop. [Facies 5: FA3]

**49-07 (2GX-042)** – planar cross-stratified sandstone above the heterolithic strata. [Facies 4: FA3]

#### **Measured Section 50**

Lat: 45<sup>0</sup> 45.450 N      Lon: 108<sup>0</sup> 49.191 W

**50-01 (2GX-043)** – planar cross-stratified sandstone above the interpreted regressive surface of marine erosion. [Facies 2: FA1]

**50-02 (2GX-044)** – sandstone above the interpreted basal incision surface. [Facies 4: FA3]

### **Measured Section 51**

Lat: 45<sup>0</sup> 49.079 N      Lon: 108<sup>0</sup> 39.111 W

**51-02 (2GX-045)** – sandstone bed from the interbedded sand and shale interval near the base of the outcrop. [Facies 1: FA1]

**51-03 (2GX-046)** – horizontal planar sandstone beds gradational from underlying interbedded sand and shale near the base of the outcrop. [Facies 1: FA1]

**51-04 (2GX-049)** – sandstone just above the interpreted regressive surface of marine erosion. This is the interval with abundant shell fragments and fish fossil. [Facies 2: FA1]

**51-08 (2GX-047)** – erosionally based crossbedded sandstone beds. MS51-08 is from the base of one such bed, where there are abundant angular mud clasts. [Facies 4: FA3]

### **THIN SECTION DATA: Point Counts, Grain Size, Rounding**

Point count, grain size, and rounding data were collected from 18 thin section samples. Point count analysis recorded the composition of 500 individual grains for each sample. The number of counts on pore space was also recorded but was not applied to the 500 grain counts per sample. In order to evaluate error, two samples (36-05, 36-10) were counted twice. Compositions recorded included monocrystalline quartz (Qm), polycrystalline quartz (Qp), chert, plagioclase feldspar (Plag), potassium feldspar (Kspar), clay matrix, biotite, muscovite, chlorite, lithic volcanic fragments (Lithic volc), lithic sedimentary fragments (Lithic sed), lithic metamorphic fragments (Lithic meta), organic fragments (org), glauconite (G), and pores. The resulting QFL plot is shown in Figure 1. Point count data are shown in Figure 2.

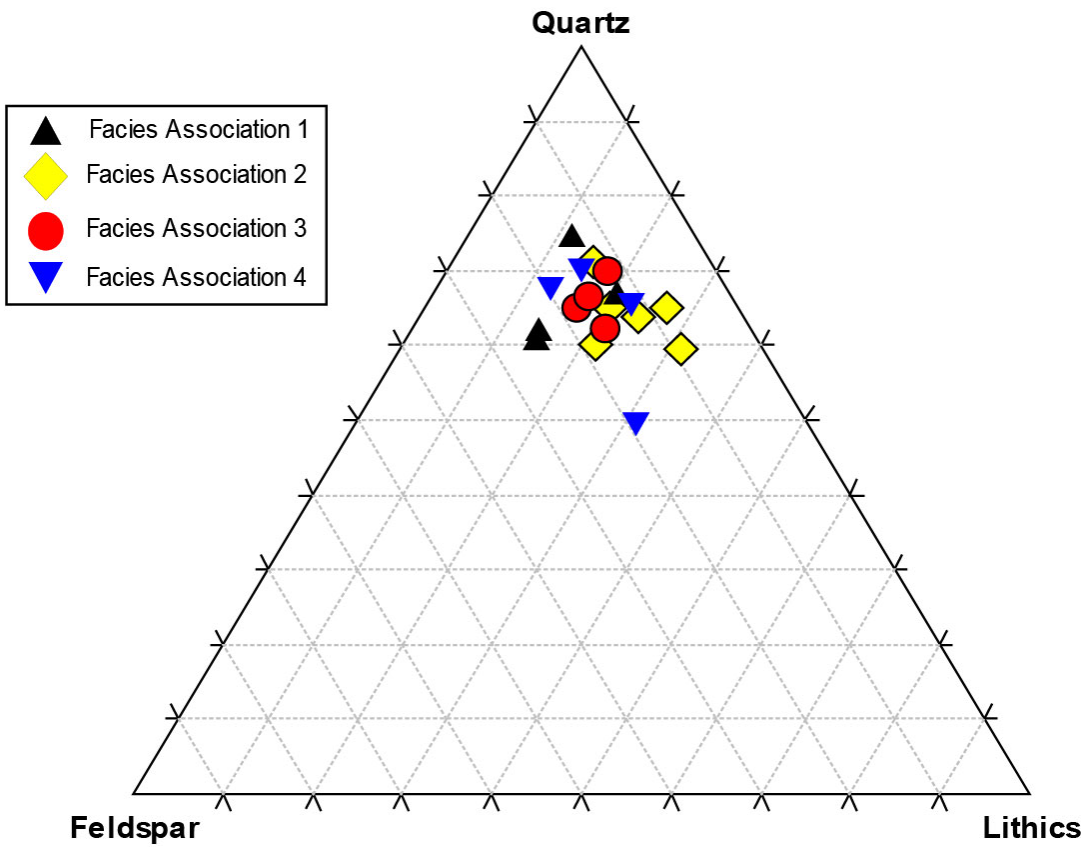


**Figure 1.** QFL plot from point count data. Points are marked according to their interpreted facies association.

Slide ID	Facies Association	Qm	Qm %	Qp	Qp %	Chert	Chert %	Plag	Plag %	Kspar
36-05	1	366	73.2	1	0.2	0	0	0	0	70
36-06	2	299	59.8	22	4.4	3	0.6	3	0.6	69
36-07	2	248	49.6	45	9	5	1	2	0.4	43
36-08	2	183	36.6	74	14.8	67	13.4	6	1.2	34
36-10	2	292	58.4	21	4.2	39	7.8	13	2.6	52
36-11	3	265	53	27	5.4	41	8.2	7	1.4	51
36-14	4	258	51.6	26	5.2	45	9	21	4.2	48
36-15	4	316	63.2	3	0.6	16	3.2	19	3.8	76
33-03	2	282	56.4	5	1	14	2.8	16	3.2	75
33-05	2	282	56.4	12	2.4	21	4.2	4	0.8	54
33-07	4	201	40.2	15	3	28	5.6	26	5.2	67
16-02	1	296	59.2	13	2.6	23	4.6	13	2.6	51
16-05	3	268	53.6	15	3	40	8	19	3.8	71
46-03	1	280	56	10	2	15	3	23	4.6	96
46-05	3	247	49.4	22	4.4	37	7.4	34	6.8	46
47-02	1	268	53.6	4	0.8	24	4.8	32	6.4	89
47-03	4	293	58.6	18	3.6	14	2.8	20	4	57
47-07	4	252	50.4	24	4.8	37	7.4	15	3	39
36-05 (again)		329	65.8	0	0	5	1	20	4	87
36-10 (again)		265	53	12	2.4	26	5.2	19	3.8	56

Slide ID	Kspar	Clay matrix	Clay mtrx %	Biotite	Biotite %	Muscovite	Musc %	Chlorite	Chl %	Lith volc	Lv %
36-05	14	2	0.4	0	0	1	0.2	0	0	0	0
36-06	13.8	0	0	0	0	0	0	0	0	0	0
36-07	8.6	0	0	0	0	0	0	0	0	0	0
36-08	6.8	0	0	0	0	0	0	0	0	0	0
36-10	10.4	0	0	1	0.2	0	0	0	0	0	0
36-11	10.2	12	2.4	6	1.2	0	0	2	0.4	0	0
36-14	9.6	25	5	3	0.6	3	0.6	0	0	0	0
36-15	15.2	0	0	1	0.2	0	0	0	0	0	0
33-03	15	0	0	0	0	0	0	0	0	0	0
33-05	10.8	0	0	0	0	0	0	1	0.2	0	0
33-07	13.4	2	0.4	6	1.2	3	0.6	0	0	0	0
16-02	10.2	0	0	0	0	0	0	0	0	0	0
16-05	14.2	0	0	0	0	2	0.4	0	0	0	0
46-03	19.2	0	0	4	0.8	0	0	0	0	0	0
46-05	9.2	0	0	2	0.4	1	0.2	2	0.4	0	0
47-02	17.8	0	0	2	0.4	0	0	0	0	1	0.2
47-03	11.4	2	0.4	0	0	0	0	0	0	2	0.4
47-07	7.8	1	0.2	8	1.6	1	0.2	8	1.6	0	0
36-05 (again)	17.4	0	0	1	0.2	1	0.2	1	0.2	0	0
36-10 (again)	11.2	0	0	1	0.2	1	0.2	1	0.2	0	0

Slide ID	Lith sed	LS %	Lith meta	Lm %	Lith org	Lorg %	Lith un	Lu %	G	G%	Pores
36-05	60	12	0	0	0	0	0	0	0	0	129
36-06	103	20.6	0	0	0	0	0	0	1	0.2	63
36-07	156	31.2	0	0	0	0	1	0.2	0	0	7
36-08	134	26.8	0	0	0	0	1	0.2	1	0.2	38
36-10	77	15.4	0	0	0	0	0	0	5	1	117
36-11	78	15.6	5	1	2	0.4	0	0	4	0.8	87
36-14	45	9	13	2.6	9	1.8	1	0.2	3	0.6	26
36-15	55	11	5	1	1	0.2	0	0	8	1.6	78
33-03	107	21.4	1	0.2	0	0	0	0	0	0	78
33-05	118	23.6	1	0.2	2	0.4	0	0	5	1.1	71
33-07	118	23.6	13	2.6	21	4.2	0	0	0	0	36
16-02	98	19.6	4	0.8	1	0.2	0	0	1	0.2	62
16-05	75	15	3	0.6	6	1.2	0	0	1	0.2	73
46-03	70	14	1	0.2	0	0	0	0	1	0.2	89
46-05	99	19.8	3	0.6	3	0.6	0	0	4	0.8	54
47-02	62	12.4	11	2.2	0	0	0	0	7	2.2	46
47-03	77	15	11	2.2	6	0	0	0	6	1.2	74
47-07	95	19	10	2	1	0.2	1	0.2	8	1.6	18
36-05 (again)	50	10.2	0	0	0	0	0	0	5	1	145
36-10 (again)	119	23.8	0	0	0	0	0	0	0	0	104

Figure 2. Point count data

Each of the 18 samples used for point count data were re-analyzed for grain size and rounding measurements. Measurements were taken from 100 grains per sample. Grain size was recorded in millimeters to the nearest 0.05 mm. Rounding and sphericity were recorded based on the roundness scale of Powers (1953): very angular (vA), angular (A), sub-angular (sA), sub-rounded (sR), rounded (R), well-rounded (wR) and high sphericity (H) or low sphericity (L). Grain size and rounding data are listed as follows:

**Sample 36-05**

<b>Count</b>	<b>Size (mm)</b>	<b>Rounding</b>	<b>Sphericity (H/L)</b>
1	0.15	Sub-Rounded	High
2	0.1	Sub-Rounded	Low
3	0.25	Rounded	High
4	0.2	Well-Rounded	High
5	0.2	Well-Rounded	High
6	0.3	Well-Rounded	High
7	0.15	Rounded	Low
8	0.15	Well-Rounded	High
9	0.2	Well-Rounded	High
10	0.2	Sub-Rounded	Low
11	0.25	Well-Rounded	High
12	0.3	Sub-Rounded	Low
13	0.25	Well-Rounded	Low
14	0.2	Rounded	Low
15	0.15	Well-Rounded	High
16	0.1	Rounded	High
17	0.1	Sub-Rounded	Low
18	0.3	Well-Rounded	High
19	0.3	Sub-Rounded	Low
20	0.2	Sub-Rounded	High
21	0.3	Rounded	High
22	0.15	Rounded	High
23	0.15	Well-Rounded	High
24	0.1	Rounded	Low
25	0.2	Rounded	High
26	0.2	Rounded	Low
27	0.2	Sub-Rounded	Low
28	0.2	sub-Angular	Low
29	0.2	Round	High
30	0.1	Well-Rounded	High

31	0.2	Sub-Rounded	High
32	0.35	Rounded	High
33	0.25	Rounded	Low
34	0.2	Well-Rounded	High
35	0.2	Well-Rounded	High
36	0.2	Well-Rounded	High
37	0.25	Sub-Rounded	High
38	0.15	sub-Angular	High
39	0.2	Rounded	High
40	0.25	Sub-Rounded	High
41	0.2	Well-Rounded	High
42	0.3	Sub-Rounded	Low
43	0.2	Well-Rounded	High
44	0.1	Well-Rounded	High
45	0.25	sub-Angular	Low
46	0.2	Rounded	Low
47	0.3	Rounded	High
48	0.25	Rounded	High
49	0.2	Well-Rounded	High
50	0.1	Well-Rounded	High
51	0.2	Rounded	High
52	0.15	Rounded	High
53	0.2	Well-Rounded	High
54	0.2	sub-Angular	High
55	0.2	Well-Rounded	High
56	0.15	Rounded	Low
57	0.15	Rounded	Low
58	0.2	Well-Rounded	High
59	0.2	Sub-Rounded	Low
60	0.25	Rounded	Low
61	0.2	Well-Rounded	High
62	0.2	Rounded	Low
63	0.2	Sub-Rounded	Low
64	0.25	Well-Rounded	High
65	0.15	Rounded	High
66	0.2	Well-Rounded	High
67	0.25	sub-Angular	Low
68	0.2	Rounded	High
69	0.2	Rounded	High
70	0.25	Well-Rounded	High
71	0.15	Well-Rounded	High

72	0.2	Sub-Rounded	Low
73	0.3	Rounded	Low
74	0.2	Well-Rounded	High
75	0.2	Sub-Rounded	Low
76	0.4	Well-Rounded	High
77	0.2	Sub-Rounded	Low
78	0.15	Sub-Rounded	Low
79	0.25	Sub-Rounded	Low
80	0.1	Sub-Rounded	High
81	0.2	Well-Rounded	High
82	0.25	Rounded	Low
83	0.15	Well-Rounded	High
84	0.15	Sub-Rounded	Low
85	0.2	Sub-Rounded	Low
86	0.25	Sub-Rounded	Low
87	0.2	Rounded	High
88	0.25	Sub-Rounded	Low
89	0.15	Well-Rounded	High
90	0.3	sub-Angular	Low
91	0.25	Rounded	Low
92	0.2	Well-Rounded	High
93	0.25	Rounded	Low
94	0.2	Sub-Rounded	Low
95	0.15	Rounded	High
96	0.15	Rounded	High
97	0.2	Rounded	High
98	0.25	Well-Rounded	High
99	0.2	Well-Rounded	High
100	0.25	Well-Rounded	High

Average 0.2055

**Sample 36-06**

Count	Size (mm)	Rounding	Sphericity
1	0.25	R	L
2	0.2	R	L
3	0.25	sR	L
4	0.15	sR	L
5	0.45	sR	L
6	0.4	R	L



7	0.15	A	L
8	0.2	R	H
9	0.25	sA	L
10	0.25	wR	H
11	0.3	sR	L
12	0.35	A	L
13	0.35	sA	L
14	0.15	sA	L
15	0.3	sA	L
16	0.3	sR	H
17	0.2	sA	L
18	0.3	sR	L
19	0.15	sR	H
20	0.3	wR	H
21	0.25	R	L
22	0.4	R	L
23	0.15	sR	H
24	0.3	wR	L
25	0.25	sR	L
26	0.2	sA	L
27	0.35	sA	L
28	0.25	sR	L
29	0.25	R	H
30	0.25	wR	H
31	0.4	sA	L
32	0.25	sR	L
33	0.3	sA	L
34	0.1	A	L
35	0.25	sA	L
36	0.25	sR	H
37	0.25	R	L
38	0.3	sA	L
39	0.3	R	H
40	0.2	R	H
41	0.15	A	L
42	0.25	wR	H
43	0.3	R	H
44	0.2	R	H
45	0.3	R	L
46	0.25	R	H
47	0.25	wR	L

48	0.2	wR	H
49	0.3	A	L
50	0.15	sR	L
51	0.3	sR	L
52	0.25	sR	L
53	0.35	sR	L
54	0.15	sA	L
55	0.3	sR	L
56	0.3	sR	H
57	0.2	R	H
58	0.4	sA	L
59	0.4	sA	L
60	0.3	R	H
61	0.15	sA	L
62	0.2	R	L
63	0.25	sA	L
64	0.3	sR	H
65	0.2	R	H
66	0.4	sA	L
67	0.2	R	H
68	0.4	wR	H
69	0.3	sR	L
70	0.2	R	H
71	0.4	sR	L
72	0.3	sA	L
73	0.15	A	L
74	0.25	R	L
75	0.25	sR	L
76	0.3	sA	L
77	0.2	R	H
78	0.3	R	L
79	0.25	R	H
80	0.3	sA	L
81	0.2	sA	L
82	0.15	R	H
83	0.3	wR	L
84	0.15	sR	L
85	0.2	sR	H
86	0.2	sR	H
87	0.2	wR	H
88	0.3	sR	L

89	0.35	wR	L
90	0.4	R	L
91	0.35	R	L
92	0.4	sA	L
93	0.2	R	H
94	0.25	wR	H
95	0.25	sR	H
96	0.25	R	H
97	0.15	R	L
98	0.25	wR	H
99	0.15	sR	L
100	0.25	R	H

Average            0.2605

**Sample 36-07**

<b>Count</b>	<b>Size (mm)</b>	<b>Rounding</b>	<b>Sphericity</b>
1	0.2	sA	L
2	0.15	A	L
3	0.15	sR	L
4	0.2	sR	L
5	0.25	sR	H
6	0.1	A	L
7	0.15	sR	L
8	0.1	A	L
9	0.2	wR	H
10	0.2	R	L
11	0.15	R	H
12	0.25	wR	H
13	0.2	R	H
14	0.1	A	L
15	0.2	sA	L
16	0.15	sR	H
17	0.15	R	H
18	0.1	sA	L
19	0.15	sR	L
20	0.2	sR	H
21	0.1	A	L
22	0.15	wR	H
23	0.15	sR	L

24	0.2	wR	H
25	0.15	R	H
26	0.15	sR	L
27	0.1	sR	H
28	0.15	R	H
29	0.25	A	L
30	0.25	sA	L
31	0.2	R	H
32	0.15	R	H
33	0.2	R	H
34	0.1	wR	H
35	0.15	R	H
36	0.2	A	L
37	0.15	wR	H
38	0.15	R	H
39	0.2	sA	L
40	0.15	R	H
41	0.1	sA	H
42	0.1	R	H
43	0.15	sR	L
44	0.3	R	L
45	0.15	sR	L
46	0.15	R	H
47	0.15	R	H
48	0.15	sR	H
49	0.15	sA	H
50	0.15	R	H
51	0.15	sR	L
52	0.1	R	H
53	0.25	wR	H
54	0.15	wR	H
55	0.2	wR	H
56	0.2	sR	L
57	0.1	sA	L
58	0.1	sR	H
59	0.1	wR	H
60	0.1	sA	L
61	0.2	R	H
62	0.1	R	H
63	0.15	R	H
64	0.1	R	H

65	0.15	R	H
66	0.2	sR	H
67	0.15	R	H
68	0.15	A	L
69	0.2	wR	H
70	0.2	R	L
71	0.15	R	L
72	0.15	R	H
73	0.2	R	H
74	0.25	R	L
75	0.15	R	H
76	0.2	R	H
77	0.15	R	H
78	0.1	R	H
79	0.2	sA	L
80	0.2	sR	H
81	0.2	A	L
82	0.2	sA	L
83	0.1	R	H
84	0.25	sA	L
85	0.25	sA	H
86	0.2	sA	L
87	0.25	sR	L
88	0.2	sR	H
89	0.1	R	H
90	0.2	A	L
91	0.2	R	L
92	0.2	sA	L
93	0.15	wR	H
94	0.15	R	H
95	0.15	sR	H
96	0.15	sA	L
97	0.15	sA	L
98	0.25	R	L
99	0.1	R	L
100	0.2	A	L

Average 0.1665

**Sample 36-08**

<b>Count</b>	<b>Size (mm)</b>	<b>Rounding</b>	<b>Sphericity</b>
1	0.15	sA	L
2	0.2	sR	L
3	0.1	sR	L
4	0.15	sA	L
5	0.2	sR	L
6	0.2	sR	L
7	0.1	sR	L
8	0.15	R	L
9	0.1	R	H
10	0.2	R	h
11	0.15	sR	L
12	0.15	R	L
13	0.2	sR	L
14	0.15	R	H
15	0.2	R	L
16	0.15	R	H
17	0.2	sR	L
18	0.15	sR	L
19	0.15	wR	H
20	0.15	R	L
21	0.05	wR	H
22	0.1	sA	L
23	0.1	sA	L
24	0.15	sA	L
25	0.15	R	H
26	0.1	A	L
27	0.25	R	H
28	0.2	wR	H
29	0.15	sA	L
30	0.2	sR	L
31	0.25	sA	l
32	0.15	R	H
33	0.15	sA	L
34	0.2	sR	L
35	0.05	sA	L
36	0.25	sR	L
37	0.2	sA	L
38	0.2	R	L
39	0.15	sR	H
40	0.2	sA	L

41	0.2	R	L
42	0.2	R	H
43	0.15	sR	L
44	0.15	wR	H
45	0.1	A	L
46	0.15	R	H
47	0.15	sR	L
48	0.25	wR	L
49	0.2	R	L
50	0.2	sR	L
51	0.25	sR	L
52	0.15	sR	L
53	0.15	wR	H
54	0.1	wR	H
55	0.1	sR	L
56	0.2	sR	H
57	0.2	wR	L
58	0.15	sR	L
59	0.2	sA	L
60	0.15	sR	H
61	0.1	A	L
62	0.25	sA	L
63	0.2	R	H
64	0.15	sR	H
65	0.2	sR	L
66	0.25	R	L
67	0.15	sA	L
68	0.15	sR	H
69	0.25	sA	L
70	0.25	R	H
71	0.15	sA	L
72	0.1	wR	H
73	0.15	R	H
74	0.1	sA	H
75	0.2	sR	L
76	0.1	R	H
77	0.15	sR	H
78	0.2	R	L
79	0.15	wR	H
80	0.05	wR	H
81	0.2	sA	L

82	0.2	sA	L
83	0.2	sA	L
84	0.1	sA	L
85	0.15	sR	H
86	0.15	sA	L
87	0.15	R	H
88	0.15	sA	L
89	0.2	R	L
90	0.2	R	H
91	0.1	sR	H
92	0.15	sR	L
93	0.15	wR	H
94	0.2	sR	L
95	0.1	A	L
96	0.1	A	L
97	0.15	sA	L
98	0.2	R	l
99	0.15	wR	L
100	0.15	sR	H

Average            0.163

**Sample 36-10**

<b>Count</b>	<b>Size (mm)</b>	<b>Rounding</b>	<b>Sphericity</b>
1	0.25	sR	H
2	0.2	R	H
3	0.2	sA	H
4	0.25	R	H
5	0.15	sR	L
6	0.2	A	L
7	0.25	sR	L
8	0.25	sA	L
9	0.1	Sa	H
10	0.25	R	H
11	0.15	R	H
12	0.25	wR	H
13	0.2	R	H
14	0.2	sR	L
15	0.3	sR	L
16	0.2	R	L



17	0.1	R	H
18	0.2	R	H
19	0.15	R	h
20	0.15	sR	H
21	0.3	wR	L
22	0.3	R	L
23	0.15	A	L
24	0.15	sR	H
25	0.25	wR	H
26	0.25	R	H
27	0.25	wR	H
28	0.25	sA	L
29	0.2	sR	L
30	0.2	R	L
31	0.3	sA	L
32	0.15	R	H
33	0.1	sR	H
34	0.15	sR	L
35	0.25	R	L
36	0.2	R	H
37	0.2	sA	H
38	0.2	wR	H
39	0.15	A	L
40	0.15	R	H
41	0.25	R	L
42	0.2	R	H
43	0.2	sR	H
44	0.3	sR	L
45	0.3	A	L
46	0.2	sR	H
47	0.3	R	H
48	0.2	R	H
49	0.3	sA	L
50	0.3	sA	L
51	0.15	sR	H
52	0.2	sR	L
53	0.1	wR	H
54	0.25	R	H
55	0.2	R	L
56	0.1	sR	H
57	0.3	sR	L

58	0.2	R	L
59	0.3	A	L
60	0.3	R	L
61	0.15	R	L
62	0.3	R	L
63	0.1	sA	H
64	0.25	sR	L
65	0.3	R	H
66	0.2	R	H
67	0.35	R	L
68	0.25	sR	H
69	0.15	sA	L
70	0.25	sR	L
71	0.2	sR	L
72	0.2	wR	H
73	0.35	sA	H
74	0.3	A	L
75	0.15	A	L
76	0.2	sR	L
77	0.25	R	H
78	0.2	sA	L
79	0.15	A	L
80	0.3	A	L
81	0.3	R	H
82	0.3	R	L
83	0.2	A	L
84	0.2	sR	L
85	0.1	A	L
86	0.15	sR	H
87	0.2	wR	L
88	0.25	R	H
89	0.15	A	L
90	0.15	sA	H
91	0.1	sR	H
92	0.2	sA	L
93	0.35	sA	L
94	0.2	R	L
95	0.15	sA	L
96	0.2	sA	L
97	0.3	sA	L
98	0.1	A	L

99	0.25	sR	L
100	0.25	R	H
Average	0.215		

**Sample 36-11**

<b>Count</b>	<b>Size (mm)</b>	<b>Rounding</b>	<b>Sphericity</b>
1	0.15	sA	L
2	0.2	sA	L
3	0.15	sA	H
4	0.1	sR	L
5	0.05	sR	H
6	0.15	sA	L
7	0.1	wR	H
8	0.15	sA	L
9	0.1	sA	H
10	0.2	sA	L
11	0.05	wR	H
12	0.1	sR	L
13	0.15	sR	H
14	0.1	wR	H
15	0.2	R	L
16	0.15	R	H
17	0.1	sA	L
18	0.1	A	L
19	0.2	R	H
20	0.15	sA	L
21	0.15	R	H
22	0.1	sR	H
23	0.25	R	H
24	0.15	wR	H
25	0.1	A	H
26	0.15	A	L
27	0.2	A	L
28	0.15	R	H
29	0.2	sR	L
30	0.2	R	H
31	0.1	A	L
32	0.1	sR	H
33	0.25	sR	L

34	0.15	R	H
35	0.1	wR	H
36	0.15	R	L
37	0.15	A	L
38	0.15	sA	L
39	0.15	A	L
40	0.1	R	H
41	0.15	wR	H
42	0.05	wR	H
43	0.15	sR	L
44	0.15	sR	L
45	0.1	R	H
46	0.15	R	H
47	0.1	sR	H
48	0.05	sA	L
49	0.15	R	H
50	0.1	R	H
51	0.1	R	H
52	0.1	R	L
53	0.1	sR	H
54	0.15	sA	H
55	0.2	R	L
56	0.15	sA	H
57	0.2	sA	L
58	0.1	sR	H
59	0.1	A	L
60	0.15	R	H
61	0.15	A	L
62	0.15	sR	H
63	0.15	sR	H
64	0.15	sR	H
65	0.1	R	L
66	0.15	R	L
67	0.15	R	L
68	0.05	sR	L
69	0.2	sR	L
70	0.1	sR	H
71	0.1	A	L
72	0.15	R	H
73	0.15	R	L
74	0.05	wR	H

75	0.2	sA	L
76	0.3	A	L
77	0.1	R	H
78	0.1	A	L
79	0.15	wR	H
80	0.15	A	L
81	0.15	A	L
82	0.05	A	L
83	0.1	R	H
84	0.2	A	L
85	0.35	A	L
86	0.15	sA	H
87	0.2	sR	L
88	0.5	A	L
89	0.15	sA	H
90	0.15	A	L
91	0.1	R	H
92	0.15	A	L
93	0.1	R	H
94	0.15	A	L
95	0.1	A	L
96	0.1	A	L
97	0.05	wR	H
98	0.15	A	L
99	0.2	sR	L
100	0.1	A	L

Average 0.142

**Sample 36-14**

<b>Count</b>	<b>Size (mm)</b>	<b>Rounding</b>	<b>Sphericity</b>
1	0.1	sA	H
2	0.25	A	L
3	0.1	A	L
4	0.1	sA	L
5	0.15	R	L
6	0.15	R	H
7	0.15	sR	L
8	0.2	A	L
9	0.1	sA	L

10	0.1	A	L
11	0.2	sR	L
12	0.1	A	L
13	0.1	A	L
14	0.15	vA	L
15	0.1	A	H
16	0.1	A	L
17	0.1	sA	H
18	0.15	R	H
19	0.1	sR	H
20	0.15	A	L
21	0.15	R	H
22	0.15	sR	H
23	0.15	A	H
24	0.15	R	L
25	0.15	wR	H
26	0.05	A	L
27	0.15	vA	L
28	0.15	A	L
29	0.1	R	L
30	0.1	sR	L
31	0.15	A	L
32	0.05	A	H
33	0.15	A	L
34	0.15	sA	L
35	0.2	vA	L
36	0.05	sA	L
37	0.1	sR	H
38	0.1	vA	L
39	0.1	sR	L
40	0.05	vA	L
41	0.1	A	L
42	0.1	sR	L
43	0.05	R	H
44	0.2	A	L
45	0.05	wR	H
46	0.1	R	H
47	0.15	A	L
48	0.1	sA	H
49	0.1	sR	L
50	0.1	A	L

51	0.1	A	L
52	0.05	wR	H
53	0.1	sA	H
54	0.15	R	L
55	0.1	sR	L
56	0.15	sA	L
57	0.1	sA	L
58	0.3	A	L
59	0.15	A	L
60	0.15	A	L
61	0.15	sA	L
62	0.2	sA	L
63	0.1	A	H
64	0.15	R	H
65	0.1	A	L
66	0.15	A	L
67	0.1	sA	L
68	0.1	A	L
69	0.15	sA	L
70	0.15	A	L
71	0.15	A	L
72	0.15	R	H
73	0.15	A	L
74	0.15	vA	L
75	0.2	R	L
76	0.15	A	L
77	0.1	wR	H
78	0.15	A	L
79	0.1	wR	H
80	0.15	sR	L
81	0.1	A	H
82	0.05	sR	H
83	0.15	A	L
84	0.15	sA	L
85	0.1	A	H
86	0.3	vA	L
87	0.1	A	H
88	0.15	A	H
89	0.1	A	L
90	0.1	sR	L
91	0.15	R	H

92	0.05	R	H
93	0.15	A	L
94	0.1	R	H
95	0.1	vA	L
96	0.15	sA	L
97	0.15	sR	L
98	0.15	sA	L
99	0.1	wR	H
100	0.1	sA	L

Average 0.1275

**Sample 36-15**

Count	Size (mm)	Rounding	Sphericity
1	0.1	wR	H
2	0.25	sR	L
3	0.2	sR	L
4	0.1	R	H
5	0.1	sR	H
6	0.15	sR	L
7	0.1	sA	L
8	0.1	sA	L
9	0.15	R	H
10	0.1	sA	L
11	0.2	sR	H
12	0.15	R	H
13	0.2	sA	H
14	0.15	sR	L
15	0.1	sR	H
16	0.1	sA	L
17	0.05	sR	H
18	0.1	R	H
19	0.2	sR	L
20	0.15	R	H
21	0.1	sA	L
22	0.1	sR	H
23	0.15	R	H
24	0.15	sA	L
25	0.05	sR	L
26	0.2	R	H



27	0.15	A	L
28	0.1	sA	L
29	0.1	wR	H
30	0.15	sA	H
31	0.2	sA	L
32	0.15	sA	L
33	0.25	R	H
34	0.05	sA	H
35	0.15	sA	L
36	0.25	sA	L
37	0.25	sA	L
38	0.25	sA	L
39	0.1	wR	H
40	0.15	R	H
41	0.1	R	H
42	0.2	wR	H
43	0.15	R	H
44	0.25	sR	H
45	0.15	R	H
46	0.15	R	H
47	0.15	sR	R
48	0.15	sR	H
49	0.2	wR	H
50	0.05	sR	H
51	0.2	sA	H
52	0.05	sA	H
53	0.15	wR	H
54	0.1	sA	H
55	0.1	sA	L
56	0.1	sA	L
57	0.15	sR	L
58	0.15	A	L
59	0.15	sR	L
60	0.15	sA	L
61	0.2	R	L
62	0.15	sA	L
63	0.1	R	L
64	0.2	wR	H
65	0.1	wR	H
66	0.2	A	L
67	0.15	sA	L

68	0.1	sR	H
69	0.2	R	H
70	0.15	sA	L
71	0.25	sR	H
72	0.1	sR	H
73	0.1	wR	H
74	0.15	sR	H
75	0.2	Sa	l
76	0.05	R	H
77	0.1	wR	H
78	0.25	R	L
79	0.2	sA	H
80	0.1	R	H
81	0.25	R	L
82	0.1	sA	L
83	0.1	sA	H
84	0.15	sA	L
85	0.1	sA	L
86	0.05	sR	H
87	0.2	sA	L
88	0.1	wR	H
89	0.1	sA	H
90	0.25	wR	H
91	0.1	A	L
92	0.15	sA	L
93	0.1	sR	H
94	0.2	R	L
95	0.1	sR	L
96	0.2	R	L
97	0.2	sR	H
98	0.2	sR	H
99	0.1	sR	H
100	0.15	R	H

Average 0.146

**Sample 33-03**

Count	Size (mm)	Rounding	Sphericity
1	0.15	sR	L
2	0.2	sA	L

3	0.2	sR	L
4	0.2	sR	H
5	0.25	sR	L
6	0.2	sR	L
7	0.05	sA	H
8	0.25	sA	L
9	0.2	sR	h
10	0.25	sA	L
11	0.15	sR	H
12	0.15	sA	H
13	0.1	sA	H
14	0.1	sA	H
15	0.25	sR	L
16	0.2	sA	L
17	0.25	sR	L
18	0.2	sA	L
19	0.25	sA	L
20	0.2	sR	L
21	0.15	sA	L
22	0.3	wR	H
23	0.2	sA	H
24	0.1	sA	L
25	0.3	R	L
26	0.05	R	H
27	0.2	sR	H
28	0.2	R	H
29	0.2	sR	H
30	0.1	R	H
31	0.15	R	L
32	0.25	sR	L
33	0.1	sR	H
34	0.2	R	L
35	0.2	sA	L
36	0.25	sA	H
37	0.2	R	H
38	0.25	wR	H
39	0.15	sA	L
40	0.15	sR	H
41	0.05	wR	H
42	0.2	sR	H
43	0.15	sA	L

44	0.2	R	H
45	0.05	wR	H
46	0.15	sA	L
47	0.1	wR	H
48	0.2	R	L
49	0.15	A	L
50	0.1	R	L
51	0.25	sR	L
52	0.2	sA	L
53	0.15	R	H
54	0.25	sR	L
55	0.15	R	H
56	0.1	sA	l
57	0.15	R	L
58	0.2	wR	h
59	0.15	wR	H
60	0.1	R	H
61	0.1	sA	H
62	0.1	R	H
63	0.05	sR	H
64	0.2	sr	h
65	0.25	sA	L
66	0.15	sR	L
67	0.15	A	L
68	0.15	sA	H
69	0.05	wR	H
70	0.15	sR	H
71	0.2	sA	H
72	0.25	sR	H
73	0.15	sA	L
74	0.25	sA	L
75	0.15	R	H
76	0.15	R	H
77	0.15	R	H
78	0.25	sA	L
79	0.15	sR	H
80	0.15	wR	H
81	0.15	sA	H
82	0.2	sA	L
83	0.1	R	H
84	0.2	sA	L

85	0.2	A	L
86	0.1	A	L
87	0.2	sA	L
88	0.1	R	H
89	0.05	sR	H
90	0.25	wR	H
91	0.1	sR	H
92	0.2	sR	L
93	0.15	wR	H
94	0.15	sA	L
95	0.2	A	L
96	0.1	sA	L
97	0.15	sR	h
98	0.1	A	L
99	0.25	R	L
100	0.2	sA	L

Average 0.169

**Sample 33-05**

Count	Size (mm)	Rounding	Sphericity
1	0.2	sR	L
2	0.1	sA	H
3	0.1	A	l
4	0.2	A	L
5	0.2	sA	L
6	0.1	wR	H
7	0.15	R	H
8	0.1	A	L
9	0.2	sR	H
10	0.2	sA	L
11	0.2	A	L
12	0.2	A	L
13	0.15	sR	H
14	0.05	wR	H
15	0.1	sA	H
16	0.15	sA	L
17	0.15	sR	L
18	0.1	sA	H
19	0.15	sA	L

20	0.2	sR	L
21	0.1	sA	L
22	0.2	R	L
23	0.2	sR	L
24	0.1	R	H
25	0.2	R	L
26	0.15	R	H
27	0.15	A	L
28	0.1	A	L
29	0.2	R	H
30	0.2	wR	H
31	0.15	sA	L
32	0.2	A	L
33	0.15	R	L
34	0.1	R	A
35	0.05	R	H
36	0.05	A	L
37	0.1	R	L
38	0.15	R	H
39	0.15	wR	H
40	0.25	R	L
41	0.15	A	L
42	0.15	A	L
43	0.1	sR	L
44	0.2	R	L
45	0.25	sA	L
46	0.1	A	L
47	0.05	R	H
48	0.2	R	H
49	0.1	wR	H
50	0.05	wR	H
51	0.1	A	L
52	0.05	wR	H
53	0.1	R	H
54	0.1	A	L
55	0.2	sA	L
56	0.1	sR	H
57	0.15	sR	L
58	0.15	A	L
59	0.15	wR	H
60	0.25	R	L

61	0.1	R	H
62	0.15	wR	H
63	0.15	sR	L
64	0.2	sR	L
65	0.2	sR	L
66	0.2	R	H
67	0.2	sA	L
68	0.15	sA	L
69	0.15	R	H
70	0.1	sA	L
71	0.2	sR	L
72	0.2	sA	L
73	0.15	A	L
74	0.15	sA	L
75	0.1	sA	L
76	0.1	A	L
77	0.25	A	L
78	0.2	sA	L
79	0.2	sA	L
80	0.15	A	L
81	0.2	wR	H
82	0.15	sR	H
83	0.2	A	L
84	0.1	sA	H
85	0.25	R	L
86	0.2	sA	L
87	0.2	sA	L
88	0.1	sR	L
89	0.15	sR	L
90	0.15	A	L
91	0.15	sA	L
92	0.15	sR	L
93	0.15	wR	H
94	0.2	vA	L
95	0.2	sA	H
96	0.1	R	H
97	0.15	sA	L
98	0.1	sA	H
99	0.15	vA	L
100	0.05	A	L

Average 0.1505

**Sample 33-07**

<b>Count</b>	<b>Size (mm)</b>	<b>Rounding</b>	<b>Sphericity</b>
1	0.15	sR	L
2	0.15	R	H
3	0.1	sR	L
4	0.15	wR	H
5	0.15	A	L
6	0.05	R	H
7	0.15	sA	H
8	0.05	wR	H
9	0.15	A	L
10	0.15	R	H
11	0.15	sA	L
12	0.3	vA	L
13	0.15	A	L
14	0.1	vA	L
15	0.15	sR	L
16	0.15	sA	L
17	0.25	R	h
18	0.15	sA	L
19	0.2	R	H
20	0.15	sR	H
21	0.1	sA	L
22	0.1	R	H
23	0.05	sR	H
24	0.15	sA	L
25	0.05	A	L
26	0.1	vA	L
27	0.05	R	H
28	0.2	A	L
29	0.2	A	L
30	0.1	R	H
31	0.1	R	H
32	,2	sR	L
33	0.3	A	L
34	0.1	A	L
35	0.2	sA	L
36	0.1	R	H



37	0.2	vA	L
38	0.05	vA	L
39	0.2	sR	H
40	0.2	vA	L
41	0.15	A	L
42	0.05	wR	H
43	0.1	A	L
44	0.2	R	H
45	0.15	sR	L
46	0.1	A	L
47	0.1	wR	H
48	0.2	wR	H
49	0.1	wR	H
50	0.1	R	H
51	0.4	R	L
52	0.15	A	L
53	0.15	sR	L
54	0.1	A	L
55	0.1	A	L
56	0.05	R	H
57	0.2	sR	L
58	0.15	A	L
59	0.1	A	L
60	0.15	A	L
61	0.1	vA	L
62	0.1	R	L
63	0.15	sR	L
64	0.15	sA	L
65	0.1	vA	L
66	0.1	sA	L
67	0.1	wR	H
68	0.15	sA	L
69	0.35	R	L
70	0.2	R	H
71	0.15	A	L
72	0.4	sR	L
73	0.25	A	L
74	0.1	R	H
75	0.1	A	L
76	0.1	vA	L
77	0.15	sR	H

78	0.15	A	L
79	0.2	A	L
80	0.15	R	H
81	0.1	sR	L
82	0.2	R	H
83	0.15	R	L
84	0.05	R	H
85	0.1	sR	H
86	0.1	sR	H
87	0.1	sA	L
88	0.1	R	H
89	0.2	R	H
90	0.1	sA	L
91	0.15	sR	L
92	0.15	A	L
93	0.4	sA	L
94	0.05	A	L
95	0.1	A	L
96	0.1	R	L
97	0.1	sR	L
98	0.2	R	H
99	0.1	wR	H
100	0.1	wR	H

Average 0.143939394

**Sample 16-02**

<b>Count</b>	<b>Size (mm)</b>	<b>Rounding</b>	<b>Sphericity</b>
1	0.05	sA	H
2	0.15	sA	H
3	0.5	R	H
4	0.2	A	L
5	0.15	sR	L
6	0.1	R	H
7	0.15	wR	H
8	0.2	R	H
9	0.15	sA	L
10	0.2	A	L
11	0.1	vA	L
12	0.15	sR	L

13	0.1	R	L
14	0.1	A	L
15	0.2	R	H
16	0.1	A	L
17	0.2	R	L
18	0.2	vA	L
19	0.25	A	L
20	0.2	A	L
21	0.2	sA	L
22	0.1	R	H
23	0.1	wR	H
24	0.15	A	L
25	0.15	A	L
26	0.15	A	L
27	0.25	A	L
28	0.15	A	L
29	0.3	sR	L
30	0.25	sR	L
31	0.2	A	L
32	0.15	sA	L
33	0.3	R	L
34	0.2	sA	L
35	0.3	A	L
36	0.2	R	H
37	0.25	sA	L
38	0.25	sR	H
39	0.25	A	L
40	0.25	A	L
41	0.05	sA	l
42	0.15	A	L
43	0.2	sA	L
44	0.2	R	L
45	0.15	`sR	L
46	0.45	sA	L
47	0.1	R	H
48	0.1	vA	L
49	0.25	sA	L
50	0.15	sR	L
51	0.15	vA	L
52	0.15	sR	L
53	0.15	A	L

54	0.2	sA	L
55	0.25	A	L
56	0.25	wR	H
57	0.15	wR	H
58	0.3	sA	L
59	0.25	A	L
60	0.3	A	L
61	0.1	R	H
62	0.1	A	L
63	0.25	sR	L
64	0.15	A	L
65	0.3	sA	L
66	0.15	A	L
67	0.1	sR	L
68	0.25	sR	L
69	0.15	R	L
70	0.1	A	L
71	0.2	sR	L
72	0.15	R	H
73	0.2	vA	L
74	0.1	A	H
75	0.2	R	L
76	0.2	A	L
77	0.2	A	L
78	0.1	R	H
79	0.1	A	L
80	0.2	R	H
81	0.15	A	L
82	0.1	A	L
83	0.05	R	H
84	0.05	A	L
85	0.25	sR	L
86	0.25	A	L
87	0.25	sR	L
88	0.2	sA	L
89	0.25	A	L
90	0.1	sR	L
91	0.2	A	L
92	0.15	R	H
93	0.1	A	L
94	0.1	A	L

95	0.15	A	L
96	0.2	vA	L
97	0.25	sA	L
98	0.15	wR	H
99	0.05	A	L
100	0.1	sA	L

Average 0.1795

**Sample 16-05**

Count	Size (mm)	Rounding	Sphericity
1	0.1	A	L
2	0.1	vA	L
3	0.25	vA	L
4	0.2	R	H
5	0.2	R	H
6	0.2	A	L
7	0.15	R	H
8	0.15	A	L
9	0.2	A	L
10	0.15	R	H
11	0.15	A	L
12	0.1	A	L
13	0.15	R	H
14	0.25	sA	L
15	0.15	A	L
16	0.2	sA	L
17	0.15	wR	L
18	0.15	R	L
19	0.2	vA	L
20	0.1	sA	L
21	0.15	sA	L
22	0.3	sA	L
23	0.1	A	L
24	0.2	R	H
25	0.2	A	L
26	0.2	sR	H
27	0.15	A	L
28	0.25	A	L
29	0.1	vA	L

30	0.15	sR	H
31	0.1	sA	H
32	0.1	wR	H
33	0.05	A	L
34	0.1	sR	H
35	0.2	sR	L
36	0.3	R	L
37	0.2	sR	H
38	0.15	wR	H
39	0.15	A	L
40	0.15	vA	L
41	0.15	sA	H
42	0.15	R	L
43	0.2	wR	L
44	0.15	A	L
45	0.05	sR	H
46	0.05	R	H
47	0.3	sR	L
48	0.25	sA	L
49	0.2	sR	L
50	0.15	R	L
51	0.1	R	H
52	0.2	A	L
53	0.2	A	L
54	0.2	A	L
55	0.2	A	L
56	0.2	A	L
57	0.25	A	L
58	0.15	R	H
59	0.25	R	L
60	0.2	R	L
61	0.3	R	H
62	0.2	sA	L
63	0.15	R	H
64	0.1	A	L
65	0.1	A	L
66	0.25	R	L
67	0.2	R	H
68	0.2	sA	L
69	0.2	A	L
70	0.2	A	L

71	0.3	sR	L
72	0.2	sA	H
73	0.1	sA	H
74	0.15	sA	H
75	0.15	sR	L
76	0.2	sA	L
77	0.15	wR	H
78	0.15	A	L
79	0.1	vA	L
80	0.25	A	L
81	0.2	wR	H
82	0.2	A	L
83	0.1	A	L
84	0.05	wR	H
85	0.2	R	L
86	0.15	wR	H
87	0.2	wR	H
88	0.15	A	L
89	0.2	sA	L
90	0.15	sA	L
91	0.2	A	L
92	0.2	A	L
93	0.15	R	H
94	0.25	A	L
95	0.25	A	L
96	0.15	A	L
97	0.15	sR	H
98	0.25	sR	L
99	0.05	wR	H
100	0.25	sR	L

Average 0.1735

**Sample 46-03**

Count	Size (mm)	Rounding	Sphericity
1	0.2	sR	H
2	0.1	wR	H
3	0.3	sA	H
4	0.1	sA	L
5	0.05	A	L

6	0.25	A	L
7	0.2	A	L
8	0.25	sR	L
9	0.15	sR	H
10	0.2	R	H
11	0.2	R	L
12	0.1	wR	H
13	0.2	A	L
14	0.2	wR	L
15	0.15	sR	H
16	0.15	R	L
17	0.15	R	H
18	0.25	sR	L
19	0.15	R	H
20	0.2	R	H
21	0.2	sR	H
22	0.2	sR	L
23	0.15	sR	H
24	0.15	sR	L
25	0.15	A	L
26	0.15	A	L
27	0.15	A	L
28	0.2	sR	H
29	0.2	sA	L
30	0.15	wR	H
31	0.15	A	L
32	0.15	A	L
33	0.1	R	H
34	0.15	vA	L
35	0.1	R	H
36	0.1	R	H
37	0.1	R	H
38	0.15	sR	H
39	0.25	sA	L
40	0.25	sA	L
41	0.1	sR	L
42	0.15	sA	H
43	0.2	sR	L
44	0.15	R	L
45	0.15	sA	L
46	0.15	wR	H



47	0.15	sA	L
48	0.15	A	L
49	0.15	sR	L
50	1.5	sA	L
51	0.2	A	L
52	0.15	A	L
53	0.2	R	H
54	0.1	R	H
55	0.2	R	L
56	0.05	A	L
57	0.2	R	H
58	0.1	sA	H
59	0.15	R	H
60	0.2	sR	L
61	0.2	A	L
62	0.1	sA	H
63	0.1	wR	H
64	0.15	A	L
65	0.1	wR	H
66	0.15	sA	H
67	0.15	A	L
68	0.25	wR	L
69	0.2	A	L
70	0.2	sR	H
71	0.15	sR	L
72	0.15	sR	L
73	0.15	A	L
74	0.1	R	H
75	0.15	wR	H
76	0.2	R	H
77	0.1	sA	H
78	0.05	A	L
79	0.2	R	L
80	0.15	wR	H
81	0.1	wR	H
82	0.15	sR	L
83	0.1	sA	H
84	0.1	wR	H
85	0.2	sR	L
86	0.2	R	L
87	0.3	R	H

88	0.1	A	L
89	0.15	A	L
90	0.2	R	L
91	0.25	R	L
92	0.1	R	H
93	0.2	sR	H
94	0.05	sR	H
95	0.1	sA	L
96	0.15	R	H
97	0.25	wR	L
98	0.1	A	L
99	0.25	A	L
100	0.15	wR	H

Average            0.1735

**Sample 46-05**

<b>Count</b>	<b>Size (mm)</b>	<b>Rounding</b>	<b>Sphericity</b>
1	0.05	wR	L
2	0.2	A	L
3	0.2	sR	H
4	0.15	A	L
5	0.1	A	L
6	0.15	A	L
7	0.2	sA	L
8	0.1	vA	L
9	0.25	A	H
10	0.2	sR	L
11	0.2	sR	L
12	0.2	sR	L
13	0.15	sA	L
14	0.2	sR	L
15	0.2	R	L
16	0.15	sR	H
17	0.1	sR	H
18	0.1	R	L
19	0.25	R	L
20	0.2	sA	H
21	0.2	A	L
22	0.2	wR	H

23	0.15	A	L
24	0.2	sR	H
25	0.15	A	L
26	0.2	R	H
27	0.15	sR	L
28	0.1	sR	H
29	0.1	A	L
30	0.05	sA	H
31	0.2	R	H
32	0.25	R	L
33	0.2	A	L
34	0.1	A	L
35	0.3	sA	L
36	0.1	vA	L
37	0.05	R	H
38	0.2	A	H
39	0.1	sA	H
40	0.1	A	L
41	0.15	A	`L
42	0.25	sA	H
43	0.25	vA	L
44	0.2	sR	H
45	0.3	sA	L
46	0.2	A	L
47	0.2	sA	L
48	0.25	sR	L
49	0.2	sA	L
50	0.1	A	L
51	0.15	sA	L
52	0.15	A	L
53	0.2	sA	H
54	0.15	sR	H
55	0.2	A	L
56	0.15	R	H
57	0.2	sR	L
58	0.1	R	H
59	0.15	sR	H
60	0.15	wR	H
61	0.2	sR	L
62	0.2	A	L
63	0.2	A	L

64	0.2	A	L
65	0.15	wR	H
66	0.1	sA	H
67	0.05	sR	H
68	0.3	R	L
69	0.15	wR	H
70	0.3	sR	L
71	0.1	A	L
72	0.2	R	H
73	0.25	sA	L
74	0.15	sA	H
75	0.2	R	L
76	0.15	sA	L
77	0.2	A	L
78	0.2	A	L
79	0.25	A	L
80	0.2	A	L
81	0.3	R	L
82	0.15	R	H
83	0.1	sA	L
84	0.15	A	L
85	0.4	A	L
86	0.15	A	L
87	0.2	sR	L
88	0.05	wR	H
89	0.15	A	L
90	0.15	sr	H
91	0.2	R	H
92	0.45	vA	L
93	0.15	wR	H
94	0.15	A	H
95	0.2	sA	L
96	0.25	sR	L
97	0.15	sA	L
98	0.2	sR	L
99	0.15	sA	H
100	0.2	A	L
Average	0.178		

**Sample 47-02**

<b>Count</b>	<b>Size (mm)</b>	<b>Rounding</b>	<b>Sphericity</b>
1	0.05	wR	H
9	0.15	wR	H
18	0.1	wR	H
19	0.15	wR	L
38	0.15	wR	H
46	0.15	wR	H
61	0.15	wR	H
84	0.1	wR	H
68	0.1	vA	L
91	0.15	vA	L
6	0.15	sR	H
11	0.25	sR	H
12	0.15	sR	H
13	0.2	sR	L
25	0.1	sR	H
30	0.25	sR	H
40	0.2	sR	L
45	0.2	sR	L
47	0.2	sR	L
49	0.15	sR	H
52	0.2	sR	L
55	0.1	sR	L
62	0.15	sR	H
69	0.2	sr	H
74	0.15	sR	L
75	0.15	sR	L
79	0.1	sR	L
85	0.15	sR	L
86	0.1	sR	H
90	0.15	sR	L
95	0.1	sR	L
5	0.2	sA	L
7	0.15	sA	L
16	0.25	sA	L
22	0.15	sA	L
26	0.15	sA	H
27	0.2	sA	H
41	0.1	sA	L
44	0.2	sA	L

54	0.2	sA	L
56	0.3	sA	L
57	0.2	sA	L
63	0.1	sA	L
65	0.05	sA	L
67	0.15	sA	L
77	0.3	sA	L
78	0.1	sA	H
80	0.15	sA	L
93	0.1	sA	L
94	0.05	sA	L
100	0.15	sA	H
8	0.15	R	H
14	0.2	R	H
15	0.2	R	H
20	0.2	R	H
23	0.15	R	H
31	0.1	R	H
34	0.15	R	L
36	0.15	R	H
37	0.2	R	L
39	0.15	R	H
42	0.05	R	H
43	0.1	R	H
50	0.15	R	L
60	0.15	R	L
70	0.1	R	H
73	0.15	R	H
82	0.1	R	L
83	0.15	R	L
87	0.15	R	H
92	0.15	R	H
97	0.25	R	L
98	0.15	R	L
2	0.1	A	L
3	0.15	A	L
4	0.1	A	L
10	0.1	A	L
17	0.15	A	L
21	0.1	A	L
24	0.2	A	L

28	0.25	A	L
29	0.1	A	L
32	0.15	A	L
33	0.1	A	L
35	0.2	A	L
48	0.15	A	L
51	0.25	A	L
53	0.15	A	L
58	0.1	A	L
59	0.15	A	L
64	0.1	A	L
66	0.15	A	L
71	0.2	A	L
72	0.1	A	L
76	0.1	A	L
81	0.2	A	L
88	0.25	A	L
89	0.15	A	L
96	0.2	A	L
99	0.25	A	L

Average 0.154

**Sample 47-03**

Count	Size (mm)	Rounding	Sphericity
1	0.3	R	H
2	0.15	A	L
3	0.3	sR	L
4	0.25	sR	L
5	0.3	R	L
6	0.2	sR	L
7	0.25	sR	H
8	0.25	sA	L
9	0.45	R	L
10	0.35	sA	L
11	0.25	sA	L
12	0.2	sA	H
13	0.2	sR	H
14	0.25	sA	L
15	0.25	sr	L

16	0.25	sR	H
17	0.25	A	L
18	0.25	sR	H
19	0.25	A	L
20	0.35	sR	L
21	0.2	sA	L
22	0.35	A	L
23	0.25	A	L
24	0.2	A	L
25	0.25	R	H
26	0.3	A	H
27	0.2	sA	H
28	0.3	sR	H
29	0.25	R	H
30	0.2	A	L
31	0.25	A	H
32	0.25	A	H
33	0.3	wR	L
34	0.25	sA	L
35	0.25	sR	L
36	0.25	A	L
37	0.2	sA	H
38	0.2	sA	L
39	0.24	sR	H
40	0.25	sA	L
41	0.2	vA	L
42	0.15	wR	H
43	0.2	sR	H
44	0.2	wR	H
45	0.35	sR	L
46	0.25	sR	L
47	0.2	sA	L
48	0.35	sR	L
49	0.1	sR	H
50	0.15	R	H
51	0.25	wR	H
52	0.25	sA	H
53	0.25	sR	L
54	0.35	sA	L
55	0.25	sR	H
56	0.45	vA	L



57	0.35	sR	L
58	0.25	A	L
59	0.25	sA	H
60	0.2	A	L
61	0.15	sA	H
62	0.2	R	H
63	0.25	sR	H
64	0.2	A	L
65	0.2	sR	L
66	0.3	R	H
67	0.25	sR	H
68	0.25	A	L
69	0.25	A	L
70	0.25	R	L
71	0.1	sR	L
72	0.2	sR	L
73	0.35	sR	L
74	0.25	sA	L
75	0.25	sA	H
76	0.3	sR	L
77	0.4	sR	L
78	0.25	sA	L
79	0.25	R	H
80	0.3	sR	L
81	0.25	vA	L
82	0.2	sR	L
83	0.3	sR	H
84	0.2	sA	L
85	0.2	sR	L
86	0.2	R	H
87	0.2	A	L
88	0.4	vA	L
89	0.35	A	L
90	0.3	sR	L
91	0.25	sR	L
92	0.25	sA	L
93	0.2	sA	L
94	0.35	A	L
95	0.2	sA	L
96	0.15	A	L
97	0.25	R	H

98	0.15	R	H
99	0.3	A	L
100	0.25	sR	H

Average            0.2514

**Sample 47-07**

Count	Size (mm)	Rounding	Sphericity
1	0.1	A	L
2	0.1	A	L
3	0.2	sR	H
4	0.05	A	L
5	0.15	sR	L
6	0.15	sA	L
7	0.15	A	L
8	0.2	A	L
9	0.2	A	L
10	0.05	A	L
11	0.15	sA	L
12	0.25	R	L
13	0.15	vA	L
14	0.05	R	H
15	0.2	sR	L
16	0.15	R	L
17	0.1	R	H
18	0.2	R	H
19	0.2	A	L
20	0.1	A	L
21	0.2	A	L
22	0.15	R	H
23	0.1	wR	h
24	0.1	sA	H
25	0.1	A	L
26	0.15	sA	H
27	0.2	A	L
28	0.1	A	L
29	0.1	A	H
30	0.2	A	L
31	0.1	A	L
32	0.1	A	L

33	0.15	R	H
34	0.1	R	H
35	0.15	A	L
36	0.1	sR	L
37	0.1	sR	L
38	0.1	R	H
39	0.1	sR	L
40	0.15	A	L
41	0.1	sA	H
42	0.1	A	L
43	0.25	A	L
44	0.25	R	L
45	0.15	sR	H
46	0.05	A	L
47	0.1	sR	L
48	0.2	sA	L
49	0.15	A	L
50	0.1	R	H
51	0.2	A	L
52	0.1	R	H
53	0.2	sR	L
54	0.1	sA	H
55	0.05	A	L
56	0.1	A	L
57	0.05	R	H
58	0.01	R	H
59	0.1	sR	L
60	0.15	vA	L
61	0.1	R	H
62	0.2	A	L
63	0.1	A	L
64	0.15	vA	L
65	0.2	sR	H
66	0.15	vA	L
67	0.2	sR	H
68	0.2	A	L
69	0.15	A	L
70	0.1	sR	H
71	0.2	sR	L
72	0.2	A	L
73	0.1	R	H

74	0.1	R	L
75	0.3	vA	L
76	0.1	sA	L
77	0.15	R	H
78	0.1	A	L
79	0.15	A	L
80	0.2	A	L
81	0.2	sR	L
82	0.15	sR	H
83	0.2	vA	L
84	0.1	sR	H
85	0.1	R	H
86	0.1	sR	L
87	0.1	sR	L
88	0.2	sR	H
89	0.1	sA	L
90	0.2	A	L
91	0.2	sR	L
92	0.1	sR	H
93	0.2	R	H
94	0.25	sR	L
95	0.1	A	L
96	0.2	A	L
97	0.15	wR	H
98	0.15	R	L
99	0.15	R	H
100	0.1	wR	H

Average            0.1416

### References

Powers, M.C., 1953, A new roundness scale for sedimentary particles. *Journal of Sedimentary Petrology*, v. 23, p. 117-119.